UNIVERSITÀ DEGLI STUDI FIRENZE

DOTTORATO DI RICERCA IN SCIENZE CLINICHE

CICLO XXXI

COORDINATORE Prof. Matucci Cerinic Marco

Phenotyping COPD: correlazione clinico-radiologica dei fenotipi della BPCO

Settore Scientifico Disciplinare MED/10

Dottorando

Dr.ssa Occhipinti Mariaelena

Tutore

Prof. Pistolesi Massimo

Coordinatore

Prof. Matucci Cerinic Marco

Anni 2015/2018

Contents

Chapter 1 - Thesis topic and outline

This thesis describes the use and development of innovative tools, both radiological and bioengineering, in supporting clinical diagnosis of chronic obstructive pulmonary disease (COPD). Radiology was coupled with pulmonary function to better understand this complex and heterogeneous disease and to describe its phenotypes and endotypes. An overview of the clinical and radiological complexity of COPD and the current role of imaging is presented in the first part (Chapters 1 and 2). The second part (Chapters 3 to 7) focuses on statistical and mathematical models that classify patients for having the emphysematous phenotype based uniquely on clinical and functional data. Innovative imaging techniques have been tested and used as gold standards. The third part (Chapter 8 and 9) examines the ongoing questions and future directions of research in the field.

Part I

Chapter 1 COPD: a complex and heterogeneous disease

Chapter 2 Radiology and Radiomics

Part II

Chapter 3 Emphysematous and nonemphysematous gas trapping in COPD

Chapter 4 Statistical models: lung function and BMI

Chapter 5 Statistical models: maximal expiratory flow-volume curve

Chapter 6 Mathematical model and radiomics

Chapter 7 Validation ESI model

Part III

Chapter 8 Which criteria to define COPD?

Chapter 9 Future directions

Chapter 10 Conclusions

Chapter 2 - COPD: a complex and heterogeneous disease

Chronic obstructive pulmonary disease (COPD) is characterized by expiratory airflow limitation caused by increased resistance of the small airways and/or increased compliance of the lung as a result of emphysema. The volume of air that can be expired within 1 s after the beginning of a forced expiration (FEV_1) is the hallmark of COPD, as expiratory airflow is affected by inflammation and remodeling of the small airways as well as by emphysematous destruction of lung parenchyma. Spirometric detection of not fully reversible airflow limitation unifies under the acronym COPD a spectrum of heterogeneous conditions, different from the clinical, functional, and pathological perspective.

Fifty years ago Burrows described the distinctive clinical, functional, radiological, and pathological characteristics that differentiate those patients with COPD during life who presented with parenchymal destruction or involvement of the small airways at autopsy (1). The terms type A (pink puffer) and type B (blue bloater) introduced to empirically differentiate COPD patients with the emphysematous type from those with the small airway disease type of chronic airways obstruction are no longer in use because a direct association between clinically defined phenotypes and lung pathologic findings, such as centrilobular and panlobular emphysema, has never been demonstrated (2). The observation that the pathological findings of small airways disease and parenchymal destruction often coexist in the same patient has substantially contributed to the introduction and wide use of the term "COPD" for the whole population of patients with chronic irreversible airflow limitation. However, spirometric parameters, such as FEV_1 and forced vital capacity (FVC), cannot provide a panoramic view of the complexity and heterogeneity of COPD. Different types of emphysema may coexist in the same patient and the mechanical properties of the lung differ according to the predominant type.

In 2009 Ogawa et al. elegantly brought back to life and strengthened Burrows' findings of the sixties by using high resolution computed tomography (CT) (3). They found that patients with COPD who had low attenuation areas (compatible with emphysematous destruction of lung parenchyma) were thinner than those who had bronchial wall thickening (compatible with chronic inflammatory changes of the small airways). A significant inverse relationship was found between body mass index (BMI) and emphysema extent at CT, whereas there was no correlation between BMI and thickness of the bronchial wall. FEV_1 inversely correlated with BMI, CT emphysema extent and bronchial wall thickness, but there was no significant difference in FEV_1 between the two CT phenotypes of COPD (3). These findings suggest that patients with COPD may have different systemic clinical manifestations (*phenotypes*), reflecting different pathophysiological mechanisms (*endotypes*) of expiratory airflow limitation (4). Moreover, the various endotypes may respond differently to therapy, which could possibly explain the deceiving results of some pharmacological trials (8).

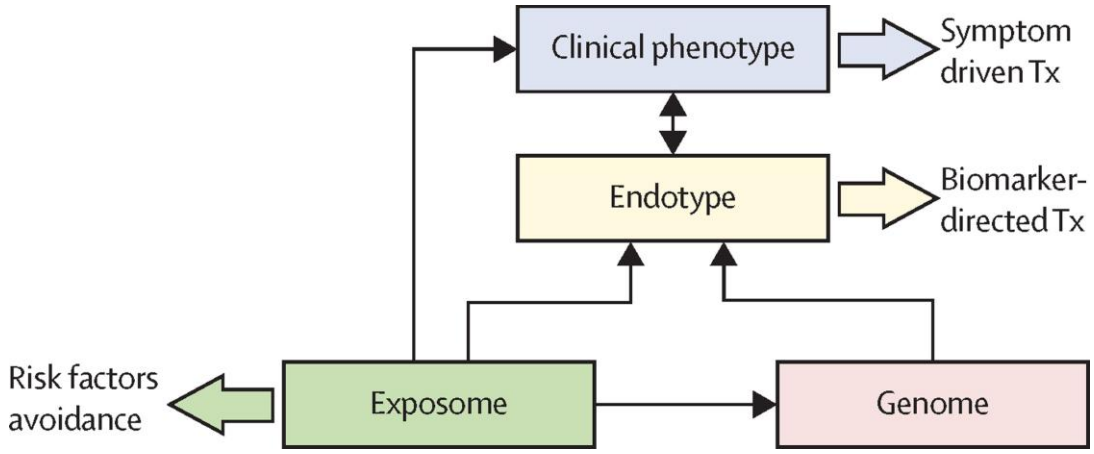

From: Woodruff P et al. The Lancet 2015 385, 1789-98.

Endotypes can be characterized *in vivo* by using CT. Together with the emphysema extent, airway wall thickness on CT has been used to help classifying patients with expiratory airflow limitation as having either a predominant emphysema phenotype (increased lung compliance) or a predominant small airway disease phenotype (increased airway resistance) (5-7). The recent technological advances in imaging acquisition and post-processing of image data have brought to advances into the understanding of such a complex and heterogeneous disease as COPD.

2.1 References

1. Burrows B. Diagnosis and course of chronic bronchitis and emphysema. Proc Annu Meet Med Sect Am Life Conv 1968; 56:106-116.
2. Thurlbeck WM. Chronic bronchitis and emphysema. Med Clin North Am 1973; 57:651-668.
3. Ogawa E, Nakano Y, Ohara T, Muro S, Hirai T, Sato S, et al. Body mass index in male patients with COPD: correlation with low attenuation areas on CT. Thorax 2009; 64:20-25.
4. Woodruff PG, Agusti A, Roche N, Singh D, Martinez FJ. Current concepts in targeting chronic obstructive pulmonary disease pharmacotherapy: making progress towards personalised management. Lancet 2015; 385:1789-1798.
5. Nakano Y, Wong JC, de Jong PA, Buzatu L, Nagao T, Coxson HO, et al. The prediction of small airway dimensions using computed tomography. Am J Respir Crit Care Med 2005; 171:142-146.
6. Kitaguchi Y, Fujimoto K, Kubo K, Honda T. Characteristics of COPD phenotypes classified according to the findings of HRCT. Respir Med 2006; 100:1742-1752.
7. Orlandi I, Moroni C, Camiciottoli G, Bartolucci M, Pistolesi M, Villari N, et al. Chronic obstructive pulmonary disease: thin-section CT measurement of airway wall thickness and lung attenuation. Radiology 2005; 234:604-610.
8. Calverley PM, Anderson JA, Celli B, Ferguson GT, Jenkins C, Jones PW, et al. Salmeterol and fluticasone propionate and survival in chronic obstructive pulmonary disease. N Engl J Med 2007; 356:775-789.ù

Chapter 3 - Radiology and Radiomics

Chest radiography has been used for many years to evaluate the entire chest in COPD patients. However, the advent of CT and the recent advances in acquisition as well as in post-processing of image data have lead to a significant improvement in the *in vivo* characterization of COPD.

CT is the most widely available and precise imaging method for the characterization of COPD. CT is a well-validated technique to assess qualitatively and quantitatively the presence, pattern, and extent of emphysema (1, 2). Quantification of low-attenuation areas, expiratory gas trapping, and airway wall thickness can help define specific COPD subtypes with different clinical and physiologic features (3).

The Fleischner Society in 2015 released a Statement on CT-definable subtypes of COPD that included a wide spectrum of emphysema and airway disease subtypes (4). The criteria to classify the subtypes rely on both quantitative and qualitative parameters.

Qualitative analysis defines the presence and subtype of emphysema, airway wall thickening, and the features associated, such as tracheobronchomalacia, bronchiectases, coexistence of interstitial lung disease, pulmonary hypertension, morphology of chest wall and large airways (4). Semiquantitative scores to quantify pulmonary emphysema have been used, but quantitative analysis overtakes radiologists performance (5).

Quantitative analysis can be performed nowadays by using many different software programs, either free or commercially available. Most of them execute a densitometric analysis of lung parenchyma and the segmentation of airways and lobes, providing parameters of low attenuation areas, airway wall thickening, and airway luminal area. More advanced programs can also provide parameters on pulmonary vasculature (i.e. vessel volume, vessel caliber, distinction between arteries and veins). Nowadays these software programs are fully automated and some of them allow the manual correction if any mistake occur. The time needed to perform these analyses vary according to the program used, ranging from 5 to 10 minutes per CT scan.

Inspiratory CT scan is performed at total lung capacity, whereas expiratory scan can be performed either at forced vital capacity or at residual volume. Spirometric gating allows scanning the chest at predefined lung volumes to avoid the influence of the level of lung inflation during scanning on CT attenuation measurements (6, 7). However, the level of lung inflation is not the only parameter affecting the assessment of the disease at CT. Quantitative analysis can also be affected by a large number of factors, such as variability in technical parameters of acquisition (slice thickness, convolution kernels, iterative reconstructions, kVp and mAs), calibration of CT scanners, CT vendors, patient's BMI, presence of motion or hard-beam artifacts, coexistence of other lesions, and post-processing image analysis (8). Recently a new factor has been added to this long list: the elastic deformation of paired inspiratory and expiratory scans performed at coregistration analysis. Coregistration analysis provides the relative volume of functional gas trapping, namely the gas trapped in

expiration not due to emphysema (9, 10). This deformation creates parametric response maps where each voxel has an attenuation value different from both the native paired CT scans.

The exponential growth in medical image analysis has brought to an increased number of pattern recognition tools and the increase in data set sizes. These advances have facilitated the development of processes for high-throughput extraction of quantitative features that result in the conversion of images into mineable data and the subsequent analysis of these data for decision support. This practice is termed *radiomics*. Radiomics allows the simultaneous use of a large amount of parameters extracted from imaging data. These parameters are mathematically processed with advanced statistical methodologies (11). Radiomic data contain first-, second-, and higher-order statistics (12). These data are combined with other patient data and are mined with sophisticated bioinformatics tools to develop models that may potentially improve diagnostic, prognostic, and predictive accuracy (13).

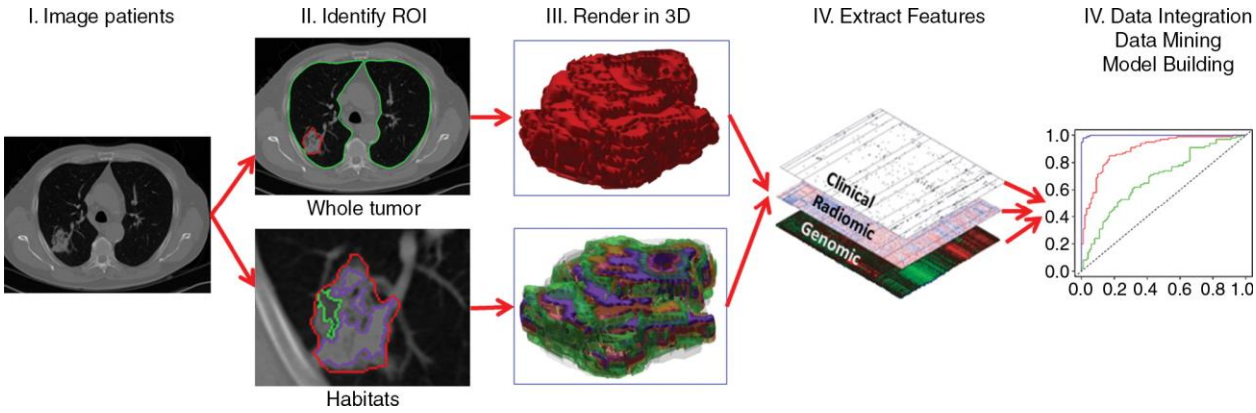

From: Gillies R et al. Radiology 2016; 278:563–77

The novelty of the methodology carries many difficulties nowadays, especially in the choice of which parameters to extract from the images. Each tool calculates a different number of features, belonging to different categories, and the initial choice may appear somehow arbitrary. Nonetheless, the methodologies for data analysis strictly depend on the number of input variables, possibly affecting the final result. One approach is to start from all the features provided by the calculation tool and to perform a preliminary analysis to select the repeatable and reproducible parameters, to subsequently reduce them by correlation and redundancy analysis. Another approach is to make an *a priori* selection of the features, based on their mathematical definition, focusing on the parameters easily interpretable in terms of visual appearance, or directly connectable to some biological properties of the tissue. Alternatively, machine-learning techniques, underlying the idea that computers may learn from past examples and detect hard-to-discern patterns from large and complex datasets, are used and emerging today as a useful tool to select appropriate features (14, 15).

Although radiomics features can be calculated by dedicated software programs, which are user-friendly and timely wise, it is still mandatory to carefully check the quality of the input data and to select the optimal parameters to guarantee reliable and robust output (16). The huge amount of information provided by this new methodology should be accurately evaluated and its clinical meaning explored.

Advances in technical equipment allowed the generation of *microCT* scans. The analysis of lung parenchyma at a 16.24μm isotropic voxel resolution allows visualizing the terminal bronchioles to the point at which they branched into respiratory bronchioles (17). An estimate of the total number of terminal bronchioles as well as the total cross-sectional area of all terminal bronchioles per lung can be obtained, providing useful information in the assessment of COPD subtypes. However, microCT can assess only frozen lung specimens, making microCT fully dedicated to research.

3.1 References

1. Muller NL, Staples CA, Miller RR, Abboud RT. "Density mask". An objective method to quantitate emphysema using computed tomography. Chest 1988; 94:782-787.
2. Madani A, Zanen J, de Maertelaer V, Gevenois PA. Pulmonary emphysema: objective quantification at multi-detector row CT--comparison with macroscopic and microscopic morphometry. Radiology 2006; 238:1036-1043.
3. Mohamed Hoesein FA, Schmidt M, Mets OM, Gietema HA, Lammers JW, Zanen P, et al. Discriminating dominant computed tomography phenotypes in smokers without or with mild COPD. Respir Med 2014; 108:136-143.
4. Lynch DA, Austin JH, Hogg JC, Grenier PA, Kauczor HU, Bankier AA, et al. CT-Definable Subtypes of Chronic Obstructive Pulmonary Disease: A Statement of the Fleischner Society. Radiology 2015:141579.
5. Bankier AA, De Maertelaer V, Keyzer C, Gevenois PA. Pulmonary emphysema: subjective visual grading versus objective quantification with macroscopic morphometry and thin-section CT densitometry. Radiology 1999; 211:851-858.
6. Camiciottoli G, Bartolucci M, Maluccio NM, Moroni C, Mascalchi M, Giuntini C, et al. Spirometrically gated high-resolution CT findings in COPD: lung attenuation vs lung function and dyspnea severity. Chest 2006; 129:558-564.
7. Kalender WA, Rienmuller R, Seissler W, Behr J, Welke M, Fichte H. Measurement of pulmonary parenchymal attenuation: use of spirometric gating with quantitative CT. Radiology 1990; 175:265-268.
8. Boes JL, Bule M, Hoff BA, Chamberlain R, Lynch DA, Stojanovska J, et al. The Impact of Sources of Variability on Parametric Response Mapping of Lung CT Scans. Tomography 2015; 1:69-77.
9. Galban CJ, Han MK, Boes JL, Chughtai KA, Meyer CR, Johnson TD, et al. Computed tomography-based biomarker provides unique signature for diagnosis of COPD phenotypes and disease progression. Nat Med 2012; 18:1711-1715.
10. Kirby M, Yin Y, Tschirren J, Tan WC, Leipsic J, Hague CJ, et al. A Novel Method of Estimating Small Airway Disease Using Inspiratory-to-Expiratory Computed Tomography. Respiration 2017; 94:336-345.
11. Aerts HJ. The Potential of Radiomic-Based Phenotyping in Precision Medicine: A Review. JAMA Oncol 2016; 2:1636-1642.
12. Gillies RJ, Kinahan PE, Hricak H. Radiomics: Images Are More than Pictures, They Are Data. Radiology 2016; 278:563-577.
13. Lambin P, Rios-Velazquez E, Leijenaar R, Carvalho S, van Stiphout RG, Granton P, et al. Radiomics: extracting more information from medical images using advanced feature analysis. Eur J Cancer 2012; 48:441-446.
14. Peeken JC, Bernhofer M, Wiestler B, Goldberg T, Cremers D, Rost B, et al. Radiomics in radiooncology - Challenging the medical physicist. Phys Med 2018; 48:27-36.

15. Giger ML. Machine Learning in Medical Imaging. J Am Coll Radiol 2018; 15:512-520.

16. Mackin D, Ger R, Dodge C, Fave X, Chi PC, Zhang L, et al. Effect of tube current on computed tomography radiomic features. Sci Rep 2018; 8:2354.

17. McDonough JE, Yuan R, Suzuki M, Seyednejad N, Elliott WM, Sanchez PG, et al. Small-airway obstruction and emphysema in chronic obstructive pulmonary disease. N Engl J Med 2011; 365:1567-1575.

Chapter 4 - Emphysematous and nonemphysematous gas trapping in chronic obstructive pulmonary disease

Emphysematous and nonemphysematous gas trapping in Chronic Obstructive Pulmonary Disease: Quantitative CT Findings and Pulmonary Function

Mariaelena Occhipinti, Matteo Paoletti, Francesca Bigazzi, Gianna Camiciottoli, Riccardo Inchingolo, Anna R. Larici, Massimo Pistolesi

Radiology 2018; 287:683–692

4.1 Introduction

The wide heterogeneity of clinical presentation makes chronic obstructive pulmonary disease (COPD) a complex disease, which deserves deeper insights beyond airflow obstruction detected at spirometry. The advent of computed tomography (CT) has brought in the last twenty years substantial progress in the assessment of the pathophysiologic mechanisms underlying airflow obstruction in COPD, namely emphysema and conductive airway disease (1). However, the possibility to accurately resolve by CT the relative contribution of emphysematous and non-emphysematous gas trapping in the determination of expiratory airflow obstruction is still matter of study, to our knowledge (2). Recently, Galban et al. proposed an innovative method called pulmonary parametric response map (pPRM), based on the co-registration of paired inspiratory and expiratory thoracic CT scans. This method can dissect and display the regional distribution of the persistent low density area (emphysematous gas trapping, due to parenchymal destruction), and the functional low density area (non-emphysematous or functional gas trapping due to conductive airway disease) (3).

Although in an individual patient one of the two pathophysiologic conditions (endotypes) may prevail, most COPD patients present (phenotype) with a mixed disorder characterized by various combinations of both components, and a corresponding mixed CT subtype (4, 5). Knowledge of the prevalent subtype in each patient may be of interest in developing clinical and pharmacological trials designed to target patient therapy to the underlying pathophysiologic mechanism of airflow obstruction. Conductive airway obstruction and parenchymal destruction may not be targetable with the same therapy. Therefore, we aimed at identifying a prevalent CT subtype, by dissecting each contribution to total gas trapping. We also evaluated the prediction and grading by clinical and functional data the contribution of emphysema to total gas trapping as assessed using non-contrast thin-section thoracic CT.

4.2 Materials and Methods

This two center study was approved by both institutional Ethics Committees of the University of Florence and the Catholic University of Sacred Heart in Rome. Written informed consent was obtained by all participants. M.O. reports consultancies from Imbio, LLC (Minnesota, MN) and a grant financed partly from MENARINI and partly from the University of Florence, during the conduct of the study. M.Pistolesi reports grants from Ministry of Health of Italy as well as from Ministry of University and Research of Italy, during the conduct of the study. The authors had control of the data and of the information submitted for publication.

Our study was based on a retrospective interpretation of prospectively acquired data. From January 2012 to December 2015, we recruited 224 consecutive eligible COPD patients (GOLD stages I-IV) meeting specific criteria, including being aged 40–85, with a smoking history of more than 10 pack-years, who showed non-reversible post-bronchodilator airflow obstruction, and who underwent chest CT within 48 hours of pulmonary function evaluation. We excluded patients within one month of an exacerbation or who had clinical conditions interfering with pulmonary function or chest CT quantitative parameters assessment, including asthma, diffuse bronchiectasis, interstitial lung disease, acute heart failure, chemotherapy and/or radiation therapy, lung cancer, lung surgery, and metal objects in the chest.

4.2.1 Pulmonary Function Testing

All patients underwent complete pulmonary function evaluation within 48 hours of the CT examination. Pre-and post-bronchodilator spirometry data, static lung volumes, and single-breath diffusing capacity for carbon monoxide (DLco) were measured according to American Thoracic Society/European Respiratory Society (ATS/ERS) guidelines (6).

4.2.2 Chest CT Scan

Volumetric chest CT scans were obtained at full inspiration and expiration using the acquisition protocol adopted in the COPDGene study (7). CT parameters were set as follows: 120 kVp, 200 mAs, rotation time 0.5s, pitch 1.1, slice thickness 0.75mm, and reconstructions kernels b31f and b70f. All CT scans were performed by the same team of diagnostic personnel in each center (lead by F.B. in Florence and A.R.L. in Rome, with 10 and 20 years of expertise in thoracic imaging, respectively) and by using the same CT scanner for all patients in each center (in Florence: SOMATOM Sensation 64, Siemens, Erlangen, Germany; in Rome: SOMATOM Definition FLASH 128, Siemens, Erlangen, Germany). Patients received prior careful instructions on how to perform the respiratory maneuvers while lying supine in the CT scanner with arms fully abducted. No contrast medium was administered. Post-processing image analysis was performed in images with reconstruction kernel b31f by a thoracic radiologist with 5 years expertise on quantitative imaging (M.O.). Thresholds at -950 Hounsfield Units (HU) and -856 HU were chosen as densitometric cut-off consistent with emphysema and total gas trapping, respectively (8-10). The relative volumes of lung attenuation area with values below -950 HU at inspiration (%$LAA_{-950insp}$) and below -856 HU at expiration (%$LAA_{-856exp}$) were

quantified by using the Pulmonary Workstation Apollo 2.1 (VIDA Diagnostics, Coralville, Iowa, USA). CT scans were also analyzed by LDA (Imbio LLC, Minneapolis, MN, USA), a U.S. FDA-cleared and CE (Conformité Européenne) mark certified medical device, which performs a deformable co-registration of paired inspiratory and expiratory CT scans, to obtain voxel-by-voxel attenuation maps. These maps, called pPRM, classify lung voxels into three different tissue patterns based on the attenuation values of each voxel: normal lung (% voxels with CT attenuation above -950HU at inspiration and above -856HU at expiration), functional low density area (%fLDA, voxels with CT attenuation above -950HU at inspiration and below -856HU at expiration), and persistent low density area (%pLDA, voxels with CT attenuation below -950HU at inspiration and below -856HU at expiration) (3). Moreover, pPRM quantify the relative volumes of each lung pattern and show their regional distribution.

4.2.3 Data analysis

Scatterplots were used to show the distribution and the relationships among CT parameters. Pearson r coefficient was used to assess association between parameters, with $p < 0.05$ indicating statistical significance.

To quantify the contribute of functional gas trapping to the CT reduced x-ray attenuation using CT density thresholds without co-registration, we used the following computation:

$$\%fGT = [\%LAA_{-856exp} - (\%LAA_{-950insp} - 6\%)]$$

where 6% of voxels below -950HU is assumed as the threshold value to diagnose emphysema by quantitative CT (1). To validate this computation we compared %fGT with %fLDA.

To help separating the contribution of functional gas trapping from emphysema, the scatterplot of %fGT and $\%LAA_{-950insp}$ of the whole series of patients was subdivided into four areas by drawing a line from the mean value of %fGT on the x-axis (36.2%) and its perpendicular from the mean value of $\%LAA_{-950insp}$ on the y-axis (14.9%). Welch's t, ANOVA, and Games-Howell post-hoc test were used to evaluate differences of clinical and functional data between the four groups of patients entailed in each area (11).

The probability to have a $\%LAA_{-950insp}$ above or below the sample mean was estimated by a ten-fold validated logistic regression model built from stepwise selection of anthropometric, clinical, and functional data (see online Supplemental Material for detail) (12). A predicted probability (P) value of 0.5 was arbitrarily selected as decision threshold. For the sake of clinical classification, patients with a P value lower than 0.5 were subdivided in two subgroups according to a P value lower or higher than 0.2. Likewise, patients with a P value higher than 0.5 were subdivided in those with a P value higher or lower than 0.8.

Data analysis and statistics were performed using S-Plus 2000 (Mathsoft, Cambridge, MA), SPSS/PC WIN 11.5.1 (SPSS, Chicago, IL), Mathcad (version 2001; Mathsoft), and C++ programming language.

4.3 Results

Two hundred and two (159 men, mean age 71, age range: 41-85; 43 women, mean age: 67, age range: 46-84) out of the 224 patients enrolled were included in the analysis. Twenty-two patients were excluded for the presence of parenchymal consolidations (16/22) or incomplete clinical (4/22) or CT scan (2/22) data. Anthropometric, smoking history, lung function, and CT metrics data of the 202 patients are shown in Table 1.

Table 2 shows the correlations between clinical, pulmonary function, and CT data. The strongest correlations were observed between %pLDA and $\%LAA_{-950insp}$, %fLDA and %fGT, $\%LAA_{-856exp}$ and FEV_1/VC, and $\%LAA_{-856exp}$ and FEV_1/FVC. Conversely, poor correlations were observed between CT metrics of functional gas trapping (i.e. %fLDA and %fGT) and functional and CT parameters compatible with emphysema (i.e. DLco%, RV/TLC, and $\%LAA_{-950insp}$). CT metrics obtained by difference of density thresholds and those obtained by co-registration analysis correlated similarly with pulmonary function parameters.

Figure 1 shows the scatterplot of the 202 patients using as coordinates $\%LAA_{-950insp}$ and $\%LAA_{-856exp}$. The dispersion of data points increased progressively, with the increase in total gas trapping ($\%LAA_{-856exp}$), indicating that there was a wide grade of interaction of emphysematous and non-emphysematous contribution to total gas trapping. In particular, patients with similar values of $\%LAA_{-950insp}$ had very different values in $\%LAA_{-856exp}$. The non-emphysematous contribution to total gas trapping is a function of the difference of the two variables at each level $\%LAA_{-950insp}$, as computed by %fGT. Figure 2 shows the strong correlation between %fGT and %fLDA, whose regression line essentially corresponds to the identity line.

Figure 3 shows the relationship between %fGT, expression of functional gas trapping, and $\%LAA_{-950insp}$, expression of emphysematous gas trapping. As can be derived from the graphical subgrouping of patients shown in Figure 3, group Emph consisted of 29/202 (14.4%) patients with prevalent emphysema ($\%LAA_{-950insp}$ higher than the mean value and %fGT lower than the mean value), whereas group Funct consisted of 46/202 (22.8%) patients with prevalent functional (non-emphysematous) gas trapping ($\%LAA_{-950insp}$ lower than the mean value and %fGT higher than the mean value). Groups Mixs 57/202 (28.2%) and Mixm 70/202 (34.6%) consisted of patients with a greater degree of severity of both components in group Mixs and a lower degree of severity of both components in group Mixm.

Table 3 shows the mean values of anthropometric, smoking history, and pulmonary function data across the four groups (Emph, Mixs, Mixm, Funct in Figure 3). BMI was significantly higher in group Mixm ($p<0.01$), with a tendency to decrease as severity of disease increased. DLco% was the only parameter to differ significantly between group Emph and Funct ($p<0.05$).

The logistic regression model was trained to classify COPD patients according to the probability to have a $\%LAA_{-950insp}$ higher than the mean value of the sample. FEV_1/VC, $FEV_1\%$, DLco%, and BMI were included as predictors of $\%LAA_{-950insp}$, and four groups were defined according to the probability output. The overall

accuracy of the probabilistic model was 81.1% in the training set and 79.2% in the validation set, with a higher accuracy (88.0%) in those patients with "milder" disease (probability of the output model <0.5) (Table 4). By combining functional indexes and BMI predictors, we classified each subject according to probability output values ranging from milder (group 1) to more severe (group 4) emphysema. The four outputs of the model had significantly different $\%LAA_{-950insp}$ (or %pLDA) ($p<0.01$), as shown in panel A of Figure 4. Panel B of Figure 4 shows the relationship between %fLDA and total gas trapping ($\%LAA_{-856exp}$). The different colors (from blue to yellow) correspond to the four groups of emphysema grade estimated by the model based on anthropometric and functional data. The regression line is fitted for data points with a model output less than 0.5 ($r=0.89$). Patients with milder emphysema (blue or dark-grey circles) are distributed mainly along the regression line. Conversely, patients with a more severe parenchymal destruction (light-grey or yellow circles) are scattered above the regression line. The data points distribution reveals that in this series of COPD patients, the emphysematous contribution to total gas trapping is absent for values of total gas trapping around or below 30%.

4.4 Discussion

Our study provides evidence that imaging metrics obtained by density thresholds difference of inspiratory and expiratory CT scans can be used to identify and quantify the relative contribution of functional (non-emphysematous) and emphysematous gas trapping and to identify a prevalent CT subtype. The evaluation of functional gas trapping obtained by density thresholds difference and co-registration analysis was comparable. The contribution of emphysema to total gas trapping, as assessed by CT, was estimated with reasonable accuracy by anthropometric and pulmonary function data.

Airflow obstruction in COPD results from parenchymal destruction as well as from small conducting airway disease, with small airway disease preceding the development of parenchymal destruction (13-15). Both pathophysiologic processes lead to gas trapping into the lungs. The differentiation of emphysematous gas trapping (due to parenchymal destruction) from functional gas trapping (due to conductive airway disease) is difficult both by pulmonary function testing and CT scan (16, 17). Recently, the pPRMs obtained through co-registration analysis of inspiratory and expiratory CT scan overcame this issue, allowing discrimination of the two contributions to total gas trapping (2, 3, 18).

We observed that the relationship between standard CT metrics ($\%LAA_{-950insp}$ and $\%LAA_{-856exp}$) was greatly dispersed, suggesting that total gas trapping ($\%LAA_{-856exp}$) included both emphysematous and non-emphysematous contributions. To determine these contributions we computed an index, called %fGT, derived from the difference between standard CT metrics ($\%LAA_{-950insp}$ and $\%LAA_{-856exp}$) obtained from inspiratory and expiratory scans. The index had a strong correlation ($r=0.99$) with %fLDA, which is the reference parameter for the non-emphysematous gas trapping derived by co-registration (2, 3, 18-20). Likewise %fLDA, %fGT provides information on the amount of functional non-emphysematous gas trapping. In contrast to %fLDA, %fGT lacks localization of gas trapping. Gas trapping regional distribution can be provided only by

pPRM, and may play a role in the assessment of symptoms severity, as well as in the selection of patients for surgical and endoscopic lung volume reduction. However, %fGT can be easily obtained by using widely available software programs on lung density analysis. This measurement can be supplemented by the qualitative evaluation of the regional distribution of the lung pathologic changes.

The weak correlation between CT metrics of parenchymal destruction (%$LAA_{-950insp}$ and %pLDA) and %fGT depicted the independent contribution of functional gas trapping and parenchymal destruction to airflow obstruction. This was in keeping with previous studies demonstrating weak correlations between indexes of emphysema severity and airway wall thickening (5, 21).

The classification in four subgroups of patients (Emph, Mixs, Mixm, Funct) to assess the relative contribution of functional gas trapping and parenchymal destruction in the definition of COPD subtypes was very similar to that proposed in other studies (14, 21, 22). Our patients displayed a continuous spectrum of pathologic alterations of both conductive airway disease and emphysema. However, knowledge of the percentage of lung destruction may be of help in assessing patient prognosis and, possibly, in selecting the individual treatment (e.g. whether to add inhaled steroids to bronchodilators). Across the four subgroups of COPD patients we observed no statistically significant differences in smoking history. Statistically significant higher DLco% values were found in patients with prevalent functional (Funct) than in those with prevalent emphysema (Emph). Patients with milder disease (Mixm) had significantly higher BMI values than other subgroups. In agreement with previous studies, we found an inverse relationship between BMI and CT indexes of emphysema, including %$LAA_{-950insp}$ and %pLDA (22, 23). Accordingly, it is reasonable that BMI was included among the regressors of the probabilistic model to predict the contribution of emphysema to total gas trapping. It has very recently been shown that BMI as well as height itself (the denominator in the BMI formula) can be used to predict emphysema risk, with odds of emphysema increasing by 5% along with one cm increase in body height (24).

Probabilistic models may help to characterize, without CT, the main pathophysiologic mechanism underlying airflow obstruction and may facilitate individualized treatment strategies. This may be of relevance considering the high prevalence of COPD in the general population and the unavailability of CT scan in most patients, even more if we consider that both inspiratory and expiratory scans are needed. We found that BMI combined in a predictive model with DLco%, FEV_1, and FEV_1/VC can be used to classify COPD patients according to CT parenchymal destruction (%$LAA_{-950insp}$) with an acceptable level of accuracy. Previous studies have shown that parenchymal destruction on CT is related to both DLco% and FEV_1, and that FEV_1/VC is better related to CT indexes (%$LAA_{-950insp}$) of airway obstruction with respect to FEV_1/FVC (25, 26). According to previous results, spirometric indexes of airflow obstruction had a moderate inverse correlation with emphysema indexes on CT (27). These findings can be explained by the absence of a linear correlation between pulmonary function data and CT attenuation values, as demonstrated in a previous analysis (26).

The probabilistic index described here may help to differentiate, with acceptable approximation, the contribution of emphysema to total gas trapping in COPD. In patients with a predicted probability lower than 0.5 as output of the model, functional gas trapping approximately corresponded to total gas trapping. In patients with a predicted probability greater than 0.5 as output of the model, parenchymal destruction added to functional gas trapping increasing the overall value of total gas trapping ($\%LAA_{-856exp}$). This is in keeping with the results obtained by McDonough and colleagues, who by measuring mean linear intercept on microCT showed that the narrowing and loss of terminal bronchioles preceded emphysematous destruction in COPD (15). In our patients, when total gas trapping was around or below 30% it had no significant emphysematous contribution, being derived almost completely from the non-emphysematous component.

The main limitation of our study was the relatively small number of patients included in the cohort to be considered representative of the whole spectrum of COPD lung structural changes. Although our cohort was smaller than those of other studies (i.e. COPDGene, SPIROMICS), both the distribution and the mean of $\%LAA_{-950insp}$ and $\%LAA_{-856exp}$ obtained in our patients are comparable to those obtained in the COPDGene study, making the described model possibly suitable for application to other populations (28, 29). Another limitation of this study was the use of the fixed ratio FEV_1/FVC according to GOLD guidelines to enroll patients, instead of using age-dependent reference equations such as the lower limit of normality (30, 31). The adoption of the fixed ratio may have over-diagnosed elderly patients, that represent the vast majority of our population. As far as CT was concerned, we lacked spirometric control of the level of lung inflation during the acquisition, and this may be an issue for reproducibility and data interpretation. However, all patients received careful instructions on how to perform the respiratory maneuvers while lying supine in the CT scanner. The presence of bronchiectasis and mucous impaction could have been another possible pitfall in the evaluation of lung density. However, none of our patients were studied during an exacerbation. Finally, the validation of the Logit model has been done on a training set (our cohort) and cross-validated by 10-fold leave-out test. It would be advisable to recruit a larger population in the near future, and to validate prospectively the model in a population different from that of the model derivation. A further limitation is the inclusion of only white Caucasian patients, which may limit the application of the observed associations to other ethnicities.

In conclusion, our study demonstrated that standard imaging metrics obtained by inspiratory and expiratory thoracic CT scans can be used to identify and quantify the relative contribution of emphysematous and non-emphysematous gas trapping, permitting a better definition of COPD subtypes. Co-registration analysis adds information on regional distribution of disease type, extent, and severity, which cannot be provided by standard densitometric analyses. Furthermore, the use of a probabilistic model including anthropometric and functional data can grade the relative contribution of parenchymal destruction to total gas trapping as assessed using CT. The application of this model may help in the definition of different COPD subtypes and may be used to design newer outcomes in developing clinical and pharmacologic trials.

4.5 Tables

Table 1. Anthropometric, pulmonary function, and CT metrics data of 202 patients with COPD. Data are reported as mean ± SD. (*: quantitative CT data calculated by Apollo 2.1 VIDA Software; †: quantitative CT data calculated by LDA Imbio Software; %fGT is calculated as described in the *Materials and Methods* section)

Age (years)	70.3 ± 8.1
BMI (kg/m^2)	26.3 ± 4.6
Smoking history (Pack-years)	50.8 ± 25.5
FEV_1%	62.7 ± 26.3
FEV_1/VC (%)	47.1 ± 12.9
FEV_1/FVC (%)	51.4 ± 12.4
FVC%	92.8 ± 25.0
FRC%	128.6 ± 33.8
TLC%	107.7 ± 17.6
DLco%	68.5 ±23.6
RV%	136.8 ± 48.3
RV/TLC (%)	50.2 ± 17.1
$\%LAA_{-950insp}$*	14.9 ± 12.4
$\%LAA_{-856exp}$*	45.1 ± 20.5
%Normal lung †	49.9 ± 21.1
%fLDA†	36.1 ± 14.0
%pLDA†	12.4 ± 12.7
%fGT	36.2 ± 13.6

Legend: BMI = body mass index, DLco% = percentage of predicted diffusing capacity of lung for carbon monoxide, FEV1% = percentage predicted forced expiratory volume in 1 second, %fGT = percentage of functional gas trapping, %fLDA = percentage of functional low density area, FRC% = percentage of predicted functional residual capacity, FVC% = percentage of predicted forced vital capacity, $\%LAA_{-950insp}$ = percentage of lung attenuation area with values below -950HU at inspiratory CT scan, $\%LAA_{-856exp}$ = percentage of lung attenuation area with values below -856HU at expiratory

CT scan, %pLDA = percentage of persistent low density area, RV% = percentage of predicted residual volume, TLC% = percentage of predicted total lung capacity, VC = vital capacity

Table 2. Pearson's correlation coefficients between %fGT and anthropometric, smoking history, pulmonary function, and CT imaging data. (*: p<0.01; †: p<0.05).

	$\%LAA_{-950insp}$	%pLDA	$\%LAA_{-856exp}$	%fLDA	%fGT
Age	0.05	0.04	0.06	0.07	0.04
BMI	-0.36*	-0.37*	-0.38*	-0.22*	-0.24*
Pack-years	0.09	0.10	0.05	-0.02	-0.004
FVC%	-0.17†	-0.20*	-0.26*	-0.21*	-0.23*
$FEV_1\%$	-0.48*	-0.50*	-0.58*	-0.43*	-0.44*
FEV_1/VC	-0.63*	-0.64*	-0.73*	-0.52*	-0.52*
FEV_1/FVC	-0.66*	-0.68*	-0.72*	-0.48*	-0.48*
TLC%	0.34*	0.33*	0.42*	0.33*	0.33*
RV%	0.41*	0.43*	0.54*	0.42*	0.43*
RV/TLC	0.35*	0.37*	0.42*	0.31*	0.31*
FRC%	0.49*	0.50*	0.57*	0.40*	0.41*
DLco%	-0.43*	-0.45*	-0.43*	-0.24*	-0.25*
$\%LAA_{-950insp}$	1	0.99*	0.76*	0.26*	0.24*
$\%LAA_{-856exp}$	0.76*	0.76*	1	0.81*	0.81*
%fLDA	0.26*	0.25*	0.81*	1	0.99*
%pLDA	0.99*	1	0.76*	0.25*	0.25*
%fGT	0.24*	0.25*	0.81*	0.99*	1

Legend: BMI = body mass index, DLco% = percentage of predicted diffusing capacity of lung for carbon monoxide, FEV1% = percentage predicted forced expiratory volume in 1 second, %fGT = percentage of functional gas trapping, %fLDA = percentage of functional low density area, FRC% = percentage of predicted functional residual capacity, FVC% = percentage of predicted forced vital capacity, $\%LAA_{-950insp}$ = percentage of lung attenuation area with values below -950HU at inspiratory CT scan, $\%LAA_{-856exp}$ = percentage of lung attenuation area with values below -856HU at expiratory CT scan, %pLDA = percentage of persistent low density area, RV% = percentage of predicted residual volume, TLC% = percentage of predicted total lung capacity, VC = vital capacity.

Table 3. Mean values of anthropometric, smoking history, and pulmonary function data among the four groups (Emph – prevalent emphysema; Mixs – mixed severe; Mixm – mixed mild; Funct– prevalent functional gas trapping) shown in Figure 3, derived by the different contributions of %fGT and $\%LAA_{-950insp}$ parameters. Differences between groups were analyzed by ANOVA and Games-Howell post-hoc tests. (*: $p<0.01$; †: $p<0.05$; NS: not significant).

	Emph	Mixs	Mixm	Funct	Differences
Age (years)	70.2	71.2	68.9	71.1	NS
BMI (kg/m^2)	25.1	24.4	28.6	25.9	Emph-Mixm * Mixs-Mixm * Funct-Mixm *
Pack-years	56.3	52	48.6	49.1	NS
DLco%	55.2	59	81.4	67.3	Emph-Mixm * Mixs-Mixm * Funct-Mixm * Emph-Funct †
FVC%	97.9	87.5	98.6	87.3	Mixs-Mixm † Mixm-Funct †
FEV_1%	61.1	46.7	79.5	58.1	Emph-Mixs † Emph-Mixm * Mixs-Mixm * Funct-Mixm * Mixs-Funct †
FEV_1/VC (%)	44.2	36.8	57.9	45.3	Emph-Mixs † Emph-Mixm † Mixs-Mixm * Mixs-Funct * Mixm-Funct *
FEV_1/FVC (%)	48.4	40.8	61.3	51.1	Emph-Mixs †

					Emph-Mixm † Mixs-Mixm * Mixs-Funct * Mixm-Funct *
TLC%	110.9	115.5	99.5	108.5	Emph-Mixm † Mixs-Mixm * Mixm-Funct †
RV%	135.6	163	109.3	140.6	Mixs-Mixm * Mixs-Funct † Mixm-Funct *
RV/TLC (%)	49.3	59.4	42.3	51.2	Mixm-Funct * Mixs-Mixm *
FRC%	131.9	150.3	109.2	129.2	Emph-Mixm * Mixs-Mixm * Mixm-Funct * Mixs-Funct *

Legend: BMI = body mass index, DLco% = percentage of predicted diffusing capacity of lung for carbon monoxide, FEV1% = percentage predicted forced expiratory volume in 1 second, FRC% = percentage of predicted functional residual capacity, FVC% = percentage of predicted forced vital capacity, RV% = percentage of predicted residual volume, TLC% = percentage of predicted total lung capacity, VC = vital capacity

Table 4. Predictors, odds ratios, and accuracy of the logistic regression model trained to classify COPD patients according to their parenchymal destruction (%$LAA_{-950insp}$) contribution to total gas trapping. The best regressors were selected after a step-wise procedure. The model classification cut-off was the predicted probability value P=0.5. Patients in class 1 included those with P<0.5 (groups 1 and 2 in Figure 4) and patients in class 2 included those with P>0.5 (groups 3 and 4 in Figure 4). In parentheses are the results obtained after ten fold cross-validation.

Predictors	Odds Ratio		p
DLco%	0.98		0.03
FEV_1/VC	0.87		<0.01
BMI	3.41		<0.01
FEV_1%	1.03		0.02
	Model estimation (cut-off P = 0.5)		
	Class 1	Class 2	% Accuracy
Observed: Class 1	103	14	88.0% (88.0%)
Class 2	24	61	71.8% (67.0%)
Overall Accuracy			81.1% (79.2%)

Legend: BMI = body mass index, DLco% = percentage of predicted diffusing capacity of lung for carbon monoxide, FEV1% = percentage predicted forced expiratory volume in 1 second, P= predicted probability; VC = vital capacity

4.6 Figures

Figure 1. Distribution of 202 patients with COPD according to CT imaging metrics of $\%LAA_{-950insp}$ and $\%LAA_{-856exp}$. The two variables showed a substantial dispersion of data points which increased progressively with increasing severity of CT metrics changes. Patients with similar values of $\%LAA_{-950insp}$ had very different values in $\%LAA_{-856exp}$.

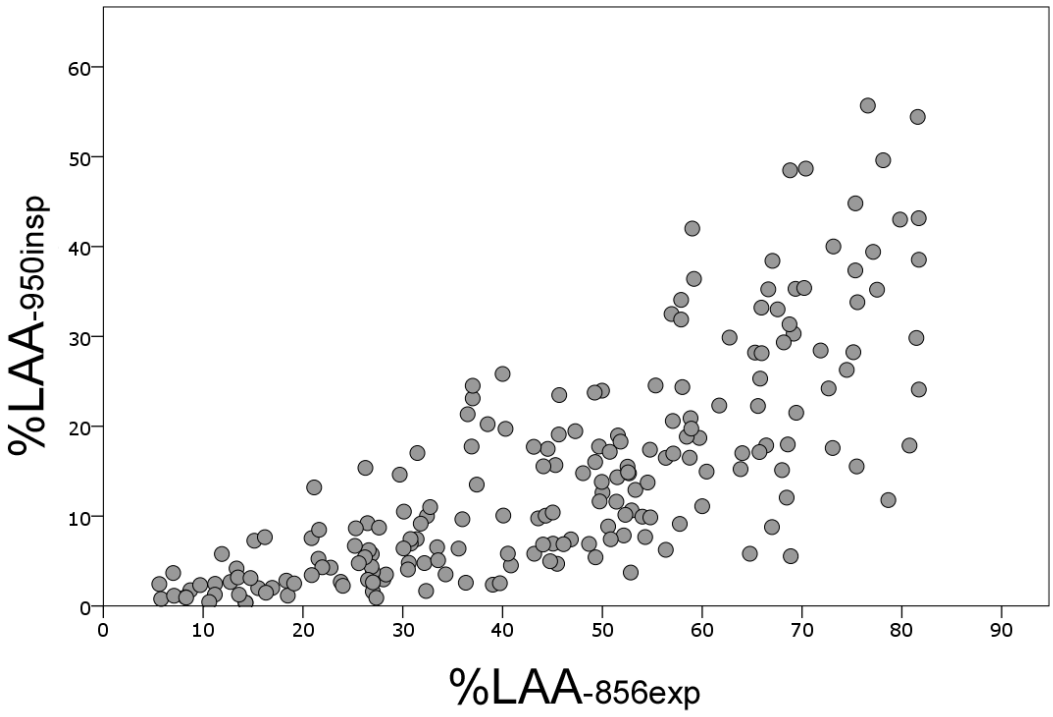

Legend: $\%LAA_{-950insp}$ = percentage of lung attenuation area with values below -950HU at inspiratory CT scan, $\%LAA_{-856exp}$ = percentage of lung attenuation area with values below -856HU at expiratory CT scan.

Figure 2. Relationship between %fLDA and %fGT. The correlation between the two variables was strong, with a very high Pearson r coefficient (r= 0.99), and a regression line essentially corresponding to the identity line.

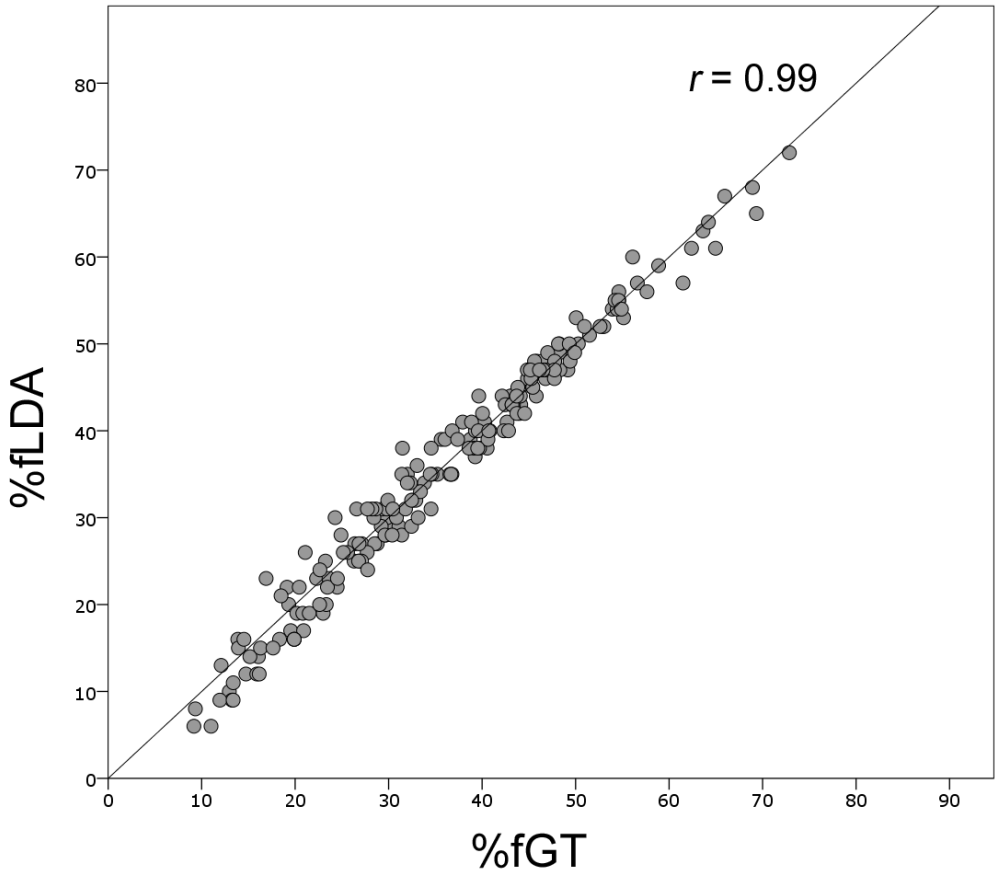

Legend: %fGT = percentage of functional gas trapping, %fLDA = percentage of functional low density area.

Figure 3. Distribution of patients according to %fGT and %LAA$_{-950insp}$. The correlation between the two variables was very weak (r=0.24, p<0.01). Lines representing mean values of %LAA$_{-950insp}$ and %fGT divide the scatterplot into four groups: group Emph (prevalent emphysema, %fGT lower than the mean value and %LAA$_{-950insp}$ higher than the mean value), group Mixs (mixed-severe disease, both %fGT and %LAA$_{-950insp}$ higher than the mean values), group Mixm (mixed-mild disease, both %fGT and %LAA$_{-950insp}$ lower than the mean values), and group Funct (prevalent functional gas trapping, %fGT higher than the mean value and %LAA$_{-950insp}$ lower than the mean value).

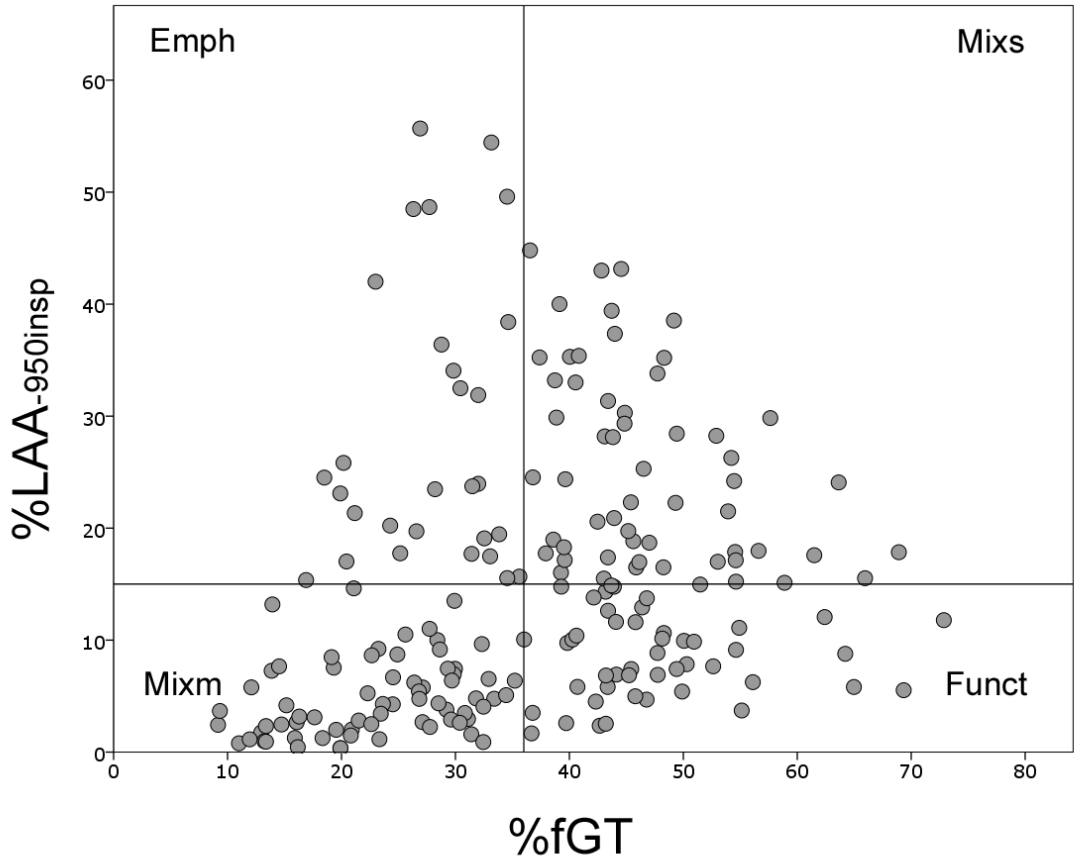

Legend: %fGT = percentage of functional gas trapping, %LAA$_{-950insp}$ = percentage of lung attenuation area with values below -950HU at inspiratory CT scan.

Figure 4. A) Modified box-and-whiskers plot of mean values with corresponding 95% CI. The plot shws the distribution of $\%LAA_{-950insp}$ across the four probability output groups of the logistic regression model. Group 1 (n=63, blue dot) represents a predicted probability output between 0 and 0.2, group 2 (n=61, dark grey dot) between 0.2 and 0.5, group 3 (n=44, light grey dot) between 0.5 and 0.8, and group 4 (n=34, yellow dot) between 0.8 and 1. These groups have significantly different $\%LAA_{-950insp}$ ($p<0.01$). **B)** Relationship between $\%LAA_{-856exp}$ and %fLDA across the four output groups of the logistic regression model. Patients with milder emphysema (blue circles) are distributed along the regression line (r=0.89), whereas patients with more severe parenchymal destruction (light grey and yellow circles) are scattered from this fitted line.

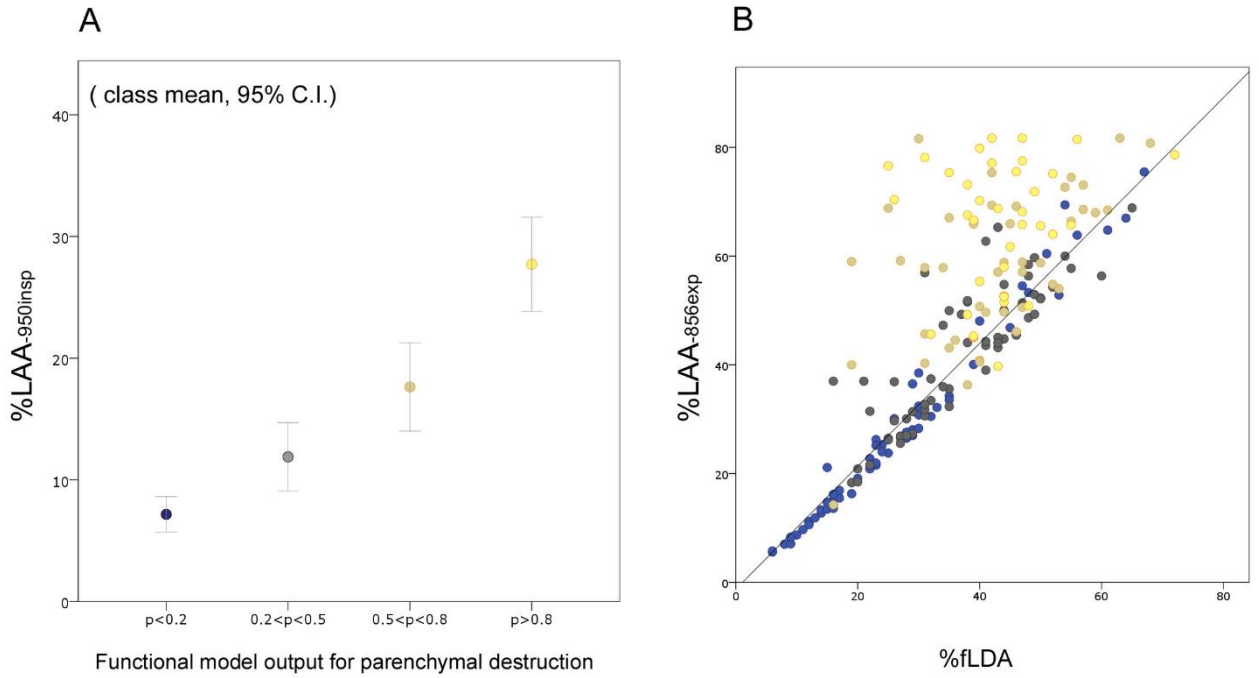

Legend: %fLDA = percentage of functional low density area, $\%LAA_{-950insp}$ = percentage of lung attenuation area with values below -950HU at inspiratory CT scan, $\%LAA_{-856exp}$ = percentage of lung attenuation area with values below -856HU at expiratory CT scan.

4.7 References

1. Lynch DA, Austin JH, Hogg JC, Grenier PA, Kauczor HU, Bankier AA, et al. CT-Definable Subtypes of Chronic Obstructive Pulmonary Disease: A Statement of the Fleischner Society. Radiology 2015; 277:192-205.

2. Bhatt SP, Soler X, Wang X, Murray S, Anzueto AR, Beaty TH, et al. Association between Functional Small Airway Disease and FEV1 Decline in Chronic Obstructive Pulmonary Disease. Am J Respir Crit Care Med 2016; 194:178-184.

3. Galban CJ, Han MK, Boes JL, Chughtai KA, Meyer CR, Johnson TD, et al. Computed tomography-based biomarker provides unique signature for diagnosis of COPD phenotypes and disease progression. Nat Med 2012; 18:1711-1715.

4. Hogg JC. Pathophysiology of airflow limitation in chronic obstructive pulmonary disease. Lancet 2004; 364:709-721.

5. Camiciottoli G, Bigazzi F, Paoletti M, Cestelli L, Lavorini F, Pistolesi M. Pulmonary function and sputum characteristics predict computed tomography phenotype and severity of COPD. Eur Respir J 2013; 42:626-635.

6. Miller MR, Hankinson J, Brusasco V, Burgos F, Casaburi R, Coates A, et al. Standardisation of spirometry. Eur Respir J 2005; 26:319-338.

7. Regan EA, Hokanson JE, Murphy JR, Make B, Lynch DA, Beaty TH, et al. Genetic epidemiology of COPD (COPDGene) study design. COPD 2010; 7:32-43.

8. Madani A, De Maertelaer V, Zanen J, Gevenois PA. Pulmonary emphysema: radiation dose and section thickness at multidetector CT quantification--comparison with macroscopic and microscopic morphometry. Radiology 2007; 243:250-257.

9. Schroeder JD, McKenzie AS, Zach JA, Wilson CG, Curran-Everett D, Stinson DS, et al. Relationships between airflow obstruction and quantitative CT measurements of emphysema, air trapping, and airways in subjects with and without chronic obstructive pulmonary disease. AJR Am J Roentgenol 2013; 201:W460-470.

10. Jain N, Covar RA, Gleason MC, Newell JD, Jr., Gelfand EW, Spahn JD. Quantitative computed tomography detects peripheral airway disease in asthmatic children. Pediatr Pulmonol 2005; 40:211-218.

11. Olejnik S, Li J, Supattathum S, Huberty CJ. Multiple testing and statistical power with modified Bonferroni procedures. J Educ Behav Stat 1997; 22:389-406.

12. Hilbe JM. Logistic Resgression Models. Science CaHCTiS, editor: CRC Press; 2009.

13. Gelb AF, Schein M, Kuei J, Tashkin DP, Muller NL, Hogg JC, et al. Limited contribution of emphysema in advanced chronic obstructive pulmonary disease. Am Rev Respir Dis 1993; 147:1157-1161.

14. Nakano Y, Muller NL, King GG, Niimi A, Kalloger SE, Mishima M, et al. Quantitative assessment of airway remodeling using high-resolution CT. Chest 2002; 122:271S-275S.

15. McDonough JE, Yuan R, Suzuki M, Seyednejad N, Elliott WM, Sanchez PG, et al. Small-airway obstruction and emphysema in chronic obstructive pulmonary disease. N Engl J Med 2011; 365:1567-1575.

16. Camiciottoli G, Bartolucci M, Maluccio NM, Moroni C, Mascalchi M, Giuntini C, et al. Spirometrically gated high-resolution CT findings in COPD: lung attenuation vs lung function and dyspnea severity. Chest 2006; 129:558-564.

17. Han MK. Clinical correlations of computed tomography imaging in chronic obstructive pulmonary disease. Ann Am Thorac Soc 2013; 10 Suppl:S131-137.

18. Martinez CH, Diaz AA, Meldrum C, Curtis JL, Cooper CB, Pirozzi C, et al. Age and Small Airway Imaging Abnormalities in Subjects With and Without Airflow Obstruction in SPIROMICS. Am J Respir Crit Care Med 2017; 195:464-472.

19. Capaldi DP, Zha N, Guo F, Pike D, McCormack DG, Kirby M, et al. Pulmonary Imaging Biomarkers of Gas Trapping and Emphysema in COPD: (3)He MR Imaging and CT Parametric Response Maps. Radiology 2016; 279:597-608.

20. Pompe E, van Rikxoort EM, Schmidt M, Ruhaak J, Estrella LG, Vliegenthart R, et al. Parametric response mapping adds value to current computed tomography biomarkers in diagnosing chronic obstructive pulmonary disease. Am J Respir Crit Care Med 2015; 191:1084-1086.

21. Subramanian DR, Gupta S, Burggraf D, Vom Silberberg SJ, Heimbeck I, Heiss-Neumann MS, et al. Emphysema- and airway-dominant COPD phenotypes defined by standardised quantitative computed tomography. Eur Respir J 2016; 48:92-103.

22. Ogawa E, Nakano Y, Ohara T, Muro S, Hirai T, Sato S, et al. Body mass index in male patients with COPD: correlation with low attenuation areas on CT. Thorax 2009; 64:20-25.

23. Lee YK, Oh YM, Lee JH, Kim EK, Lee JH, Kim N, et al. Quantitative assessment of emphysema, air trapping, and airway thickening on computed tomography. Lung 2008; 186:157-165.

24. Miniati M, Bottai M, Pavlickova I, Monti S. Body height as risk factor for emphysema in COPD. Sci Rep 2016; 6:36896.

25. Desai SR, Hansell DM, Walker A, MacDonald SL, Chabat F, Wells AU. Quantification of emphysema: a composite physiologic index derived from CT estimation of disease extent. Eur Radiol 2007; 17:911-918.

26. Paoletti M, Cestelli L, Bigazzi F, Camiciottoli G, Pistolesi M. Chronic Obstructive Pulmonary Disease: Pulmonary Function and CT Lung Attenuation Do Not Show Linear Correlation. Radiology 2015; 276:571-578.

27. Nakano Y, Muro S, Sakai H, Hirai T, Chin K, Tsukino M, et al. Computed tomographic measurements of airway dimensions and emphysema in smokers. Correlation with lung function. Am J Respir Crit Care Med 2000; 162:1102-1108.

28. Lynch DA, Al-Qaisi MA. Quantitative computed tomography in chronic obstructive pulmonary disease. J Thorac Imaging 2013; 28:284-290.

29. Nambu A, Zach J, Schroeder J, Jin G, Kim SS, Kim YI, et al. Quantitative computed tomography measurements to evaluate airway disease in chronic obstructive pulmonary disease: Relationship to physiological measurements, clinical index and visual assessment of airway disease. Eur J Radiol 2016; 85:2144-2151.

30. Brusasco V. Spirometric definition of COPD: exercise in futility or factual debate? Thorax 2012; 67:569-570.

31. Luoto JA, Elmstahl S, Wollmer P, Pihlsgard M. Incidence of airflow limitation in subjects 65-100 years of age. Eur Respir J 2016; 47:461-472.

4.8 Supplemental Material

4.8.1 Methods

Patients were recruited at the Respiratory Unit of the University of Florence (181 patients) and at the Respiratory Unit of the Catholic University of Sacred Heart in Rome (43 patients). Clinical and pulmonary function data were acquired by pulmonologists (mean years of experience: 22.5 [10 to 40]), whereas radiologists (mean years of experience: 12.5 [5 to 20]) performed CT scans and post-processing image analysis.

4.8.1.1 Pulmonary Function Testing

All patients underwent pulmonary function evaluation using a mass-flow sensor and multi-gas analyzer (in Florence: V6200 Autobox Body Plethysmograph; Sensor Medics, Yorba Linda, USA; in Rome: Platinum Elite™ Body Plethysmograph, Medical Graphics Corporation, St. Paul, MN, USA). Blood gas analysis at rest was also performed by using a blood gas analyzer (in Florence: Radiometer ABL90 FLEX, Brønshøj, Denmark; in Rome: Radiometer ABL800 FLEX, Brønshøj, Denmark).

4.8.1.2 Co-registration analysis

To quantify the contribution of non-emphysematous gas trapping to total gas trapping, we introduced an index (called %fGT in the main part of the paper) calculated from standard CT metrics ($\%LAA_{-856exp}$ and $\%LAA_{-950insp}$). The index %fGT was validated by comparison with %fLDA obtained by co-registration.

4.8.1.3 Functional-based classification

Considering the high prevalence of COPD in general practice [1E] and the unavailability of CT scans in the vast majority of patients, we also evaluated the possibility to estimate the severity of parenchymal destruction, as quantified by $\%LAA_{-950insp}$, using functional data routinely measured in clinical practice. In particular, we trained a logistic regression probabilistic model to classify patients according to the CT level of parenchymal destruction using anthropometric, clinical, and functional data as independent variables. The most statistically significant regressors of the model were identified by a step-wise procedure. Ten-fold validation was then performed to ascertain the total and partial predictive accuracy [2E]. One-way ANOVA (F-test) was used to verify the model performances in grading COPD patients according to the predicted probability (P) obtained as outputs. After the logistic regression model (Table 4 in main paper) was validated, we classified each subject according to the probability output value obtained by combining functional indexes and BMI predictors. Differences between groups of patients with progressively increasing severity of emphysema were assessed by ANOVA and F-test.

4.8.2 Results

4.8.2.1 Co-registration analysis

Figure 1E shows the distribution of the two pPRM indexes plotted with different colors according to FEV_1% predicted grade. As shown in the figure, patients with similar FEV_1 grade are randomly scattered in the diagram. The two different contributions to gas trapping could not be correctly assessed by using standard classification methods based on FEV_1% thresholds. The two relative contributions to total gas trapping were weakly correlated ($r=0.24$, $p<0.01$, Table 2 of main manuscript). Lines in Figure 1E represent mean values of %pLDA (12.4%) and %fLDA (36.1%), dividing the scatterplot into four groups, in parallel with the division done in Figure 3 in the main manuscript. The four groups include Emph (prevalent emphysema, %fLDA lower than the mean value and %pLDA higher than the mean value), group Mixs (mixed-severe disease, both %fLDA and %pLDA higher than the mean values), group Mixm (mixed-mild disease, both %fLDA and %pLDA lower than the mean values), and group Funct (prevalent functional gas trapping, %fLDA higher than the mean value and %pLDA lower than the mean value). The distribution of the data points was very similar to that of Figure 3 in the main manuscript. The small differences in data distribution were due to the differences in the mean value of %pLDA and $\%LAA_{-950insp}$ (12.4% and 14.9%, respectively), while the mean values of %fLDA and %fGT were almost identical (36.1% and 36.2%, respectively).

4.8.2.2 Functional-based classification

Differences between the mean values of $\%LAA_{-950insp}$ in the various groups are plotted in Figure 4 in the main text. Panel B of Figure 4 shows the relationship between %fLDA (x axis) and the total gas trapping amount as measured at expiration (y axis). The different colors (from blue to yellow) correspond to the four groups we introduced to grade emphysema extent estimation according to the output of the logistic regression model.

The regression line is fitted for data points characterized by a predicted probability P value (model output) less than 0.5 classified as having “milder emphysema” extent. As shown in the figure, patients with milder emphysema (blue dots) are distributed along this regression line, so that the total gas trapping is directly associated with functional gas trapping (the emphysematous contribution is absent). Other patients, characterized by a more severe parenchymal destruction (light grey-yellow dots), are scattered far from this fitted line because the contribution of the emphysematous gas trapping caused a “shifting effect” towards higher values of $\%LAA_{-856exp}$ (y values).

Figure 1E. Distribution of the two pPRM indexes plotted with different colors according to FEV1% predicted grade. Lines representing the mean values of %pLDA (12.4%) and %fLDA (36.1%) divide the scatterplot into four groups, in parallel with the division done in Figure 3 in the main manuscript. The four

groups include group Emph (prevalent emphysema, %fLDA lower than the mean value and %pLDA higher than the mean value), group Mixs (mixed-severe disease, both %fLDA and %pLDA higher than the mean values), group Mixm (mixed-mild disease, both %fLDA and %pLDA lower than the mean values), and group Funct (prevalent functional gas trapping, %fLDA higher than the mean value and %pLDA lower than the mean value).

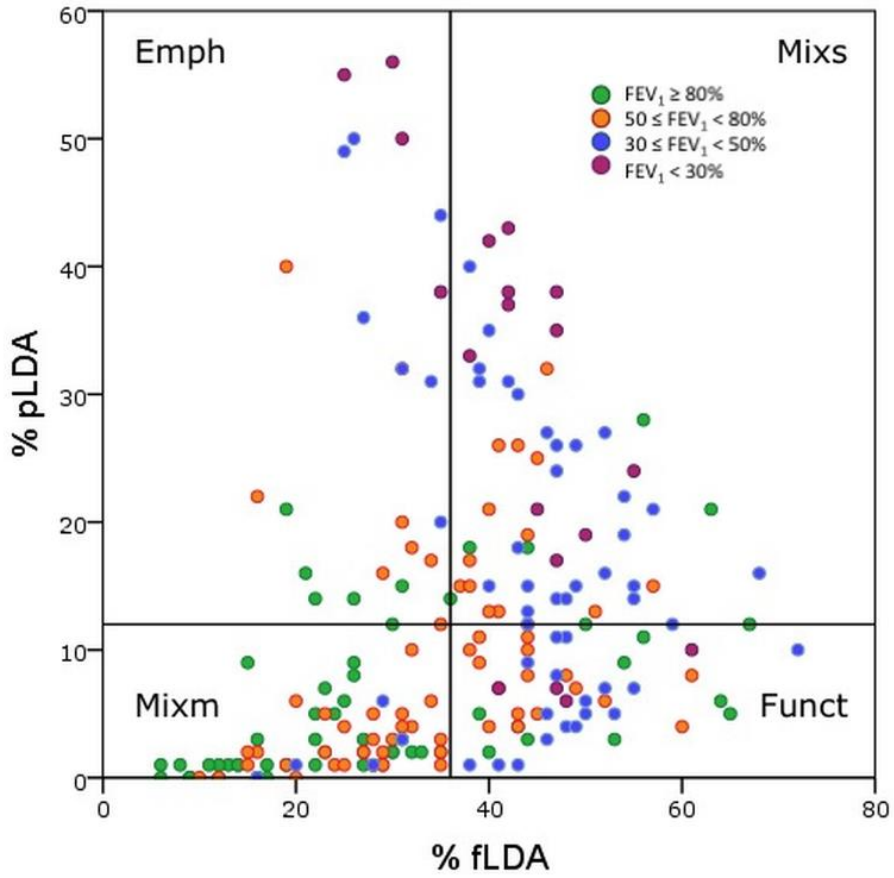

4.9 References

1E. Mannino DM, Buist AS. Global burden of COPD: risk factors, prevalence, and future trends. Lancet 2007; 370(9589): 765–773.

2E. Picard R, Cook D. Cross-validation of regression models. J Am Stat Assoc 1984; 79: 575–583.

4.10 Advances in knowledge

- As shown in 202 patients with COPD, the quantification of the relative contributions of emphysematous and non-emphysematous gas trapping was used to identify a prevalent CT subtype.
- The emphysematous (persistent low density area, %pLDA) and non-emphysematous (functional low density area, %fLDA) contributions to total gas trapping provided by a pulmonary parametric response map (pPRM) could not be adequately assessed by standard classification methods based on FEV_1%, which showed only a moderate correlation with %pLDA (r=-0.50) and %fLDA (r=-0.43).
- The non-emphysematous contribution to total gas trapping (%fLDA) was highly correlated (r=0.99), with the difference of imaging metrics at standard density thresholds ($\%LAA_{-856exp}$ and $\%LAA_{-950insp}$).
- The emphysematous contribution to total gas trapping (%pLDA) was essentially absent for values of total gas trapping around or below 30%.
- A functional model including FEV_1/VC, FEV_1%, DLco%, and BMI was used to predict the CT level of parenchymal destruction, with an overall accuracy of 81%.

Implications for Patient Care:

- The definition of the prevalent CT subtype (i.e. emphysema versus airway disease) of COPD obtained by a co-registration method as well as by standard CT metrics could potentially be used to target patient therapy to the underlying COPD endotype.
- A logistic model combining BMI and pulmonary function data can be used to predict CT-based quantification of emphysema grade, which may prove useful when assessing COPD patients who do not undergo thoracic CT.

Summary Statement:

Standard imaging metrics obtained by inspiratory and expiratory CT can be used to identify and quantify the relative contribution of emphysematous and non-emphysematous gas trapping, permitting a better definition of COPD patient subtypes.

Radiology

Emphysematous and Nonemphysematous Gas Trapping in Chronic Obstructive Pulmonary Disease: Quantitative CT Findings and Pulmonary Function[1]

Mariaelena Occhipinti, MD
Matteo Paoletti, PhD
Francesca Bigazzi, MD
Gianna Camiciottoli, MD
Riccardo Inchingolo, MD
Anna Rita Larici, MD
Massimo Pistolesi, MD, PhD

Purpose: To identify a prevalent computed tomography (CT) subtype in patients with chronic obstructive pulmonary disease (COPD) by separating emphysematous from nonemphysematous contributions to total gas trapping and to attempt to predict and grade the emphysematous gas trapping by using clinical and functional data.

Materials and Methods: Two-hundred and two consecutive eligible patients (159 men and 43 women; mean age, 70 years [age range, 41–85 years]) were prospectively studied. Pulmonary function and CT data were acquired by pulmonologists and radiologists. Noncontrast agent–enhanced thoracic CT scans were acquired at full inspiration and expiration, and were quantitatively analyzed by using two software programs. CT parameters were set as follows: 120 kVp; 200 mAs; rotation time, 0.5 second; pitch, 1.1; section thickness, 0.75 mm; and reconstruction kernels, b31f and b70f. Gas trapping obtained by difference of inspiratory and expiratory CT density thresholds (percentage area with CT attenuation values less than −950 HU at inspiration and percentage area with CT attenuation values less than −856 HU at expiration) was compared with that obtained by coregistration analysis. A logistic regression model on the basis of anthropometric and functional data was cross-validated and trained to classify patients with COPD according to the relative contribution of emphysema to total gas trapping, as assessed at CT.

Results: Gas trapping obtained by difference of inspiratory and expiratory CT density thresholds was highly correlated ($r = 0.99$) with that obtained by coregistration analysis. Four groups of patients were distinguished according to the prevalent CT subtype: prevalent emphysematous gas trapping, prevalent functional gas trapping, mixed severe, and mixed mild. The predictive model included predicted forced expiratory volume in 1 second/vital capacity, percentage of predicted forced expiratory volume in 1 second, percentage of diffusing capacity for carbon monoxide, and body mass index as emphysema regressors at CT, with 81% overall accuracy in classifying patients according to its extent.

Conclusion: The relative contribution of emphysematous and nonemphysematous gas trapping obtained by coregistration of inspiratory and expiratory CT scanning can be determined accurately by difference of CT inspiratory and expiratory density thresholds. CT extent of emphysema can be predicted with accuracy suitable for clinical purposes by pulmonary function data and body mass index.

Online supplemental material is available for this article.

[1]From the Section of Respiratory Medicine, Department of Experimental and Clinical Medicine, University of Florence, Careggi University Hospital, Largo A. Brambilla 3, 50134 Florence, Italy (M.O., M. Paoletti, F.B., G.C., M. Pistolesi); and Departments of Pulmonology (R.I.) and Radiological Sciences (A.R.L.), Gemelli University Hospital, Catholic University of the Sacred Heart, Rome, Italy. Received July 20, 2017; revision requested September 25; revision received October 9; accepted October 27; final version accepted November 3. **Address correspondence to** M.O. (e-mail: *mariaelena.occhipinti@unifi.it*).

Supported by the Ministry of Health of Italy and Ministry of University and Research of Italy.

Chapter 5 - Statistical models: lung function and BMI

In the previous study we have shown that a probabilistic model based on body mass index (BMI), FEV_1 as percent of predicted, FEV_1/VC and DLco as percent of predicted could be used to estimate emphysema quantified on CT. Limitations of that approach for clinical practice or clinical trials are that DLco is not always available and standard pulmonary function parameters have a wide inter-individual variability, even after normalization for ethnicity, age, and body size.

We aimed to ascertain whether the probability of having emphysema, as defined by quantitative CT metrics, could also be estimated with a level of accuracy suitable for clinical practice and pharmacologic trials by a probabilistic model based on functional parameters directly derived from the spirometric flow-volume curve without standardization for sex, age, and ethnicity data.

Lung function and BMI predictive models to assess CT emphysema extent in COPD

Mariaelena Occhipinti, M Paoletti, F Bigazzi, J Sieren, M Palazzi, G Camiciottoli, M Pistolesi

(Presentation at American Thoracic Society Conference, San Diego, 22-24/05/2018)

5.1 Background

Airflow limitation in COPD results from lung parenchymal destruction (emphysema) as well as from conductive airway disease. These two pathophysiologic conditions lead both to gas trapping within lungs. Spirometry cannot differentiate between emphysematous and functional gas trapping, whereas chest computed tomography (CT) with post-processing image analysis can quantify both components of gas trapping.

Although in each patient one of the two pathophysiologic conditions (endotypes) may prevail, either emphysema or conductive airway disease, most COPD patients present with a mixed phenotype characterized by various combinations of both components and a corresponding mixed CT subtype. Knowledge of the prevalent subtype in each patient may be of interest in developing clinical and pharmacological trials designed to target patients therapy to the underlying pathophysiologic mechanism of airflow obstruction. However, CT cannot be performed in all COPD patients, due to the high prevalence of COPD in the general population and the unavailability of CT scans in the vast majority of patients.

Purpose: We aimed to predict by clinical and functional data the probability of having emphysema, as assessed on CT.

5.2 Methods

From January 2014 to December 2017 we recruited 133 non-consecutive COPD patients with the following criteria.

Inclusion criteria:

- Age 40 to 85 years
- Smoking history of more than 10 pack-years
- Nonreversible post-bronchodilator airflow obstruction at PFTs
- GOLD stages I to IV
- Chest CT within 48 hours from pulmonary function evaluation

Exclusion criteria:

- History of exacerbation within one month
- History of any clinical conditions interfering with pulmonary function or chest CT quantitative parameters assessment, including asthma, diffuse bronchiectasis, interstitial lung disease, acute heart failure, chemo-radiation therapy, lung cancer, lung surgery, metal objects in the chest.

5.2.1 Pulmonary Function Tests (PFTs)

All patients underwent complete pulmonary function evaluation within 48 hours of the CT examination. Pre-and post-bronchodilator spirometry data, static and dynamic lung volumes (FEV_1, FEV_1/VC, FEV_1/FVC, VC, RV, TLC, RV/TLC, FRC), and single-breath diffusing capacity for carbon monoxide (DLco) were measured according to ATS/ERS guidelines. We also measured the lower limit of normality (LLN) according to ERS/ATS guidelines.

5.2.2 Chest CT Scan

Volumetric chest CT scans were obtained at full inspiration and expiration using the acquisition protocol adopted in the COPDGene study. All CT scans were performed by using the same CT scanner for all patients (SOMATOM Sensation 64, Siemens, Erlangen, Germany).

Patients received prior cautious instructions on how to perform the respiratory maneuvers while lying supine in the CT scanner with arms fully abducted. No contrast medium was administered.

The relative volumes of lung attenuation area with values below -950 HU at inspiration ($\%LAA_{-950insp}$) and below -856 HU at expiration ($\%LAA_{-856exp}$) were quantified by using the Pulmonary Workstation Apollo 2.1 (VIDA Diagnostics, Coralville, Iowa, USA). Thresholds at -950 Hounsfield Units (HU) and -856 HU were chosen as densitometric cut-off consistent with emphysema and total gas-trapping, respectively.

5.2.3 Predictive model

The CT level of parenchymal destruction was estimated by a ten-fold validated *logistic regression model* built from stepwise selection of anthropometric, clinical, and functional data. The most significant regressors of the model were identified by a step-wise procedure. Ten-fold validation was then performed to ascertain the total and partial predictive accuracy. The logistic regression model was trained to classify COPD patients according to the probability to have a $\%LAA_{-950insp}$ higher than the mean value of the sample. By applying the model, each subject was classified according to probability output (p_{th}) values, from milder ($p_{th}<0.5$) to more severe ($p_{th}>0.5$) emphysema.

After the logistic regression model was validated, we classified each subject according to the p_{th} value obtained by combining functional indexes and BMI predictors. ROC curve (AUC) analysis was used to calculate the accuracy of the models after tenfold cross-validation considering the logistic p_{th} at value of 0.5.

The software programs included Mathcad (version 2001; Mathsoft), SPSS/PC WIN 11.5.1 (SPSS, Chicago, IL), and C++ programming language. Values of p lower than 0.05 indicated statistical significance.

5.3 Results

Anthropometric, clinical, functional, and imaging data of patients with $FEV_1/FVC<0.70$ or $FEV_1/FVC<LLN$.

Anthropometric, clinical, functional, and imaging data of 133 patients with $FEV_1/FVC<0.70$									
Age	70 (8)	FEV_1%	63 (27)	FVC %	93 (25)	RV %	137 (48)	Imaging	
BMI	26 (5)	FEV_1/VC	47 (13)	FRC %	129 (34)	RV/TLC	50 (17)	$\%LAA_{-950insp}$	15 (12)
Pack/yrs	51 (25)	FEV_1/FVC	51 (12)	TLC %	108 (18)	DLco %	68 (24)	$\%LAA_{-856exp}$	45 (20)

Data are expressed as means (SD).

Anthropometric, clinical, functional, and imaging data of 108 patients with $FEV_1/FVC<LLN$									
Age	70 (8)	FEV_1%	56 (23)	FVC %	93 (25)	RV %	146 (45)	Imaging	
BMI	26 (5)	FEV_1/VC	44 (12)	FRC %	136 (32)	RV/TLC	53 (14)	$\%LAA_{-950insp}$	16 (12)
Pack/yrs	51 (24)	FEV_1/FVC	49 (12)	TLC %	111 (17)	DLco %	64 (22)	$\%LAA_{-856exp}$	49 (19)

Predictors of $\%LAA_{-950insp}$ in the two models, contingency tables and corresponding ROC curves in the group of patients with FEV1/FVC<0.70

MODEL A

Predictors
DLco%
FEV_1/VC
FEV_1%
BMI

	Group p_{th}<0.5	Group p_{th}>0.5	Accuracy
Group p_{th}<0.5	66	11	86.8%
Group p_{th}>0.5	10	46	80.7%
Overall accuracy			84.2%

MODEL B

Predictors
$FEF_{25\%}$
$FEF_{50\%}$
PEF
BMI

	Group p_{th}<0.5	Group p_{th}>0.5	Accuracy
Group p_{th}<0.5	67	9	88.2%
Group p_{th}>0.5	14	43	75.4%
Overall accuracy			82.7%

MODEL A

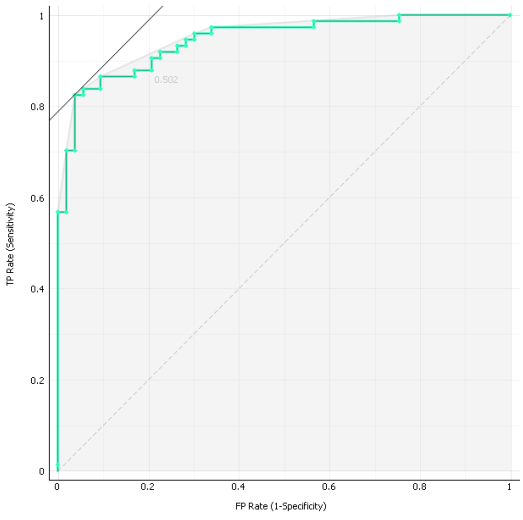

MODEL B

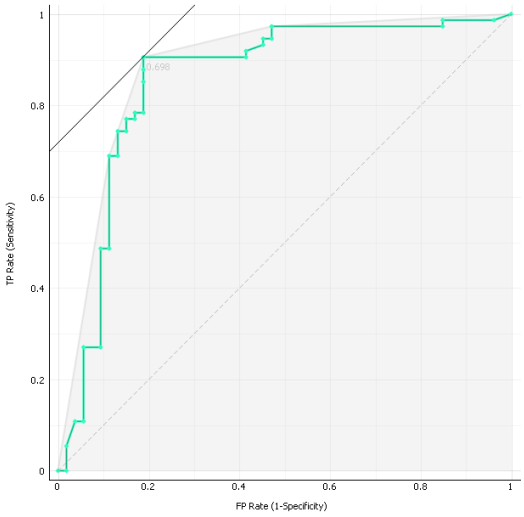

The concordance between the two models in the group of 133 patients with FEV_1/FVC<0.70 was 84%.

In the group of 108 patients with FEV1/FVC<LLN both models had 81% accuracy. The concordance between the two models in the group of patients with FEV_1/FVC<LLN was 81%.

5.4 Conclusions

The predictive models including BMI and functional data predicted with a considerable accuracy the emphysema extent as assessed on quantitative CT, regardless of the criteria used for recruiting patients with COPD. These models, if validated in larger scale studies, may be suitable for daily clinical assessment of patients with COPD, to predict treatment response, and to design newer outcomes for clinical and pharmacologic trials in which CT scan cannot be performed.

5.5 References

1. Occhipinti M, Paoletti M, Bigazzi F, Camiciottoli G, Inchingolo R, Larici AR, et al. Emphysematous and Nonemphysematous Gas Trapping in Chronic Obstructive Pulmonary Disease: Quantitative CT Findings and Pulmonary Function. Radiology 2018; 287:683-692.
2. Lynch DA, Austin JH, Hogg JC, et al. CT-Definable Subtypes of Chronic Obstructive Pulmonary Disease: A Statement of the Fleischner Society. Radiology 2015; 277: 192-205.
3. Hogg JC. Pathophysiology of airflow limitation in chronic obstructive pulmonary disease. Lancet 2004; 364: 709-721.
4. Camiciottoli G, Bigazzi F, Paoletti M, Cestelli L, et al. Pulmonary function and sputum characteristics predict computed tomography phenotype and severity of COPD. Eur Respir J 2013; 42: 626-635.
5. Hilbe JM. Logistic Resgression Models. CRC Press, 2009.
6. McDonough JE, Yuan R, Suzuki M, et al. Small-airway obstruction and emphysema in chronic obstructive pulmonary disease. N Engl J Med 2011; 365: 1567-1575.
7. Pellegrino R et al. Interpretative strategies for lung function tests. Eur Resp J 2005; 26:948-968
8. Miller MR, Crapo R, Hankinson J, Brusasco V, Burgos F, Casaburi R, et al. General considerations for lung function testing. Eur Respir J 2005; 26:153-161.
9. Topalovic M, Exadaktylos V, Peeters A, Coolen J, Dewever W, Hemeryck M, et al. Computer quantification of airway collapse on forced expiration to predict the presence of emphysema. Respir Res 2013; 14:131.

Chapter 6 - Statistical models: maximal expiratory flow-volume curve

In the previous study we have shown that the probabilistic models including BMI and functional data can estimate with a considerable accuracy the emphysema extent as assessed on quantitative CT, regardless of the criteria used for recruiting patients with COPD. The importance of the maximal expiratory flow-volume (MEFV) curve parameters lead us towards an accurate analysis of the flow-volume curve throughout its shape. Moreover, a method based on the MEFV curve has recently been proposed by Topalovic et al. to predict the presence of emphysema, showing good specificity but low sensitivity (1).

We aimed to find from the analysis of MEFV curve the parameter(s) most suitable for a probabilistic model to predict with high specificity and sensitivity the presence and extent of emphysema, as defined by quantitative CT metrics.

6.1 Methods

This was a two-centre study approved by the institutional Ethics Committees of the University of Florence and the Catholic University of Sacred Heart in Rome. The study was based on a retrospective interpretation of prospectively acquired data. From January 2012 to December 2016, subjects with clinical diagnosis of COPD were considered for inclusion if they satisfied the following inclusion criteria: age 40-85 years, smoking history >10 pack-years, no COPD exacerbations within one month, no diagnosis of asthma or cardiac disease, and acceptance to participate by written informed consent. From a total of 232 eligible subjects, 38 were excluded because incomplete data, or coexisting abnormalities on CT scan, thus 194 were included in the study.

6.1.1 Functional and imaging evaluation

Subjects underwent complete pulmonary function evaluation by using a mass-flow sensor and multigas analyser (V6200 Autobox Body Plethysmograph Sensor Medics, Yorba Linda, USA, or Platinum Elite™ Body Plethysmograph, Medical Graphics Corporation, St. Paul, MN, USA), arterial blood gases by Radiometer ABL90 FLEX or ABL800 FLEX (Brønshøj, Denmark), and CT scan within 48 hours of the clinical and functional evaluation. Pre- and post-bronchodilator spirometry, lung volumes, and single-breath DLco were obtained according to standard ATS/ERS (American Thoracic Society/European Respiratory Society) recommendations (8-10).

In each center volumetric chest CT scans were obtained by the same team and the same CT scanner (SOMATOM Sensation 64, Siemens, Erlangen, Germany, or SOMATOM Definition FLASH 128, Siemens, Erlangen, Germany). CT scans were acquired at full inspiration and forced end-expiration using the acquisition protocol adopted in the COPDGene Study (11) with the following parameters: 120 kVp, 200 mAs, rotation

time 0.5s, slice thickness 0.6mm, pitch 1.1 and reconstructions kernels b31f (smooth) and b70f (sharp). Subjects were instructed on how to perform respiratory manoeuvres while lying supine in the CT scanner with arms fully abducted. No contrast medium was injected. Post-processing image analysis was performed with reconstruction kernel b31f. Thresholds at -950 Hounsfield Units (HU) and -856 HU were chosen as densitometric cut-offs for emphysema and total gas trapping, respectively (12-14). The relative volumes of lung attenuation area with values below -950 HU at inspiration ($\%LAA_{-950insp}$) and below -856 HU at expiration ($\%LAA_{-856exp}$) were quantified by using the Pulmonary Workstation Apollo 2.1 (VIDA, Coralville, IA, USA). Percentage of functional gas trapping (%fGT) was calculated as $\%fGT = \%LAA_{-856exp} - \%LAA_{-950insp} - 6\%$, which was validated and found strongly correlated (r^2=0.98) with functional low density area (%fLDA) measured by co-registration analysis of paired inspiratory and expiratory CT scans (15). %fGT is the lung area with low attenuation values below -856HU on expiration and above -950HU on inspiration, representing the fraction of gas trapped at end expiration because of airway closure or extreme flow limitation.

6.1.2 Data analysis and statistics

The relationship between $\%LAA_{-856exp}$ and $\%LAA_{-950insp}$ was analyzed by fitting a local regression curve to CT raw data.

A binary logistic regression model was trained to classify all subjects according to the probability of being affected by less or more severe emphysema according to their value of $\%LAA_{-950insp}$ lower or higher than the mean value of the group, matching the same classification criteria published for larger cohorts (16). The input parameters were selected by a step-wise process using anthropometric data and parameters derived from the MEFV curve as independent variables.

The shape of the MEFV curve was analysed by fitting segments of the descending limb at specific fractions of FVC. Curves with a difference between PEF and FEF_{25} less than 5% of PEF were discarded by the algorithm.

ROC curve (AUC) analysis was used to calculate the accuracy of the model after tenfold cross-validation considering a logistic probability threshold (p_{th}) at value of 0.5.

Welch's *t*-test was used to evaluate differences in CT metrics among subgroups with different ranges of $\%LAA_{-950insp}$. Pearson *r* coefficient was used to describe the correlations between CT parameters.

The software programs included Mathcad (version 2001; Mathsoft), SPSS/PC WIN 11.5.1 (SPSS, Chicago, IL), and C++ programming language. Values of *p* lower than 0.05 indicated statistical significance. Data are expressed as mean and standard deviation (SD).

6.2 Results

Scatterplot of CT imaging metrics of $\%LAA_{-950insp}$ and $\%LAA_{-856exp}$ showed a non-linear monotonic relationship with two main segments with distinct slopes, different dispersion profiles (r^2= 0.45 p<0.01 and r^2= 0.30 p<0.01), and a breakpoint at the mean $\%LAA_{-950insp}$ (14%) (Figure 1). In the group of 77 subjects with $\%LAA_{-950insp}$ >14 the data points around the relative segment of the regression curve were more dispersed than in the group of 117 subjects with $\%LAA_{-950insp}$ <14 (Figure 1). CT metrics, anthropometric and functional parameters were significantly different (p<0.05) between the two groups (Table 2).

There was a significant correlation between %fGT and $\%LAA_{-856exp}$ in both groups, but it was much stronger (r^2= 0.96) in the group of subjects with $\%LAA_{-950insp}$ <14 than in those with $\%LAA_{-950insp}$ >14 (r^2= 0.45). This difference suggests that total gas trapping was completely explained by %fGT in the latter, but not in the former.

A binary logistic regression model including the slope of the flow-volume curve between 25% and 50% of FVC [S_{25-50}= (FEF_{25} – FEF_{50}) / 0.25 x FVC], BMI, and FEV_1/FVC predicted the probability of having emphysema with 87% sensitivity and 81% specificity (85% accuracy). Examples of differences in MEFV curve of two subjects with different degrees of emphysema are shown in Figure 3.

Figure 4 shows the scatterplot of $\%LAA_{-856exp}$ vs %fGT relative to the model output of each patient.

The vast majority of subjects with p_{th}<0.5 were distributed along the identity line, suggesting that $\%LAA_{-856exp}$ was almost completely explained by %fGT, whereas most subjects with p_{th}>0.5 were scattered above the identity line, suggesting that $\%LAA_{-856exp}$ could be also explained by the emphysema contribution (Figure 4). The distance of each data point above the identity line gives an estimate of the contribution of emphysema to total gas trapping.

6.3 Discussion

The main finding of this study is that the probability of having emphysema, as defined by quantitative CT metrics, was estimated with accuracy by a probabilistic model including BMI and functional parameters derived from MEFV curve not requiring normalization by reference equations.

Nowadays quantitative CT enables the definition of the relative volumes of emphysema and gas trapping in subjects with COPD by using CT metrics of low attenuation areas at inspiration ($\%LAA_{-950insp}$) and expiration ($\%LAA_{-856exp}$) (12, 13). In the present study a non-linear relationship between the above-mentioned CT metrics was observed with a breakpoint at 14 $\%LAA_{-950insp}$. This is close to the mean value observed in the COPDGene Study population (17) and recently proposed to define “severe” emphysema (16). The results of the present study show that this cut-off distinguished not only different degrees of emphysema, but also subjects with different mechanisms of airflow obstruction. Indeed, subjects with $\%LAA_{-950insp}$<14 had a

borderline (6.7%) percentage of emphysema (18) and their total gas trapping was almost completely explained by functional gas trapping, which was on average 34%, a value much higher than the 20% reported in healthy individuals (19). Therefore, in this group the gas trapping was mainly accounted for by conductive airway disease. Conversely, in subjects with $\%LAA_{-950insp} > 14$ total gas trapping was mainly accounted for by the presence of emphysema, though it is not possible to exclude that functional gas trapping was also present due to coexisting airway disease or loss of airway support by peribronchial tethering (20).

Traditionally, a reduction of DLco has been considered as a marker of emphysema in subjects with COPD (21). In this connection, a recent study from our group showed that a logistic model including DLco%, FEV_1%, FEV_1/VC, and BMI was able to accurately predict the presence of emphysema on CT (15).

As early as in 1976, it was proposed that a kinging of the descending limb of the forced MEFV curve might represent a sign of airway collapse reflecting the presence of emphysema, as assessed by DLco (22). More recently the angle between two regression lines fitted to the descending limb of the MEFV curve resulted to be predictive of the presence of emphysema on CT scan, showing a good specificity but low sensitivity (1). The kinking of MEFV curve in emphysema can be interpreted on the grounds of the wave-speed theory (23). During forced expiration, alveolar pressure increases and gas is compressed within the lung, thus reducing lung volume and elastic recoil pressure. As a result, driving pressure and distending pressure at choke point are decreased, thereby reducing maximal flow. This effect may be magnified in emphysema because of the abrupt fall of lung elastic recoil at high lung volumes (21) and the larger amount of gas to be compressed, thus flattening the MEFV curve. By contrast, the scooping of MEFV curve in airway disease may reflect a smooth decrease of lung elastic recoil and a transition of the chock point towards the lung periphery with less gas compression. Mechanisms that may contribute to the kinking of forced expiratory flow in emphysema are a sudden airway narrowing due to sharp decrease in lung elastic recoil (24) and a sharp decrease of thoracic gas compression from mid to low lung volumes. Therefore, flattening of the MEFV curve from mid-to-low lung volumes should be a predictor of emphysema. In the present study, slopes of MEFV curves were determined at different lung volumes and compared with quantitative CT metrics to derive a probabilistic model for estimating the probability of having emphysema at CT. The logistic model of the present study predicted the presence of emphysema with sensitivity considerably higher than found by Topalovic et al. (1). Furthermore, the model described in the present study had slightly higher accuracy than the model previously described by our group based on BMI, FEV_1%, FEV_1/VC, and DLco% (15). Advantages of the present model over the previous one are that it does not require any normalization of parameters for anthropometric data and it is independent of the choice of spirometric criteria to define airflow obstruction.

From a technical point of view the sensitivity of the model is critically dependent on the effort during the MEFV curve because this affects the magnitude of thoracic gas compression (25), which is a major determinant of the shape of MEFV curve, particularly in subjects with prevalent emphysema (Figure 2) (3).

This study has some limitations. First, it included a relatively small number of subjects, only white Caucasian, and cannot be considered representative of the whole spectrum of COPD subjects. However, the distribution of CT metrics and their average values were similar to that reported in the COPDGene Study, which included more than 10,000 subjects of two different ethnicities (17). Second, CT scans were acquired without spirometric control of lung inflation level during the acquisition. However, all subjects received prior cautious instruction on how to perform the respiratory manoeuvres just before undergoing CT scanning by dedicated personnel and quantitative measurements were obtained by using an objective and automated software using the thresholds for emphysema and gas trapping reported in current literature (12-14).

In conclusion, this study demonstrates that the probability of having emphysema and its extent, as defined by quantitative CT metrics, can be estimated with accuracy by a probabilistic model based on BMI and functional parameters derived from the flow-volume curve. Being independent of reference values, the model could be helpful in clinical practice and also in patients' selection for clinical trials.

6.4 Tables

Table 1. Anthropometric, pulmonary function and CT metrics data. Data are mean (SD). Smoking history is expressed as pack-years.

N	194
Sex (M:F)	154:40
Age (yr)	70.2 (8.0)
BMI (kg/m^2)	26.5 (4.6)
Smoking history	51.7 (27.0)
FEV_1 (% pred)	62.6 (25.8)
FEV_1/VC	47.5 (13.2)
FEV_1/FVC	52.3 (13.1)
TLC (% pred)	108.2 (16.5)
DLco (% pred)	68.9 (23.5)
RV (% pred)	137.0 (46.7)
FRC (% pred)	129.5 (32.6)
RV/TLC	49.9 (14.1)
$\%LAA_{-950insp}$	14.3 (11.7)
$\%LAA_{-856exp}$	45.2 (20.3)
%fGT	36.9 (13.7)

Legend: BMI = body mass index, DLco = lung diffusing capacity of lung for carbon monoxide, FEV_1% = forced expiratory volume in 1 s, %fGT = percentage of functional gas-trapping, FRC = functional residual capacity, FVC = forced vital capacity, % $LAA_{-950insp}$ = percentage of lung attenuation area with values <-950 Hounsfield Units at inspiratory CT scan, $\%LAA_{-856exp}$ = percentage of lung attenuation area with values <-856 Hounsfield Units at expiratory CT scan, RV = residual volume, TLC = total lung capacity, VC = vital capacity.

Table 2. Mean values of CT metrics, anthropometric and functional data in relation to emphysema extent ($\%LAA_{-950insp}$).

	$\%LAA_{-950insp} < 14$	$\%LAA_{-950insp} \geq 14$	p
N	117	77	
$\%LAA_{-950insp}$	6.7	25.9	<0.01*
$\%LAA_{-856exp}$	34.5	61.4	<0.01*
%fGT	33.8	41.5	<0.01*
Age (yr)	69.2	71.6	0.04*
BMI (kg/m^2)	27.7	24.7	<0.01*
Smoking history	49.7	54.7	0.19
FEV_1 (%)	70.2	50.9	<0.01*
FVC (%)	92.8	92.9	<0.01*
FEV_1/VC	53.5	38.5	<0.01*
FEV_1/FVC	58.7	42.6	<0.01*
TLC (%)	103.8	114.9	<0.01*
RV (%)	125.1	155.1	<0.01*
RV/TLC	46.3	55.5	<0.01*
FRC (%)	118.0	146.8	<0.01*
DLco (%)	77.6	55.9	<0.01*
PEF (%)	77.9	54.5	<0.01*
S_{25-50} (degrees)	65.1	37.7	<0.01*

PEF= peak of expiratory flow, S_{75-50} = slope of the descending limb of flow-volume curve between 75 and 50% of FVC. Other notations as in Table 1.

6.5 Figures

Figure 1. Scatterplot of $\%LAA_{-950insp}$ and $\%LAA_{-856exp}$ in 194 patients with COPD. The local regression curve (*grey line*) of the two CT metrics depicts the non-linear monotonic relationship of the variables. The dashed line indicates the *breakpoint* corresponding approximately to the mean value of $\%LAA_{-950insp}$ of the 194 patients. Pearson's correlation coefficient value is r^2= 0.45 (p<0.01) in the first segment and r^2= 0.30 (p<0.01) in the second segment.

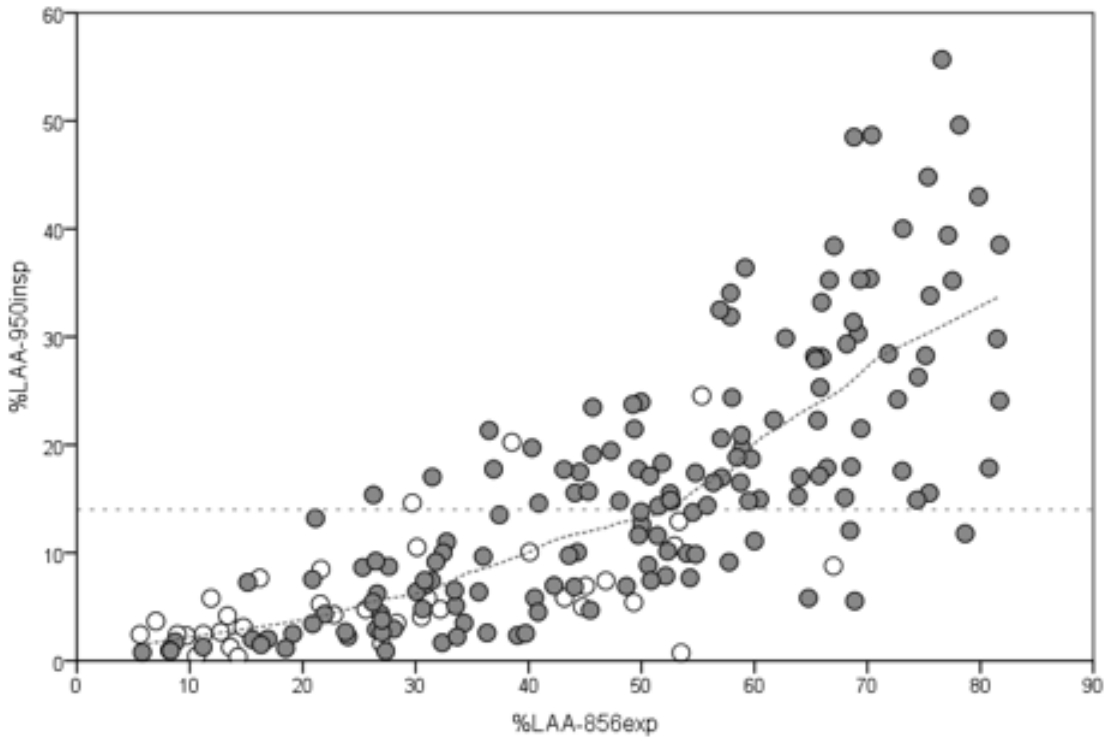

Legend: $\%LAA_{-950insp}$ = percentage of lung attenuation area with values below -950 Hounsfield Units at inspiratory CT scan; $\%LAA_{-856exp}$ = percentage of lung attenuation area with values below -856 Hounsfield Units at expiratory CT scan. (Open circles are 37 subjects with FEV_1/FVC<0.70 but greater than lower limit of normality)

Figure 2. ROC curves of the two logistic models. The curves represent the DLco-based model (*left panel*) and the MEFV curve-based model (*right panel*).

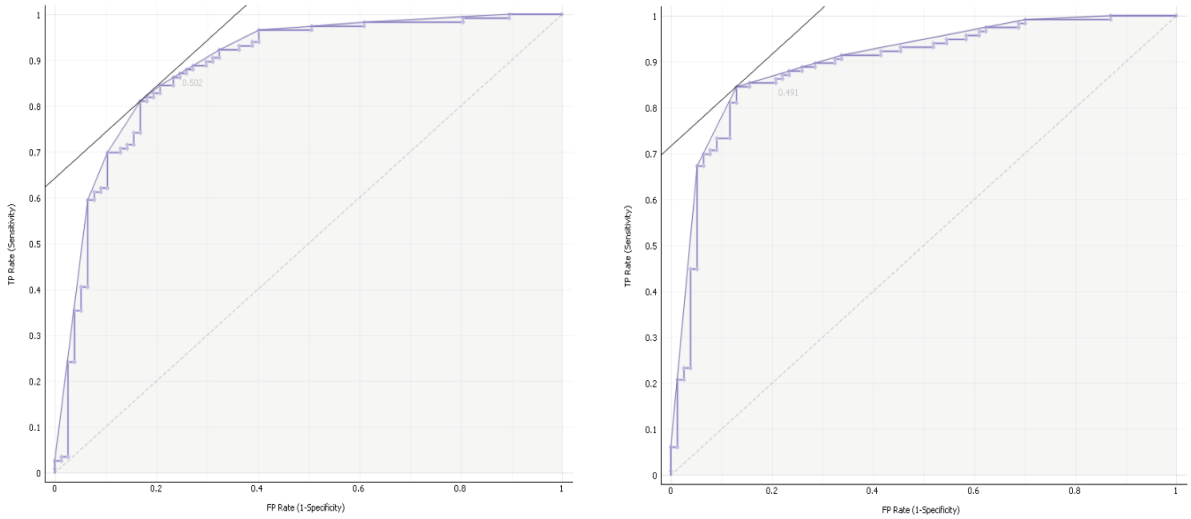

Figure 3. Maximal expiratory flow-volume curves of two representative subjects, with severe emphysema (*left panel*: 24% $LAA_{-950insp}$, 50% LAA_{-856}) or airway disease (*right panel*: 4% $LAA_{-950insp}$, 53% $LAA_{-856exp}$). Note the flatter slope between 25 and 50% of FVC in the former when flow was plotted against expired volume (*black lines*) but not pletysmographic thoracic volume (*grey lines*), indicating greater thoracic gas compression at high-to-mid lung volumes.

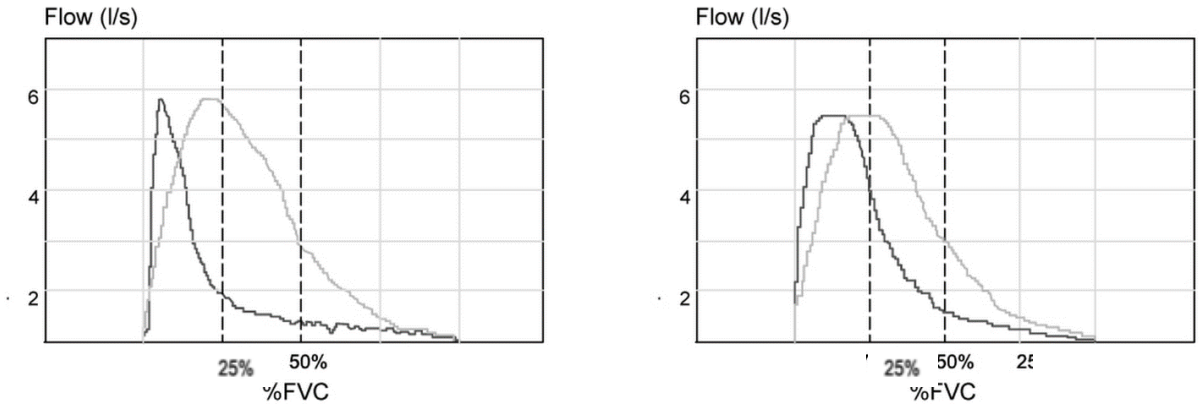

Figure 4. Scatterplot of %LAA$_{-856exp}$ and %fGT with colours ranging from white to black according to the probability values estimated by the logistic model. Data points lying on the identity line indicate subjects in whom the total gas trapping can be totally explained by functional gas trapping. The distance of each data point above the identity line quantifies the contribution of emphysema to total gas trapping.

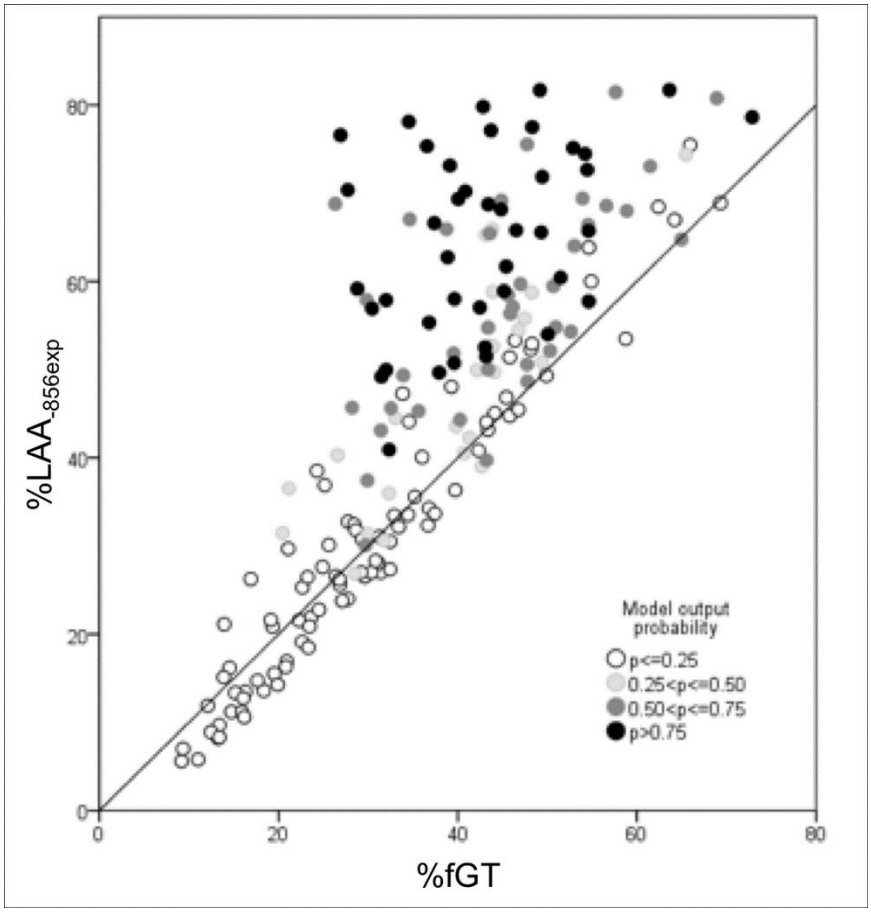

6.6 References

1. Topalovic M, Exadaktylos V, Peeters A, Coolen J, Dewever W, Hemeryck M, et al. Computer quantification of airway collapse on forced expiration to predict the presence of emphysema. Respir Res 2013; 14:131.
2. Pauwels RA, Buist AS, Calverley PM, Jenkins CR, Hurd SS, Committee GS. Global strategy for the diagnosis, management, and prevention of chronic obstructive pulmonary disease. NHLBI/WHO Global Initiative for Chronic Obstructive Lung Disease (GOLD) Workshop summary. Am J Respir Crit Care Med 2001; 163:1256-1276.
3. Pellegrino R, Viegi G, Brusasco V, Crapo RO, Burgos F, Casaburi R, et al. Interpretative strategies for lung function tests. Eur Respir J 2005; 26:948-968.
4. Brusasco V. Spirometric definition of COPD: exercise in futility or factual debate? Thorax 2012; 67:569-570.
5. Camiciottoli G, Bigazzi F, Paoletti M, Cestelli L, Lavorini F, Pistolesi M. Pulmonary function and sputum characteristics predict computed tomography phenotype and severity of COPD. Eur Respir J 2013; 42:626-635.
6. Paoletti M, Cestelli L, Bigazzi F, Camiciottoli G, Pistolesi M. Chronic Obstructive Pulmonary Disease: Pulmonary Function and CT Lung Attenuation Do Not Show Linear Correlation. Radiology 2015; 276:571-578.
7. Castaldi PJ, Benet M, Petersen H, Rafaels N, Finigan J, Paoletti M, et al. Do COPD subtypes really exist? COPD heterogeneity and clustering in 10 independent cohorts. Thorax 2017; 72:998-1006.
8. Miller MR, Hankinson J, Brusasco V, Burgos F, Casaburi R, Coates A, et al. Standardisation of spirometry. Eur Respir J 2005; 26:319-338.
9. Macintyre N, Crapo RO, Viegi G, Johnson DC, van der Grinten CP, Brusasco V, et al. Standardisation of the single-breath determination of carbon monoxide uptake in the lung. Eur Respir J 2005; 26:720-735.
10. Wanger J, Clausen JL, Coates A, Pedersen OF, Brusasco V, Burgos F, et al. Standardisation of the measurement of lung volumes. Eur Respir J 2005; 26:511-522.
11. Regan EA, Hokanson JE, Murphy JR, Make B, Lynch DA, Beaty TH, et al. Genetic epidemiology of COPD (COPDGene) study design. COPD 2010; 7:32-43.
12. Madani A, De Maertelaer V, Zanen J, Gevenois PA. Pulmonary emphysema: radiation dose and section thickness at multidetector CT quantification-comparison with macroscopic and microscopic morphometry. Radiology 2007; 243:250-257.
13. Schroeder JD, McKenzie AS, Zach JA, Wilson CG, Curran-Everett D, Stinson DS, et al. Relationships between airflow obstruction and quantitative CT measurements of emphysema, air trapping, and airways in subjects with and without chronic obstructive pulmonary disease. AJR Am J Roentgenol 2013; 201:W460-470.
14. Jain N, Covar RA, Gleason MC, Newell JD, Jr., Gelfand EW, Spahn JD. Quantitative computed tomography detects peripheral airway disease in asthmatic children. Pediatr Pulmonol 2005; 40:211-218.
15. Occhipinti M, Paoletti M, Bigazzi F, Camiciottoli G, Inchingolo R, Larici AR, et al. Emphysematous and Nonemphysematous Gas Trapping in Chronic Obstructive Pulmonary Disease: Quantitative CT Findings and Pulmonary Function. Radiology 2018; 287:683-692.
16. Hersh CP, Washko GR, Estepar RS, Lutz S, Friedman PJ, Han MK, et al. Paired inspiratory-expiratory chest CT scans to assess for small airways disease in COPD. Respir Res 2013; 14:42.
17. Lynch DA, Al-Qaisi MA. Quantitative computed tomography in chronic obstructive pulmonary disease. J Thorac Imaging 2013; 28:284-290.
18. Lynch DA, Austin JH, Hogg JC, Grenier PA, Kauczor HU, Bankier AA, et al. CT-Definable Subtypes of Chronic Obstructive Pulmonary Disease: A Statement of the Fleischner Society. Radiology 2015:141579.
19. Silva M, Nemec SF, Dufresne V, Occhipinti M, Heidinger BH, Chamberlain R, et al. Normal spectrum of pulmonary parametric response map to differentiate lung collapsibility: distribution of densitometric classifications in healthy adult volunteers. Eur Radiol 2016; 26:3063-3070.
20. Dayman H. Mechanics of airflow in health and in emphysema. J Clin Invest 1951; 30:1175-1190.

21. Blakemore WS, Forster RE, Morton JW, Ogilvie CM. A standardized breath holding technique for the clinical measurement of the diffusing capacity of the lung for carbon monoxide. J Clin Invest 1957; 36:1-17.

22. Saltzman HP, Ciulla EM, Kuperman AS. The spirographic "kink". A sign of emphysema. Chest 1976; 69:51-55.

23. Dawson SV, Elliott EA. Wave-speed limitation on expiratory flow-a unifying concept. J Appl Physiol Respir Environ Exerc Physiol 1977; 43:498-515.

24. Gibson GJ, Pride NB. Lung distensibility. The static pressure-volume curve of the lungs and its use in clinical assessment. Br J Dis Chest 1976; 70:143-184.

25. Sharafkhaneh A, Officer TM, Goodnight-White S, Rodarte JR, Boriek AM. Novel method for measuring effects of gas compression on expiratory flow. Am J Physiol Regul Integr Comp Physiol 2004; 287:R479-484.

Chapter 7 - Mathematical model and radiomics

In the previous studies we have shown that the statistical models including either BMI and functional data or parameters of the flow-volume curve can estimate with a considerable accuracy the emphysema extent as assessed on quantitative CT, regardless of the criteria used for recruiting patients with COPD ($FEV_1/FVC<0.70$ or $FEV_1/FVC<LLN$). The most relevant limitation of these approaches is the intrinsic nature of the statistical models, namely they rely on regression coefficients reflecting the characteristics of the training set. Mathematical models can overcome this limitation and in the past they have been developed to study the biomechanical characteristics of the lung function.

We aimed at developing a mathematical model, based on the analysis of the maximal expiratory flow-volume (MEFV) curve, to provide an emphysema severity index (ESI) and to compare it with the COPD subtypes defined by quantitative CT and CT-based radiomics.

Spirometric assessment of emphysema presence and severity as measured by quantitative CT and CT-based radiomics in COPD

Mariaelena Occhipinti, Matteo Paoletti, Brian J. Bartholmai, Srinivasan Rajagopalan, Ronald A. Karwoski, Cosimo Nardi, Riccardo Inchingolo, Anna R. Larici, Gianna Camiciottoli, Federico Lavorini, Stefano Colagrande, Vito Brusasco, Massimo Pistolesi

Submitted – under review

7.1 Introduction

Chronic obstructive pulmonary disease (COPD) is a complex condition with a wide spectrum of clinical presentations and pathological features unified under the spirometric definition of airflow obstruction. Airway narrowing and parenchymal destruction are recognized as the mechanisms responsible for airflow obstruction in COPD, but they cannot be distinguished by standard spirometry. However, standard spirometry is one of the most employed variables for patients enrollment and outcome evaluation in clinical and pharmacologic studies.

In recent years, chest computed tomography (CT) allows to depict and measure *in vivo* the lung pathologic changes of COPD by quantifying parenchymal destruction, the direct sign of emphysema, as well as bronchial wall thickening and gas trapping, which represent direct and indirect signs of conductive airway disease, respectively. (1,2) A closer imaging definition of whether conductive airway disease or emphysema is the predominant mechanism of airflow obstruction has been lately obtained by using co-registration analysis of inspiratory and expiratory CT scans. (3) Nowadays more information is extracted from imaging data using advanced feature analysis representing what is called “radiomics”. (4) Artificial neural networks and statistical

models are available to provide radiologists and clinicians with objective and reproducible computer-based evaluations of lung parenchyma. In particular, CALIPER (Computer Aided Lung Informatics for Pathology Evaluation and Rating) recently developed at Mayo Clinic (Rochester, MN), is a computational platform for the near real-time characterization and quantification of lung parenchymal patterns on CT scan. (5,6)

Altogether, quantitative and qualitative studies have shown that CT can allow distinguishing not only between airway and parenchymal abnormalities, but also between subtypes of emphysema, i.e. centrilobular, panlobular, and paraseptal. (7) However, a widespread routine use of CT for the assessment of COPD in clinical practice and clinical and pharmacologic studies cannot be currently foreseen due to radiation exposure and limited instrumental availability in the face of the COPD rapidly increasing prevalence of the disease. (8)

In a previous study we have shown that a probabilistic model based on body mass index, FEV_1 as percent of predicted, FEV_1/VC and DLco as percent of predicted could be used to estimate emphysema quantified on CT. (9) Limitations of that approach for clinical practice or clinical and pharmacologic trials are that DLco is not always available and that standard pulmonary function parameters have a wide inter-individual variability, even after normalization for ethnicity, age, and body size. (10) Furthermore, probabilistic models rely on regression coefficients that reflect the characteristics of the training set. These limitations may be possibly overcome by mathematical models studying directly the biomechanical characteristics of airway function of each patient. (11)

The aim of the present study was to assess whether a mathematical model designed to fit the shape of the maximum expiratory flow-volume curve (MEFV) obtained by standard spirometry could provide estimates of the presence and the severity of emphysema comparable with parameters used to assess emphysema extent derived from quantitative CT and CT-based radiomics.

7.2 Methods

This two-center study was approved by the institutional Ethics Committees of the University of Florence and of the Catholic University of Sacred Heart in Rome. The study is based on a retrospective interpretation of prospectively acquired data. From January 2012 to December 2016, subjects with diagnosis of COPD (post-bronchodilator FEV_1/VC<0.70) (12,13) were considered for inclusion if they satisfied the following inclusion criteria: age 40-85 years, smoking history >10 pack-years, no COPD exacerbations within one month, no diagnosis of asthma or cardiac disease, and acceptance to participate by written informed consent. Thirty-eight out of 232 eligible subjects were excluded because of incomplete data or coexisting abnormalities on CT scan.

7.2.1 Functional evaluation

Subjects underwent complete pulmonary function evaluation by using a mass-flow sensor and multigas analyser (V6200 Autobox Body Plethysmograph Sensor Medics, Yorba Linda, CA, USA, or Platinum Elite™ Body Plethysmograph, Medical Graphics Corporation, St. Paul, MN, USA), arterial blood gases by

Radiometer ABL90 FLEX or ABL800 FLEX (Brønshøj, Denmark). Pre- and post-bronchodilator spirometry, lung volumes, and single-breath DLco were obtained according to standard ATS/ERS (American Thoracic Society/European Respiratory Society) recommendations. [14]

7.2.2 CT scanning technique and analysis

In each center volumetric chest CT scans were obtained by the same team and the same CT scanner (SOMATOM Sensation 64 or SOMATOM Definition FLASH 128, Siemens, Erlangen, Germany) within 48 hours of the functional evaluation. CT scans were acquired at full inspiration and forced end-expiration using the acquisition protocol adopted in the COPDGene Study (15) with the following parameters: 120 kVp, 200 mAs, rotation time 0.5 sec, slice thickness 0.6 mm, pitch 1.1 and reconstructions kernels b31f (smooth) and b70f (sharp). Subjects were instructed on how to perform respiratory maneuvers while lying supine in the CT scanner with arms fully abducted. No contrast medium was injected. Post-processing image analysis was performed on images with reconstruction kernel b31f by using three different software programs: VIDA, Imbio LDA, CALIPER (Figure 1A-F).

- **VIDA analysis** (Figure 1B). We used the Pulmonary Workstation Apollo 2.1 (VIDA, Coralville, IA, USA) installed onsite to segment airways and lungs and to calculate the relative volumes of lung attenuation area with values below -950 Hounsfield Units (HU) at inspiration ($\%LAA_{-950insp}$) and below -856HU at expiration ($\%LAA_{-856exp}$). Thresholds at -950 HU and -856HU were chosen as densitometric cut-offs for emphysema and total gas trapping, respectively. (1,16,17) The analysis was fully automated with the possibility to correct manually any mistake in airway or lobe segmentation.
- **Imbio LDA analysis** (Figure 1C-D). Co-registration analysis performed by Imbio LDA (Minneapolis, MN, US) automatically pairs inspiratory and expiratory CT scans to provide percentages of normal lung (percentage of voxels with CT attenuation greater than -950 HU at inspiration and greater than -856HU at expiration), persistent low density area (%pLDA, voxels with CT attenuation below -950HU at inspiration and below -856HU at expiration), and functional low density area (%fLDA, voxels with CT attenuation above -950HU at inspiration and below -856HU at expiration). (3) %fLDA represents the non-emphysematous contribution to total gas trapping, namely the fraction of gas trapped at end expiration because of airway closure or extreme flow limitation. Moreover, Imbio LDA provides parametric response maps showing the regional distribution of each lung pattern. The analysis was fully automated and performed on an online platform called Imbio Launchpad.
- **CALIPER analysis** (Figure 1E-F). Inspiratory CT scans were post-processed by using CALIPER (Mayo Clinic, Rochester, MN, USA), a computational platform for the near real-time characterization and quantification of seven lung parenchymal patterns on CT scans, including Normal, Mild Low Attenuation Area (LAA), Moderate LAA, Severe LAA, Ground-glass, Reticular, and Honeycombing (Figure 1E). (5) CALIPER is based on histogram signature mapping techniques trained through expert radiologist consensus assessment of pathologically confirmed datasets obtained through the Lung Tissue

Research Consortium (6,18). For each subject, CALIPER outputs a glyph similar to a radial space-filling plot providing an iconic summary of the volumetric parenchymal classification, thus facilitating the comprehension of the multidimensional source data. (6) The area of the glyph represents the computed total lung volume. The glyph is partitioned with radial lines to illustrate the relative volumes of the left and right lungs and further divided into three regions, each representing the upper/middle/lower lung zones (Figure 1F). CALIPER analysis was fully automated and was performed onsite in the laboratory.

7.2.3 Emphysema Severity Index (ESI)

ESI is based on a parametric biomechanical model representing a theoretical approximation of the shape of the descending limb of the MEFV curve computed by assuming that at a given time the pressure lost by a fluid flow conveyed in a cylindrical duct is inversely related to its diameter and directly related to the fluid specific friction factor, density, and velocity (see the Supplemental Material for theoretical and mathematical details). The computation does not require standardization of input parameters, as it is directly related to the shape of the curve. Therefore, ESI is independent from percentage predicted values of pulmonary function variables. ESI value was computed in each patient using a specifically developed software application, whose theoretical basis is reported on the online supplement. A numerical output value ranging from 0 to 10 was used to stratify the dataset of 194 COPD patients according to the estimated emphysema severity.

7.2.4 Data analysis and statistics

By using the two thresholds of $\%LAA_{-950insp}$ reported in literature to define absence of significant emphysema (6%) (7) and severe emphysema (14%) (19) we classified the patients in three subgroups: no emphysema (NE, $\%LAA_{-950insp} < 6$), moderate emphysema (ME, $6 \leq \%LAA_{-950insp} < 14$), and severe emphysema (SE, $\%LAA_{-950insp} \geq 14$).

A pairwise dissimilarity matrix was derived using SILA (**S**cale **I**ndicative of **L**ung parenchyma **A**bnormality). SILA between a pair of CALIPER quantified CT lung volumes was computed as a cumulative aggregate of the differentials of normalized distributions of ordered (as mild, moderate, and severe) CALIPER exemplars. The unique clusters representing similar groups of patients were identified by unsupervised clustering of the 194x194 dissimilarity matrix using affinity propagation. The method does not require an *a priori* specification of the number of desired clusters.

Chi-squared test was used to determine any significant differences between expected and observed frequencies in the clusters obtained by CALIPER and the three groups defined on the basis of $\%LAA_{-950insp}$ ranges (NE, ME, SE).

Analysis of variance, Welch's t, and Games-Howell post-hoc tests were used to evaluate differences of the mean values of pulmonary function tests and ESI mean values among the three groups of emphysema severity defined by VIDA and Imbio LDA, as well as the clusters obtained by CALIPER.

To evaluate the performances of the ESI software as a classification tool we used logistic regression analysis. In each patient we estimated the probability of being affected by "severe" emphysema ($\%LAA_{-950insp} \geq 14$, data computed by VIDA) given the ESI value obtained by spirometry. In a similar manner we estimated the probability of "absence" of significant emphysema ($\%LAA_{-950insp} < 6$, data computed by VIDA) given the ESI value.

A ten-fold cross validation was performed over the entire dataset and we calculated the True Positives and False Positives rates for each fold. Sensitivity, specificity and AUC were evaluated by ROC curve analysis. In particular we estimated in each patient the probability of being affected by "severe" emphysema ($\%LAA_{-950insp} > 14$, data provided by VIDA) given the value of ESI score obtained by spirometry; π = Pr (Y = "Severe" | X = ESI) and the probability of "absence" of emphysema ($\%LAA_{-950insp} < 6$, data provided by VIDA) given the value of ESI score obtained by spirometry; π = Pr (Y = "Absence" | X = ESI).

The software programs included Mathcad (version 2001; Mathsoft), SPSS/PC WIN 11.5.1 (SPSS, Chicago, IL), C++ programming language, and Orange. (20) Values of *p* lower than 0.05 indicated statistical significance. Data are expressed as mean and standard deviation (SD).

7.3 Results

Table 1 describes anthropometric, pulmonary function, and CT metrics data of the 194 subjects included in the study. Subjects were distributed across all GOLD stages: 55 stage I, 62 stage II, 56 stage III, and 21 stage IV.

Figure 1 shows CT images of a patient with advanced destructive emphysema before (Fig. 1A) and after post-processing image analysis by using the three different software programs: VIDA (Fig. 1B), Imbio LDA (Fig. 1C-D), and CALIPER (Fig. 1E-F).

Figure 2 illustrates the patients subdivision according to the pairwise dissimilarity matrix that identified three clusters (G1-G3), based on the SILA metric derived from the features extracted by CALIPER. Cluster G1 consisted of 95/194 (49%) subjects, G2 of 65/194 (33.5%) subjects, and G3 of 34/194 (17.5%) subjects. Across the three different clusters patients lungs were represented by a glyph, illustrating the regional composition of classified lung volume with color-coded sections proportional to the percentage of lung patterns within the region (Figure 1F). G1 was characterized by predominant Normal and Mild LAA patterns, G2 by predominant Moderate LAA pattern, and G3 by predominant Severe and Moderate LAA patterns. Patients clustered as G1 by CALIPER had either NE or ME at VIDA, whereas patients clustered as G2 had ME or SE and all patients clustered as G3 had SE.

Table 2 displays the mean values of ESI and the functional data of the three groups of patients stratified by quantitative CT (VIDA, Imbio LDA) according to the thresholds to define different degrees of emphysema (NE, ME, SE) and by radiomics (CALIPER) according to the clusters of progressive emphysema severity (G1,

G2, G3). Patients allocation differed within the three groups defined by each of the quantitative CT post-processing techniques. However, a significant progressive impairment from patients classified NE or G1 to patients classified SE and G3 was observed. Pulmonary function data were significantly different among the subgroups with various degrees of emphysema with a few exceptions (for further detail see the Table 1S on the online supplement). Lower ESI values (<5) were typical for MEFV curves obtained in COPD patients with NE or ME, whereas higher values (>5) were observed in patients with SE. Mean of the ESI values differed significantly among the three emphysema groups defined by $\%LAA_{-950insp}$ by VIDA ($p<.001$) as well as among the three Imbio LDA groups ($p<.001$) and CALIPER clusters ($p<.001$).

Table 3 depicts the functional differences between groups with various degrees of emphysema as classified by VIDA and Imbio LDA (NE, ME, SE) and by CALIPER (G1, G2, G3).

The graph in Figure 3A represents the ten folds averaged ROC curve obtained by varying the classification threshold over the range of the logistic regression model output π = Pr (Y = "Severe" | X = ESI) for the probability of "severe" emphysema ($\%LAA_{-950insp}$ >14, data provided by VIDA). The best results in terms of sensitivity and specificity were relative to the threshold value 0.47, with sensitivity=0.82 and specificity=0.87. The total AUC area was of 0.88.

The graph in Figure 3B represents the ten folds averaged ROC curve obtained by varying the classification threshold over the range of the logistic regression model output π = Pr (Y = "Absence" | X = ESI) for the probability of "absence" of emphysema ($\%LAA_{-950insp}$ <6, data provided by VIDA). The best results in terms of sensitivity and specificity were relative to the threshold value 0.37, with sensitivity=0.80 and specificity=0.85. The total AUC area was of 0.86.

Therefore, NE is differentiated from ME/SE with a sensitivity of 0.80 and a specificity of 0.85, whereas SE is differentiated from ME with a sensitivity of 0.82 and a specificity of 0.87 by using the MEFV curve.

Figure 4 shows differences in MEFV curves of two representative subjects with severe emphysema and no emphysema. The former has a flatter slope when flow is plotted against expired volume but not at pletysmographic thoracic volume, indicating greater thoracic gas compression at high-to-mid lung volumes.

7.4 Discussion

The extensive application of CT scan post-processing techniques has shown that presence and severity of emphysema as assessed by CT does closely reflect lung function presentation in COPD. The main finding of this study is that a mathematical model developed to fit the descending limb of the MEFV curve approximates the multimodality CT-validated emphysema stratification with an accuracy that could be suitable for clinical

and research purposes. The model is based only on MEFV curve morphology and, consequently, it is independent from percentage predicted values of pulmonary function.

In recent years quantitative CT enabled radiologists to quantify and localize the relative volumes of emphysema and gas trapping in subjects with COPD by using standard CT metrics of low attenuation areas at pre-determined inspiratory and expiratory X-ray attenuation thresholds. (1,16) Beside CT quantification of emphysema, the new computational radiomics approach allows to extract multiple features from imaging data and to process them in order to objectively and reproducibly characterize the main pathologic changes in the course of lung diseases. Radiomics artificial intelligence can be used to develop non-invasive imaging biomarkers, which could be helpful in phenotyping heterogeneous diseases, such as COPD. (21)

As shown in Table 2, patients allocation in an emphysema severity subgroups varies with the different CT metrics and radiomics approaches used. Despite this heterogeneity of classification reflecting the underlying methodological differences of the three CT post-processing analyses, ESI differentiates the progressive severity of emphysema whatever the CT method used to classify patients.

A recent study from our group showed that a probabilistic model including DLco%, FEV_1%, FEV_1/VC, and BMI dissects with accuracy emphysematous from non-emphysematous gas trapping as assessed by standard CT metrics in patients with COPD. (9) Reduction in DLco is considered a marker of emphysema in subjects with COPD. (22) However, measurement of DLco is not widely performed and standard pulmonary function parameters have a wide inter-individual variability, even after normalization for ethnicity, age, and body size. (10) In the current study we overcame these limitations by a model depending only from MEFV curve morphology that does not require normalization by reference equations and, being a mathematical model and not a probabilistic one, it does not depend from regression coefficients reflecting the characteristics of a training set.

A role for the MEFV curve in predicting the risk of emphysema was introduced as early as 1976 by Saltzman et al. (23) They proposed that a kinging of the descending limb of the MEFV curve might represent a sign of airway collapse reflecting the presence of emphysema. (23) More recently the angle between two regression lines fitted to the descending limb of the MEFV curve resulted to be predictive of the presence of emphysema on CT scan with good specificity but low sensitivity. (24)

The kinking of MEFV curve in emphysema can be interpreted on the grounds of the wave-speed theory. (25) During forced expiration, alveolar pressure increases and gas is compressed within the lung, thus reducing lung volume and elastic recoil pressure. As a result, driving pressure and distending pressure at choke point decrease, thereby reducing maximal flow. As demonstrated in a recent study, this effect may be magnified in emphysema because of the abrupt fall of lung elastic recoil at high lung volumes and the larger amount of gas to be compressed. (26) The composite result of these physical phenomena is a flattening the MEFV curve. By contrast, the scooping of MEFV curve in COPD patients with predominant conductive airway disease may

reflect a smooth decrease of lung elastic recoil and a transition of the choke point towards the lung periphery with less gas compression. (27) Mechanisms that may contribute to the kinking of forced expiratory flow in emphysema are a sudden airway narrowing due to sharp decrease in lung elastic recoil and a sharp decrease of thoracic gas compression from mid-to-low lung volumes. (28) Therefore, flattening of the MEFV curve from mid-to-low lung volumes (Figure 4) could be a predictor of emphysema. At variance with the above quoted paper on the analysis of the MEFV curve, (24) the model presented here predicts presence and severity of emphysema with a considerable level of accuracy.

This study has some limitations. First, it included a relatively small number of white Caucasian subjects that cannot be considered representative of the wide clinical spectrum of COPD in the general population. However, the distribution of CT metrics and their average values were similar to those reported from the COPDGene Study that included more than 10,000 subjects of two different ethnicities. (9,29) Second, the CT scans were acquired without spirometric control of lung inflation level during the acquisition. However, all subjects received prior cautious instruction on how to perform the respiratory maneuvers just before undergoing CT scanning by dedicated personnel. Third, radiomics is very sensitive to protocol acquisition parameters, algorithm definitions, and image processing. (21) Lack of standardization of these components severely hampers reproducibility and comparability of results. In this study all CT scans were acquired with the same protocol by the same personnel in each study center, and after calibration of CT scanner before each examination. Fourth, models based on MEFV curve strictly depend on patient effort during spirometry, as it affects the magnitude of thoracic gas compression. (30) This is a major determinant of the shape of the MEFV curve, particularly in subjects with predominant emphysema. (13) However, accurate technicians training could overcome this limitation.

7.4.1 Conclusions

This study demonstrates that the presence of emphysema and its severity in patients with COPD, as defined on inspiratory-expiratory CT scan by standard metrics and co-registration analysis, as well as by a computational unsupervised CT-based radiomics, can be accurately estimated by a mathematical model based on MEFV curve morphology. The model is independent from reference values and, if confirmed in larger populations of patients with COPD, it could be helpful in clinical practice to personalize therapy, to select patients for clinical and pharmacologic trials, and for the interpretation of their results whenever spirometry is the only available examination.

7.5 Tables

Table 1. Anthropometric, pulmonary function and CT metrics data.

N		194
Sex (M:F)		154:40
Age (yr)		70 (8.0)
BMI (kg/m^2)		27 (4.6)
Smoking history (pack-years)		52 (27)
FEV_1 (% pred)		63 (26)
FEV_1/VC		48 (13)
FEV_1/FVC		52 (13)
TLC (% pred)		108 (17)
DLco (% pred)		69 (24)
RV (% pred)		137 (47)
FRC (% pred)		130 (33)
RV/TLC		50 (14)
VIDA	$\%LAA_{-950insp}$	14 (12)
	$\%LAA_{-856exp}$	45 (20)
Imbio LDA	%pLDA	12.2 (12.5)
	%fLDA	37.1 (14.0)
	% Normal	49.1 (21.1)

Data are expressed as mean (SD). Legend: BMI = body mass index, DLco = lung diffusing capacity of lung for carbon monoxide, FEV_1% = forced expiratory volume in 1 s, %fLDA = percentage of functional low density area, FRC = functional residual capacity, FVC = forced vital capacity, % $LAA_{-950insp}$ = percentage of lung attenuation area with values <-950 Hounsfield Units at inspiratory CT scan, $\%LAA_{-856exp}$ = percentage of lung attenuation area with values <-856 Hounsfield Units at expiratory CT scan, % Normal= percentage of normal lung, %pLDA= percentage of persistent low density area, %pred= percentage of predicted, RV = residual volume, TLC = total lung capacity, VC = vital capacity.

Table 2. Relationship among ESI values and functional data across the groups of patients with various degrees of emphysema.

	Emphysema severity	N	ESI score	FEV_1 %	FVC %	FEV_1/FVC %	TLC %	RV %	FRC %	DLco %
VIDA	NE	57	1.1 (1.5)	76.1 (23.6)	93.5 (22.8)	63.1 (8.0)	100.1 (11.8)	115.0 (30.5)	109.3 (18.2)	79.7 (22.9)
	ME	58	3.1 (2.6)	63.6 (23.9)	91.4 (21.0)	54.1 (10.2)	106.9 (18.8)	134.1 (51.7)	125.3 (31.0)	75.6 (21.6)
	SE	79	6.8 (2.5)	49.9 (23.7)	91.2 (27.8)	42.4 (10.8)	115.2 (15.1)	157.6 (48.2)	147.9 (33.7)	55.9 (19.8)
	ANOVA / Welch's test p		***<.001***	***<.001***	***.002***	***<.001***	***<.001***	***<.001***	***<.001***	***<.001***
Imbio LDA	NE	86	1.5 (1.8)	72.6 (22.9)	92.9 (20.9)	60.5 (9.2)	101.1 (15.6)	118.2 (42.0)	111.5 (23.7)	78.9 (23.2)
	ME	46	4.6 (2.7)	63.8 (27.5)	94.1 (25.2)	52.1 (10.1)	111.9 (15.0)	145.6 (47.4)	135.4 (30.5)	72.6 (18.1)
	SE	62	7.7 (3.3)	44 (18.8)	88.6 (28.2)	39.6 (9.5)	115.7 (15.5)	160.7 (46.2)	152.1 (32.5)	51.9 (18.9)
	ANOVA / Welch's test p		***<.001***	***<.001***	*.442*	***<.001***	***<.001***	***<.001***	***<.001***	***<.001***
CALIPER	G1	95	1.7 (2.1)	71.9 (23.7)	92.8 (21.9)	59.8 (9.6)	101.2 (14.6)	118.7 (39.4)	113.2 (24.3)	78.4 (23.2)
	G2	65	5.4 (2.8)	59.7 (24.9)	97.1 (26.5)	48.8 (11.0)	113.4 (16.5)	145.9 (47.6)	137.9 (30.7)	65.6 (19.0)
	G3	34	8.0 (1.7)	36.8 (14.3)	79.5 (23.2)	36.5 (8.0)	118.2 (13.6)	177.3 (44.0)	163.4 (29.9)	48.1 (18.5)
	ANOVA / Welch's test p		***<.001***	***<.001***	***.002***	***<.001***	***<.001***	***<.001***	***<.001***	***<.001***

Differences among groups were assessed by analysis of variance and Welch's tests, expressed in *italics* and in ***bold*** if significant. Values are expressed as mean (SD). DLco %= percent predicted diffusing lung capacity for carbon monoxide, FEV_1 %= percent predicted forced expiratory volume in 1 s, FRC% = percent predicted functional residual capacity, FVC% = percent predicted forced vital capacity, $\%LAA_{-950insp}$ = percentage of lung attenuation area with values <-950 Hounsfield Units at inspiratory CT scan, ME (moderate emphysema, $6 \leq \%LAA_{-950insp} < 14$ if VIDA or $6 \leq$ %pLDA <14 if Imbio LDA), NE (no emphysema, $\%LAA_{-950insp} < 6$ if VIDA or %pLDA <6 if Imbio LDA), RV% = percent predicted residual volume, SE (severe emphysema, $\%LAA_{-950insp} \geq 14$ if VIDA or $\%LAA_{-950insp} \geq 14$ if Imbio LDA), TLC% = percent predicted total lung capacity.

Table 3. Functional differences between groups with various degrees of emphysema. Groups are defined according the classification performed by VIDA and Imbio LDA (NE, ME, SE) and by CALIPER (G1, G2, G3). Differences were analyzed by Games-Howell post-hoc test and p values are displayed (significant p values are in bold). Legend: DLco %= percent predicted diffusing lung capacity for carbon monoxide, FEV_1 %= percent predicted forced expiratory volume in 1 s, FRC% = percent predicted functional residual capacity, FVC% = percent predicted forced vital capacity, $\%LAA_{-950insp}$ = percentage of lung attenuation area with values <-950 Hounsfield Units at inspiratory CT scan, ME (moderate emphysema, 6 ≤$\%LAA_{-950insp}$ <14 if VIDA or 6 ≤%pLDA <14 if Imbio LDA), NE (no emphysema, $\%LAA_{-950insp}$ <6 if VIDA or %pLDA <6 if Imbio LDA), RV% = percent predicted residual volume, SE (severe emphysema, $\%LAA_{-950insp}$ ≥14 if VIDA or $\%LAA_{-950insp}$ ≥14 if Imbio LDA), TLC% = percent predicted total lung capacity.

		FEV_1%	FVC%	FEV_1/FVC%	TLC%	RV%	FRC%	DLco%
VIDA	p NE/ME	**<.01**	**<.01**	**<.01**	.28	**<.01**	**<.01**	**<.01**
	p NE/SE	**<.01**	**<.01**	**<.01**	**<.01**	**<.01**	**<.01**	**<.01**
	p ME/SE	**<.01**	.52	**<.01**	**<.01**	**<.01**	**<.01**	**<.01**
Imbio LDA	p NE/ME	.16	.96	**<.01**	**<.01**	**<.01**	**<.01**	.21
	p NE/SE	**<.01**	.56	**<.01**	**<.01**	**<.01**	**<.01**	**<.01**
	p ME/SE	**<.01**	.54	**<.01**	.42	.23	**.02**	**<.01**
CALIPER	p G1/G2	**<.01**	.52	**<.01**	**<.01**	**<.01**	**<.01**	**<.01**
	p G2/G3	**<.01**	**<.01**	**<.01**	.28	**<.01**	**<.01**	**<.01**
	p G1/G3	**<.01**	**<.01**	**<.01**	**<.01**	**<.01**	**<.01**	**<.01**

7.6 References

1. Madani A, De Maertelaer V, Zanen J, Gevenois PA. Pulmonary emphysema: radiation dose and section thickness at multidetector CT quantification-comparison with macroscopic and microscopic morphometry. Radiology. 2007; 243:250-7.

2. Hackx M, Bankier AA, Gevenois PA. Chronic obstructive pulmonary disease: CT quantification of airways disease. Radiology. 2012; 265:34-48.

3. Galban CJ, Han MK, Boes JL, et al. Computed tomography-based biomarker provides unique signature for diagnosis of COPD phenotypes and disease progression. Nat Med. 2012; 18:1711-5.

4. Aerts HJ. The Potential of Radiomic-Based Phenotyping in Precision Medicine: A Review. JAMA Oncol. 2016; 2:1636-42.

5. Raghunath S, Rajagopalan S, Karwoski RA, et al. Quantitative stratification of diffuse parenchymal lung diseases. PLoS One. 2014; 9:e93229.

6. Bartholmai BJ, Raghunath S, Karwoski RA, et al. Quantitative computed tomography imaging of interstitial lung diseases. J Thorac Imaging. 2013; 28:298-307.

7. Lynch DA, Austin JH, Hogg JC, et al. CT-Definable Subtypes of Chronic Obstructive Pulmonary Disease: A Statement of the Fleischner Society. Radiology. 2015:141579.

8. Adeloye D, Chua S, Lee C, et al. Global and regional estimates of COPD prevalence: Systematic review and meta-analysis. J Glob Health. 2015; 5:020415.

9. Occhipinti M, Paoletti M, Bigazzi F, et al. Emphysematous and Nonemphysematous Gas Trapping in Chronic Obstructive Pulmonary Disease: Quantitative CT Findings and Pulmonary Function. Radiology. 2018; 287:683-92.

10. Miller MR, Crapo R, Hankinson J, et al. General considerations for lung function testing. Eur Respir J. 2005; 26:153-61.

11. Abboud S, Barnea O, Guber A, Narkiss N, Bruderman I. Maximum expiratory flow-volume curve: mathematical model and experimental results. Med Eng Phys. 1995; 17:332-6.

12. Pauwels RA, Buist AS, Calverley PM, Jenkins CR, Hurd SS, Committee GS. Global strategy for the diagnosis, management, and prevention of chronic obstructive pulmonary disease. NHLBI/WHO Global Initiative for Chronic Obstructive Lung Disease (GOLD) Workshop summary. Am J Respir Crit Care Med. 2001; 163:1256-76.

13. Pellegrino R, Viegi G, Brusasco V, et al. Interpretative strategies for lung function tests. Eur Respir J. 2005; 26:948-68.

14. Miller MR, Hankinson J, Brusasco V, et al. Standardisation of spirometry. The European respiratory journal. 2005; 26:319-38.

15. Regan EA, Hokanson JE, Murphy JR, et al. Genetic epidemiology of COPD (COPDGene) study design. COPD. 2010; 7:32-43.

16. Schroeder JD, McKenzie AS, Zach JA, et al. Relationships between airflow obstruction and quantitative CT measurements of emphysema, air trapping, and airways in subjects with and without chronic obstructive pulmonary disease. AJR Am J Roentgenol. 2013; 201:W460-70.

17. Jain N, Covar RA, Gleason MC, Newell JD, Jr., Gelfand EW, Spahn JD. Quantitative computed tomography detects peripheral airway disease in asthmatic children. Pediatr Pulmonol. 2005; 40:211-8.

18. Maldonado F, Moua T, Rajagopalan S, et al. Automated quantification of radiological patterns predicts survival in idiopathic pulmonary fibrosis. Eur Respir J. 2014; 43:204-12.

19. Fry DL. Theoretical considerations of the bronchial pressure-flow-volume relationships with particular reference to the maximum expiratory flow volume curve. Phys Med Biol. 1958; 3:174-94.

20. Zheng CJ, Adams AB, McGrail MP, Marini JJ, Greaves IA. A proposed curvilinearity index for quantifying airflow obstruction. Respir Care. 2006; 51:40-5.

21. Hughes WF. Theory and problems of fluid dynamics. New York: Shaum; 1967.

22. Hersh CP, Washko GR, Estepar RS, et al. Paired inspiratory-expiratory chest CT scans to assess for small airways disease in COPD. Respir Res. 2013; 14:42.

23. Stajdohar M, Demsar J. Interactive Network Exploration with Orange. J Stat Softw. 2013; 53:1-24.

24. van Griethuysen JJM, Fedorov A, Parmar C, et al. Computational Radiomics System to Decode the Radiographic Phenotype. Cancer Res. 2017; 77:e104-e07.

25. Blakemore WS, Forster RE, Morton JW, Ogilvie CM. A standardized breath holding technique for the clinical measurement of the diffusing capacity of the lung for carbon monoxide. J Clin Invest. 1957; 36:1-17.

26. Saltzman HP, Ciulla EM, Kuperman AS. The spirographic "kink". A sign of emphysema. Chest. 1976; 69:51-5.

27. Topalovic M, Exadaktylos V, Peeters A, et al. Computer quantification of airway collapse on forced expiration to predict the presence of emphysema. Respir Res. 2013; 14:131.

28. Dawson SV, Elliott EA. Wave-speed limitation on expiratory flow-a unifying concept. J Appl Physiol Respir Environ Exerc Physiol. 1977; 43:498-515.

29. Pellegrino R, Crimi E, Gobbi A, et al. Severity grading of chronic obstructive pulmonary disease: the confounding effect of phenotype and thoracic gas compression. J Appl Physiol (1985). 2015; 118:796-802.

30. Hogg JC, Pare PD, Hackett TL. The Contribution of Small Airway Obstruction to the Pathogenesis of Chronic Obstructive Pulmonary Disease. Physiol Rev. 2017; 97:529-52.

31. Gibson GJ, Pride NB. Lung distensibility. The static pressure-volume curve of the lungs and its use in clinical assessment. Br J Dis Chest. 1976; 70:143-84.

32. Lynch DA, Al-Qaisi MA. Quantitative computed tomography in chronic obstructive pulmonary disease. J Thorac Imaging. 2013; 28:284-90.

33. Sharafkhaneh A, Officer TM, Goodnight-White S, Rodarte JR, Boriek AM. Novel method for measuring effects of gas compression on expiratory flow. Am J Physiol Regul Integr Comp Physiol. 2004; 287:R479-84.

7.7 Figures

Figure 1. Lung parenchyma representations at CT scan after post-processing with different software programs in a patient with severe emphysema. A. Axial CT scan shows advanced destructive emphysema with a giant bulla in the right lower lobe adjacent to an area of passive atelectasis. B. Volume rendering of the densitometric analysis performed by VIDA shows the location and severity of emphysema at inspiratory scan (threshold -950HU) displaying spheres whose diameter is proportional to the relative volume of emphysema in each region. C-D. Coronal and Sagittal 2D images obtained by co-registration of inspiratory and expiratory CT scans by Imbio LDA show the location of emphysema (*red*), functional airways gas trapping (*yellow*), and normal lung (*green*). E. Volume rendering of the lung texture analysis performed by CALIPER shows the 3D distribution of the different lung patterns, including Normal (*dark green*), Mild Low Attenuation Area (LAA, *light green*), Moderate LAA (*light blue*), Severe LAA (*dark blue*), Ground-glass (*yellow*), Reticular (*orange*). The glyph (F) provided by CALIPER summarizes the location and amount of the different lung patterns. The overall area of the glyph represents the computed total lung volume, the partitions with thick radial lines illustrate the relative volumes of the left (L) and right (R) lungs, which are further divided with thin radial lines into three regions, each representing the upper (U), middle (M), lower (L) lung zones. In this patient severe LAA dominates in the right lower and middle lung zones, whereas middle and lower left zones are characterized by mild and moderate LAA.

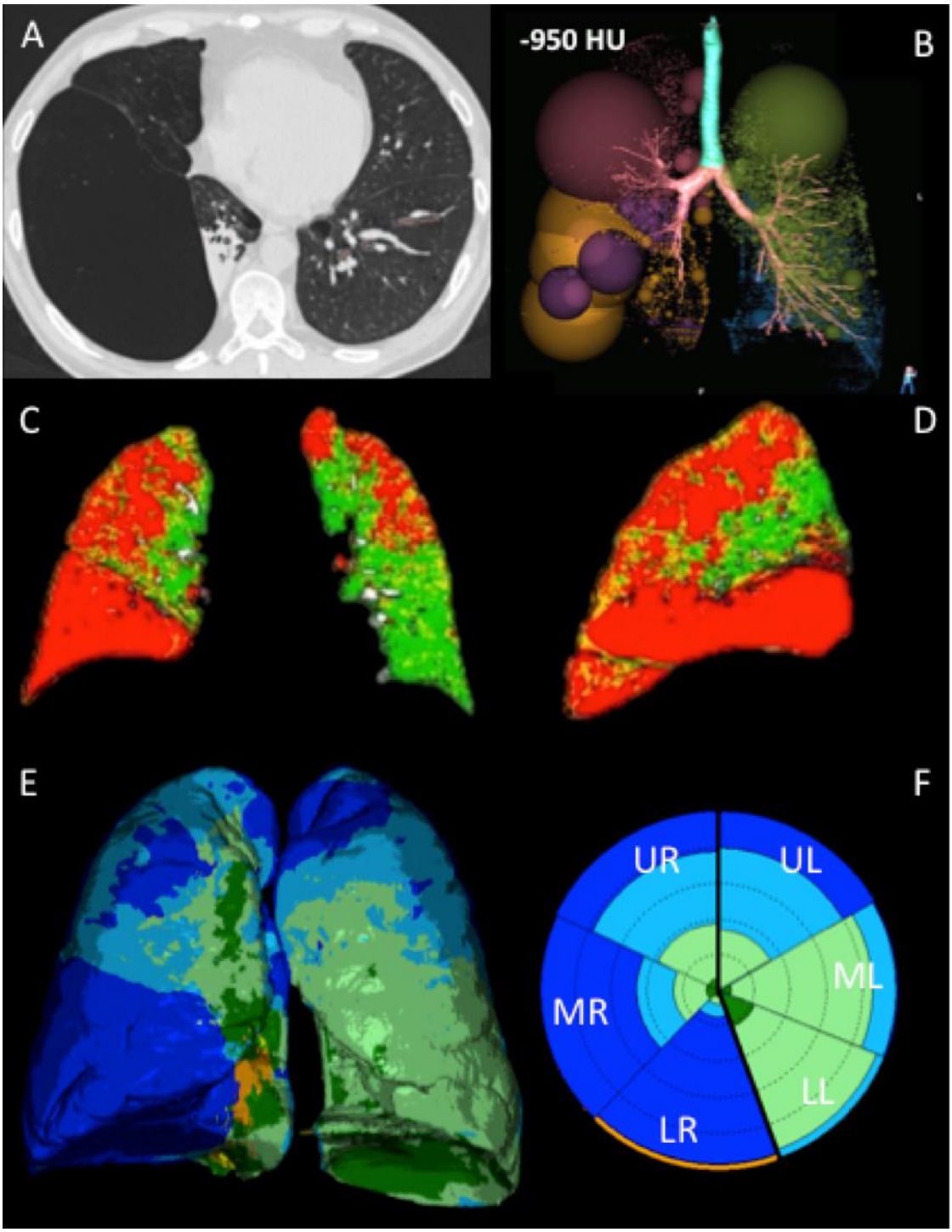
A
-950 HU
B
C
D
E
F
UR
UL
ML
MR
LL
LR

Figure 2. The three clusters of COPD patients stratified represented as glyphs. Clusters (G1 to G3) were the result of quantitative unsupervised clustering based on a dissimilarity matrix that captures the distribution of classified parenchymal patterns recognized by CALIPER. G1 was characterized by predominant Normal (*dark green*) and Mild LAA (*light green*) patterns, whereas G2 by predominant Moderate LAA (*light blue*) pattern and G3 by predominant Severe (*dark blue*) and Moderate LAA (*light blue*) patterns. The size of each glyph represents patient lung volume.

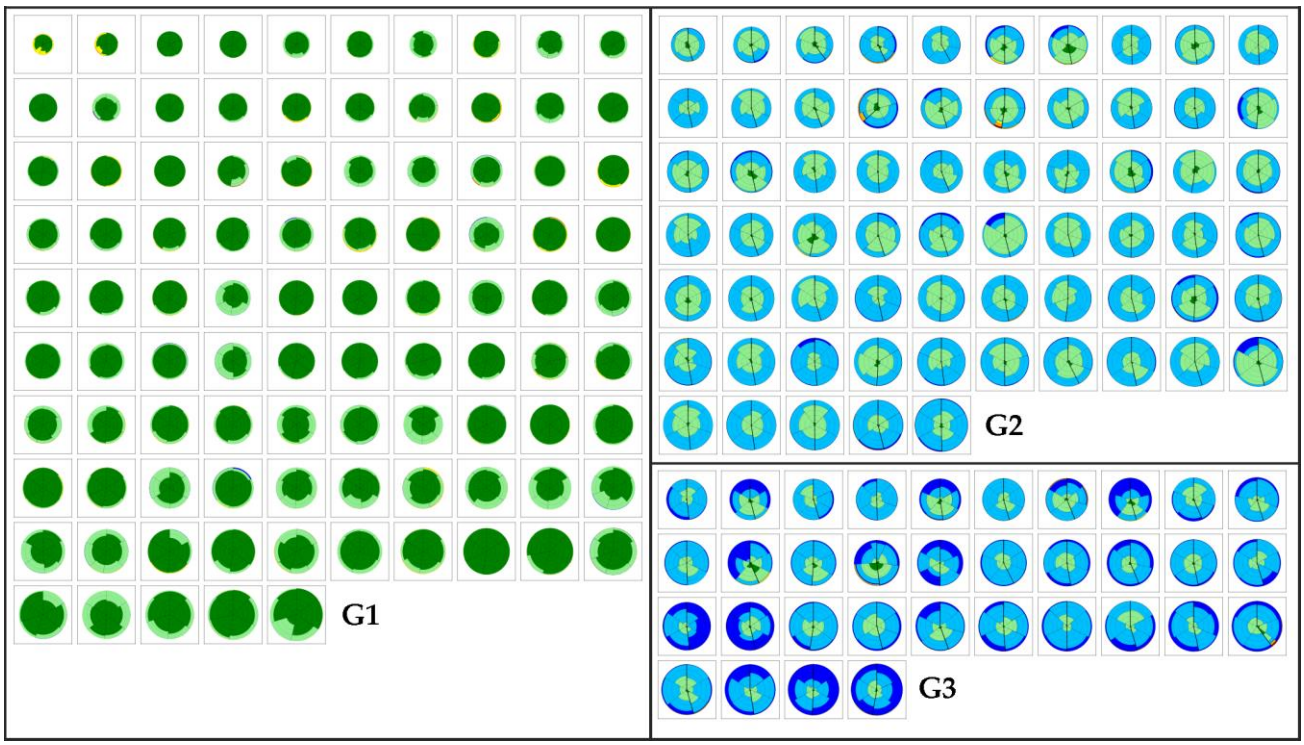

Figure 3. ROC curve over the range of the logistic regression model output for severe emphysema (A) and no emphysema (B). Severe emphysema was defined at CT scan as $\%LAA_{-950insp} \geq 14$ by VIDA whereas no emphysema was defined at CT scan as $\%LAA_{-950insp} < 6$ by VIDA. The total AUC area was of 0.88 for severe emphysema and 0.86 for no emphysema.

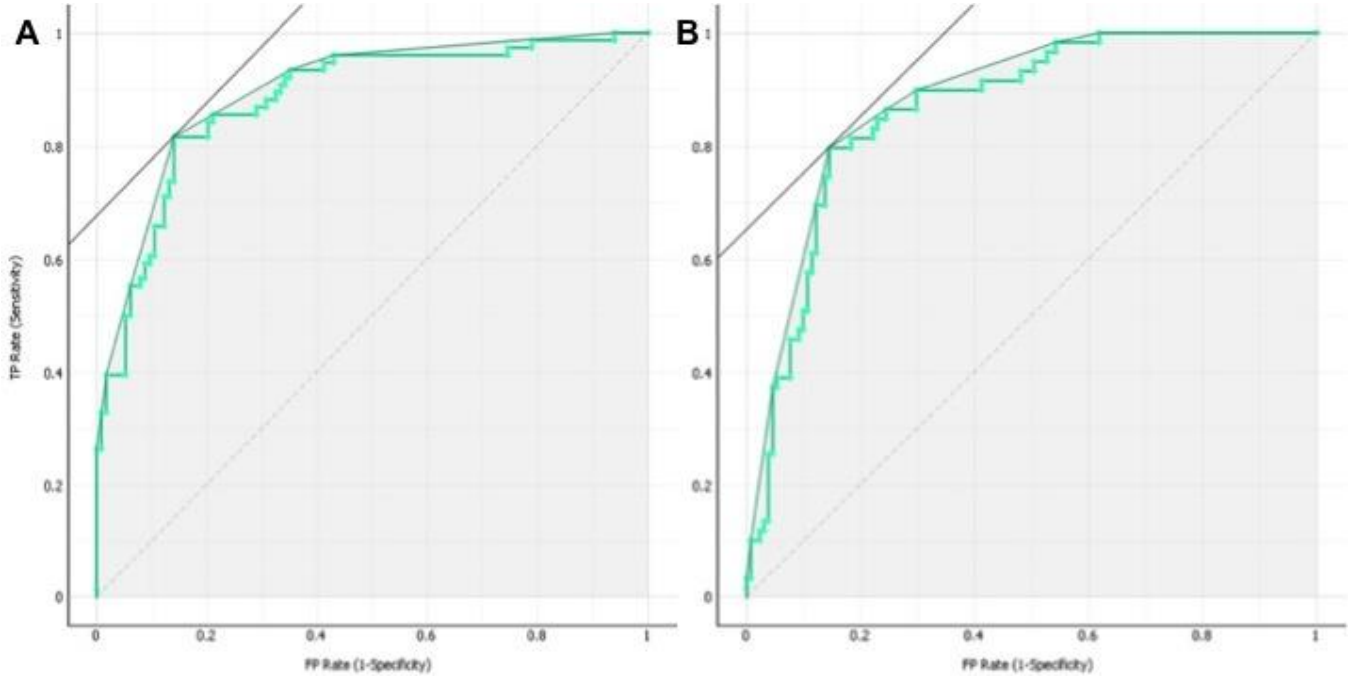

Figure 4. Maximal expiratory flow-volume curves of two representative subjects with severe emphysema or no emphysema. Patient with severe emphysema (*left panel*) had $\%LAA_{-950insp}$ =24 whereas the patient with no emphysema (*right panel*) had $\%LAA_{-950insp}$=4 at CT. Note the flatter slope in the former when flow was plotted against expired volume (*black lines*) but not pletysmographic thoracic volume (*grey lines*), indicating greater thoracic gas compression at high-to-mid lung volumes.

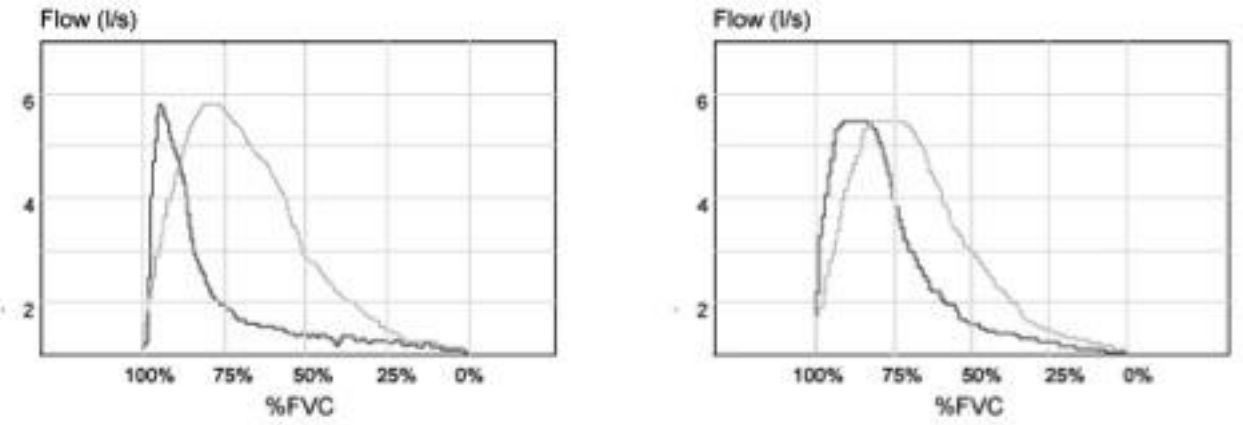

7.8 Supplemental Material

7.8.1 Theoretical background and description of ESI method

In the past many studies in human subjects have shown the presence of a functional association between the airflow at mouth, the instantaneous volume of the lung, and the pressure applied on the surface of the lung. (11,31,32) In particular the analysis of the MEFV curve has been used for many years to characterize the functional behavior of the bronchial tree and the surrounding parenchyma.

In this study we tested a parametric biomechanical model representing a theoretical approximation of the shape of the descending limb of the MEFV curve to assess the severity of emphysema in patients with COPD by spirometry. The Emphsyema Severity Index (ESI) application software is based on a mathematical model developed to approximate the MEFV curve of each subject to ultimately provide a quantitative score ranging from 1 to 10. The ESI score represents a practical application of a biomechanical model developed a priori. No retrospective statistical inference or standardization of input parameters was required.

The main physical principle inspiring this approach is that the pressure lost (*Pl*) at a given time *t* along an airway segment could be considered proportional to a specific friction factor (*Ff*), the air density (*d*) and the air velocity (*v*), similarly to the theory of the circular ducts. An inverse relationship between the pressure lost

and the mean diameter (*D*) of the airway is also supposed obtaining the following equation (better known as Darcy equation):

$$Pl = \frac{Ff \cdot d \cdot v^2}{2 \cdot D} \quad [1]$$

By considering the hypothesis of laminar flow, the calculus of the friction factor depends uniquely on the Reynolds number *Rn*

$$Ff = \frac{k1}{Rn} \quad [2] \text{ where } \quad Rn = \frac{v \cdot D}{vis} \quad [3]$$

k1 is a constant and the variable *vis* is the dynamic viscosity of the air fluid.

Substituting equations [2] and [3] into equation [1] we obtain the pressure drop in the case of laminar flow as:

$$Pl = \frac{k1/2 \cdot vis \cdot d \cdot v}{D^2} \quad [5]$$

Considering a circular airway section we can write the air velocity in the segment as:

$$v = \frac{4 \cdot \Phi}{D^2 \cdot \pi} \quad [6]$$

where Φ is the resulting flow and *D* is the mean inner diameter of the airway segment. Substituting equation [6] into [5] we obtain the association between the airflow and the pressure lost, as of laminar flow hypothesis.

$$Pl = \frac{k2 \cdot vis \cdot d \cdot \Phi}{D^4} \quad [7]$$

Equation [7] shows that the relationship between the pressure lost and the airflow seems to be linear in laminar flow approximation.

In the past some authors proposed lumped parametric models to fit the MEFV curve acquired during maximal effort test, taking into account linear association profiles between airways resistance and airflow. The studies obtained acceptable waveforms and good fitting of the curve. (32)

At variance with past models, we proposed a mathematical model for the approximation of the MEFV curve developed under the hypothesis that the airflow measured at the mouth through standard spirometry could not be considered as a laminar flow. As a consequence the *Ff* variable could not be calculated as a scaled inverse of the Reynolds number *Rn* (laminar flow), but a more complex calculation is required to estimate the pressure drop. Colebrook proposed the following equation for the calculation of the friction factor, where *Ru* is the mean relative roughness of the airway segment (4):

$$\frac{1}{Ff^{0.5}} = -2 \cdot log10\left(\frac{Ru}{3.7 \cdot D} + \frac{2{,}51}{Rn \cdot Ff^{0.5}}\right) \quad [8]$$

Although the Colebrook's equation is usually solved numerically due to its implicit nature, simplified versions have been proposed in the past (i.e. the Altshul-Tsal (33) formulation to estimate an approximated *Ff* factor). Nonetheless, despite of the analytical procedure for the estimation of *Ff,* the final equation that describes the pressure drop is the following:

$$Pl = \frac{K3 \cdot Ff \cdot d \cdot \Phi^2}{D^5} \quad [9]$$

where *K3* and *Ff* are constant values for a specific patient and airway segment, *d* is the air density, *Φ* is the resulting flow and *D* is the mean inner diameter.

One interesting observation deriving from these mathematical models is that the pressure drop *Pl* along a segment is inversely proportional to the diameter of the airway power 4 or 5. It follows that a minimal variation in airway diameter is amplified to cause a significant pressure drop along the whole segment. This shows how the regulation of the respiratory airways walls efficiently modulates the airflow.

Another important characteristic of the non-laminar flow hypothesis is the quadratic association between the airflow and the pressure lost along the airways, while this relationship would be linear if the measured flow at the mouth was hypothesized as laminar.

As a consequence the lumped parametric model of a maximal flow volume curve implemented in the ESI model is based on the following non-linear equation:

$$\Phi(V) = \frac{1 - a1 \cdot V^2}{a2 + a3 \cdot V^2} \quad [10]$$

where the numerator represents a simple model of the quadratic pressure profile during a maximal function test and the denominator represents the model of the exhaled volume-dependent quadratic airways resistance profiles. The best *a1*, *a2* and *a3* coefficients are estimated iteratively by the software, which performs a Least Mean Squares fitting of the descending limb of the MEFV curve.

Once the best mathematical model fitting the raw data is obtained, the software then proceeds to the calculus of the first and second derivatives for the specific fitted MEFV curve. This procedure is performed to search the inflection point *Vf* of the descending limb of the MEFV curve.

$$\frac{\partial'' \Phi(V)}{\partial V} = 0 \quad [11]$$

The point *Vf* is very important in assessing emphysema severity, as its abscissa represents the lung volume (in liters) at which the resistance profile becomes influenced by the lost in elastic recoil due to the parenchymal destruction. This creates an inversion in the concavity of the descending limb of the MEFV curve.

This type of analysis was not possible before because of the hypothesis of the above-mentioned linear models. Indeed, in those models the second derivatives profiles did not admit acceptable solutions to the equation [11].

After the solutions of equation [11] are calculated, the first derivative is then evaluated in correspondence of the acceptable solution (volume value) *Vf* and re-mapped between 0-10 over the angle range *(20° - 80°)* generating the quantitative index called ESI. The computation does not require standardization of input parameters, as it is directly related to the shape of the curve. Therefore, ESI is independent from percentage predicted values of pulmonary function variables. ESI value was computed in each patient using a specifically developed software application, based on the above theoretical basis. A numerical output value ranging from 0 to 10 was used to stratify the dataset of 194 COPD patients according to the estimated emphysema severity.

The Figure 1S shows a box-plot representing the $\%LAA_{-950insp}$ distribution (I-III quartiles) in the validation dataset in three subgroups: no emphysema (NE, $\%LAA_{-950insp} < 6$), moderate emphysema (ME, $6 \leq \%LAA_{-950insp} < 14$), and severe emphysema (SE, $\%LAA_{-950insp} \geq 14$). The intersection of the ESI values (*red line*) with the corresponding box indicates the most probable severity class for the case analyzed. In this example the case analyzed had a low probability of having SE.

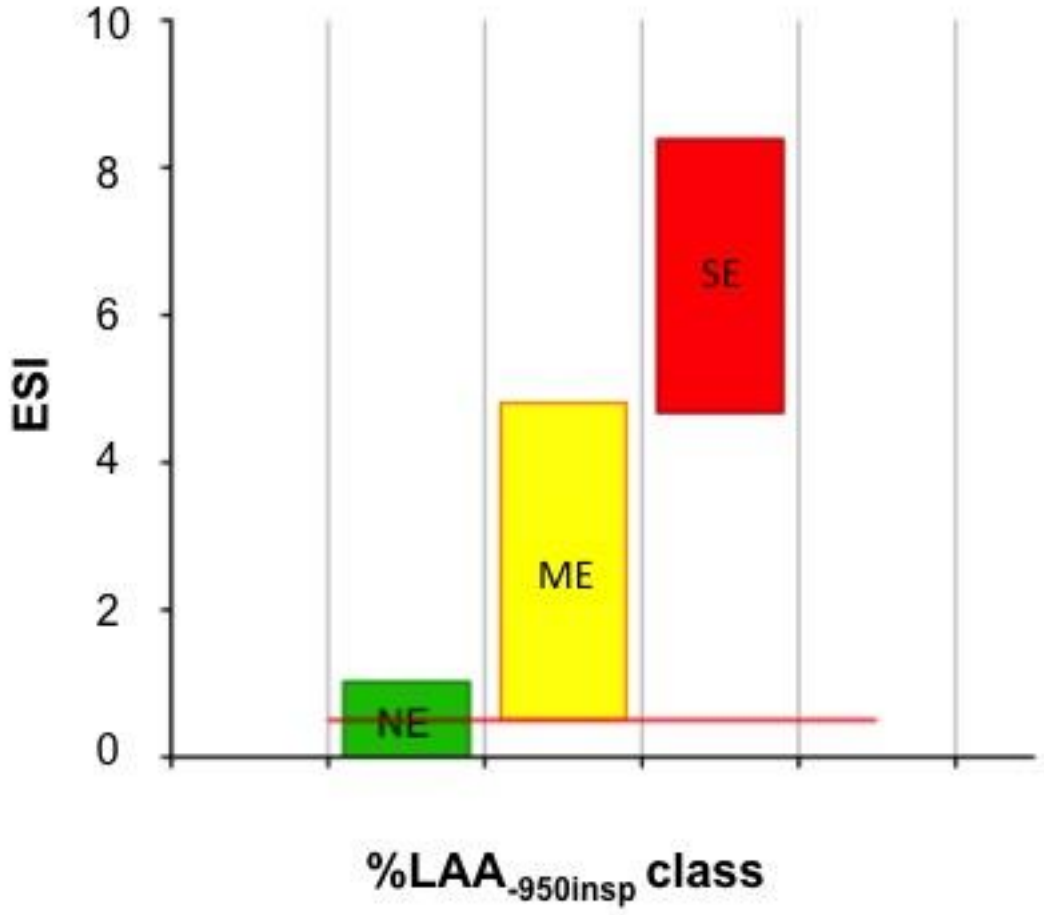

7.8.2 Post-processing imaging techniques

Figure 2S show images obtained by using VIDA software program in two COPD patients. Panel A shows the results obtained in a patient with advanced destructive emphysema whereas panel B shows the results obtained in a patient with small airway disease. In panel A the parenchymal destruction at axial CT scan correlates with the big bullae of $\%LAA_{-950insp}$ detected by VIDA analysis. Vessels are lacking in emphysematous areas. In panel B the thickening of airway walls and the tiny bilateral ground-glass micronodules on axial CT scan are consistent with small airway disease. Although no significant areas of emphysema were found by VIDA analysis, the gas trapping at end-expiration due to airway disease was evident.

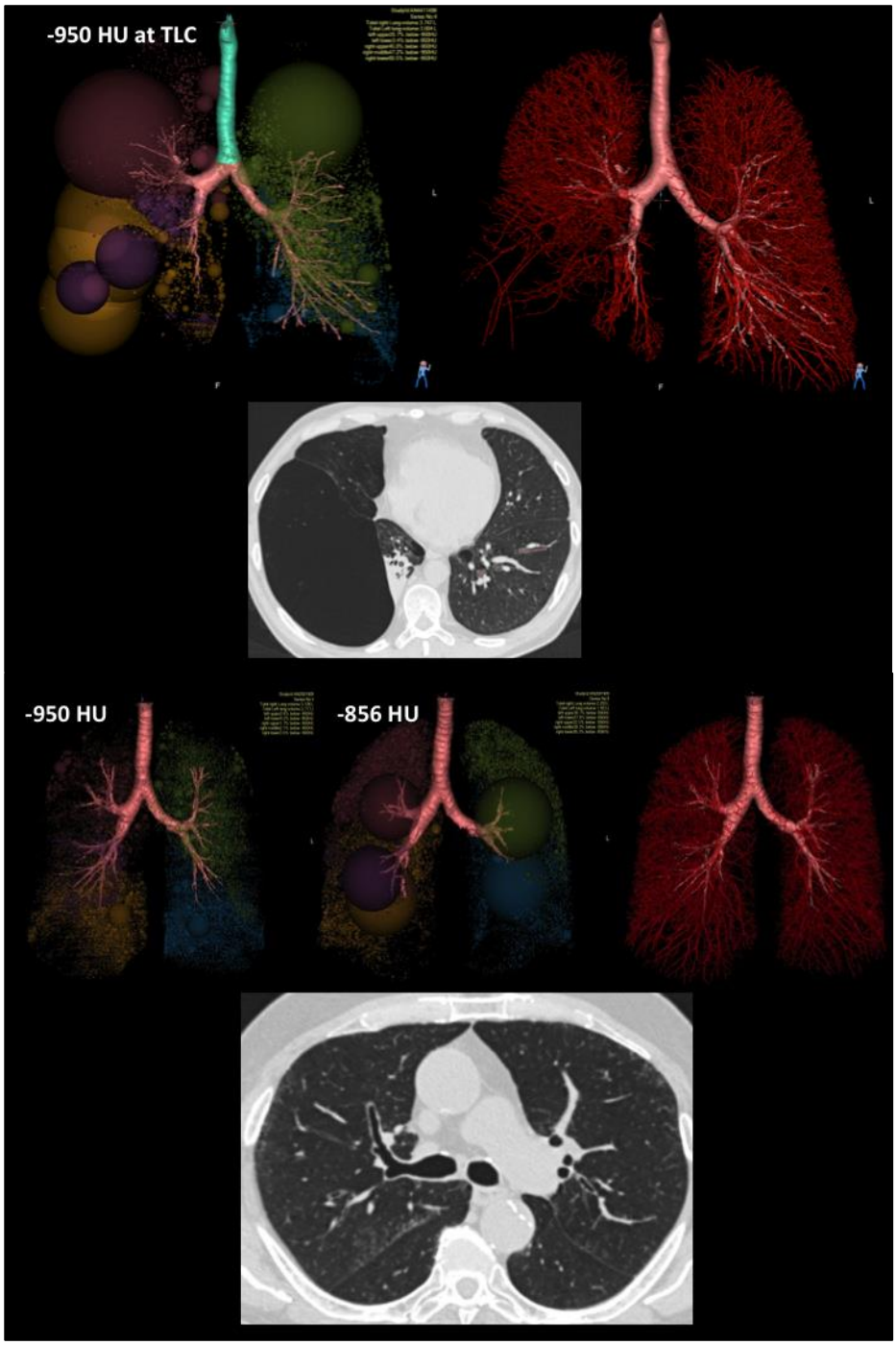

A

B

Figure 3S shows coronal and sagittal pulmonary parametric response maps obtained by using Imbio LDA analysis in a subject with emphysema predominantly located in lower lobes. The parametric response maps identify and localize the three color-coded density patterns at co-registration analysis: normal lung in green (percentage of voxels with CT attenuation greater than -950 HU at inspiration and greater than -856 HU at expiration), persistent low density area in red (%pLDA, voxels with CT attenuation below -950HU at inspiration and below -856HU at expiration), and functional low density area in yellow (%fLDA, voxels with CT attenuation above -950HU at inspiration and below -856HU at expiration).

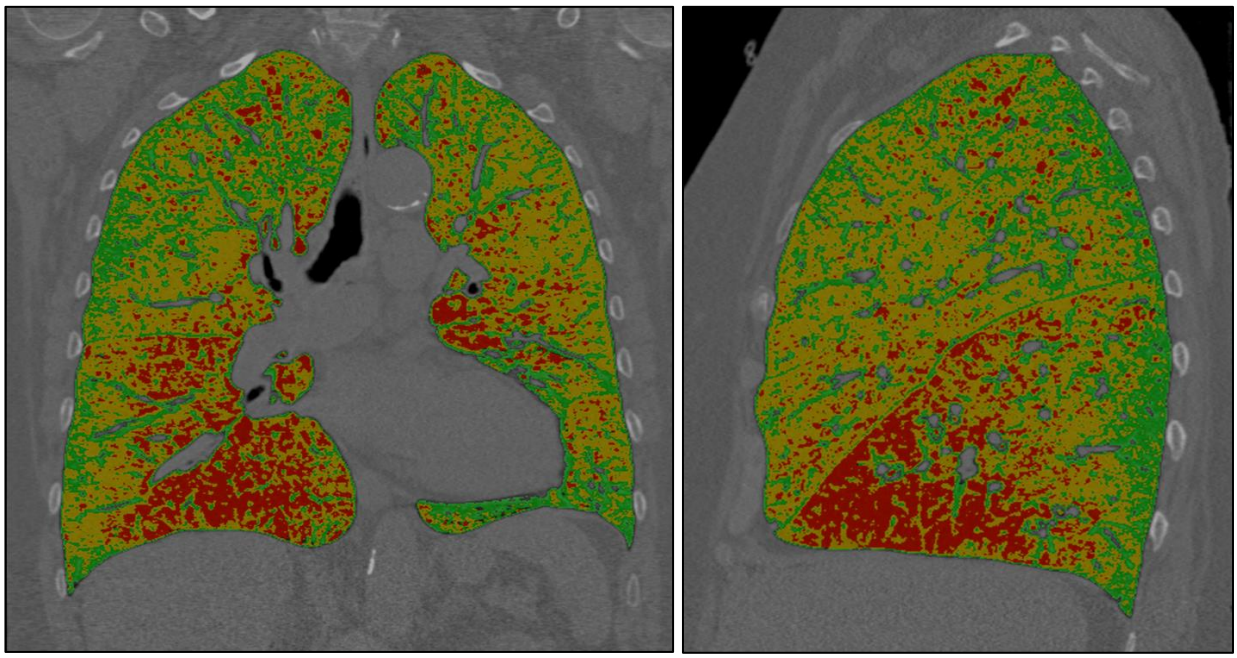

Figure 4S shows the permuted dissimilarity matrix illustrating the abnormality based pairwise dissimilarities (brighter the shade higher the dissimilarity) among the features extracted by CALIPER and obtained with SILA. The nine blocks represent the first-pass clusters and the three diagonal blocks represent the final three unique stratified clusters (G1, G2, G3).

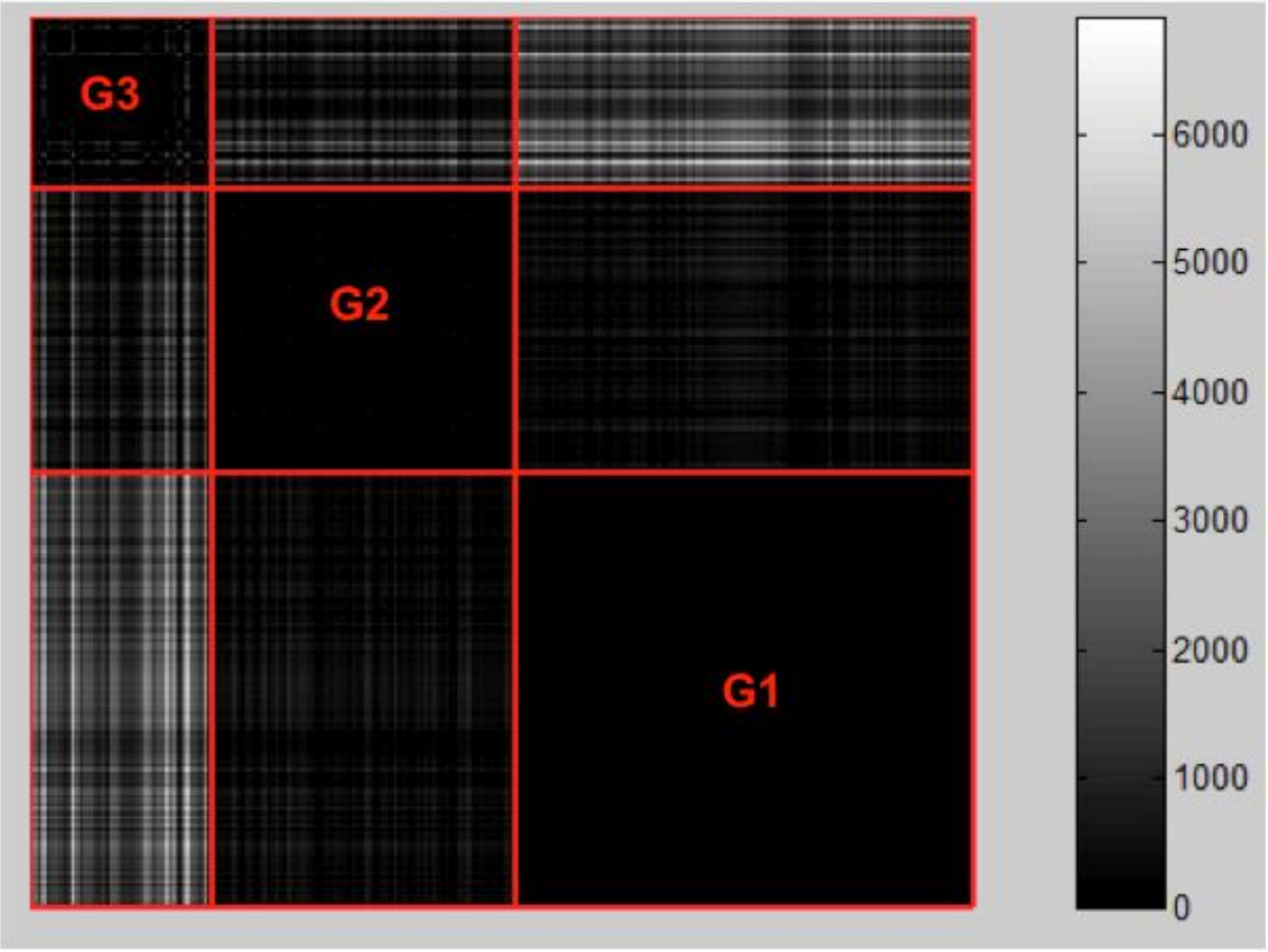

Chapter 8 - Validation ESI model

In the previous chapter we have proposed a mathematical model (ESI method) to predict the presence of emphysema as assessed at CT by using functional parameters derived from MEFV curve. The model was built using the Italian cohort of CLIP-COPD Study. To validate our model we tested it in the largest population of COPD patients available worldwide: the COPDGene Study population. Despite our cohort, this population included thousands of subjects and different ethnicities.

The value of maximal expiratory flow-volume curve in estimating the presence and severity of emphysema as assessed on CT

Mariaelena Occhipinti, Matteo Paoletti, Elizabeth Regan, David A. Lynch, James D. Crapo, Stefano Colagrande, Edwin K. Silverman, Massimo Pistolesi and the COPDGene investigators

(Accepted for Presentation at American Thoracic Society Conference, Dallas, 17-18/05/2019)

Rationale: To assess whether a mathematical model derived from the maximal expiratory flow-volume (MEFV) curve could predict with accuracy the severity of emphysema as defined by parameters derived from quantitative computed tomography (CT). To validate the model in a large population of subjects with chronic obstructive pulmonary disease (COPD).

Methods: CT metrics of emphysema were assessed on the inspiratory CT scans of 194 white COPD patients who underwent pulmonary function testing. Three groups of emphysema severity were identified according to CT metrics of emphysema (low attenuation area below -950HU at inspiration, $\%LAA_{-950insp}$): no emphysema ($\%LAA_{-950insp}<6\%$), mild-moderate emphysema ($6\%<\%LAA_{-950insp}<14\%$), and severe emphysema ($\%LAA_{-950insp}>14\%$).

An index to estimate emphysema severity (ESI) as assessed by CT was developed by using a parametric mathematical model fitting the descending portion of MEFV curve. A numerical output value ranging from 0 to 10 was used to stratify the dataset according to the estimated emphysema severity. Model outputs were then compared to CT metrics to evaluate the performances of ESI model. Validation of the model was performed on 4000 COPDGene subjects, including whites and African Americans.

Analysis of variance, Welch t, and Games-Howell post-hoc tests were used to evaluate differences between the three groups of emphysema defined by CT metrics. ROC curve (AUC) analysis was used to calculate the accuracy of the model by varying the threshold over the range of the ESI score.

Results: Subjects were distributed across GOLD stages I to IV and evenly distributed across the three groups of emphysema severity (59 with no emphysema, 58 with moderate emphysema, 77 with severe

emphysema). Mean of the ESI score differed significantly among the three emphysema severity groups (p<.001) in both the first cohort and the COPDGene population, with lower scores (<5) in subjects with severe emphysema and higher scores (>5) in patients with no or mild emphysema. The model had an overall 85% accuracy (87% sensitivity and 83% specificity) in the first cohort and 82.5% accuracy (82% sensitivity and 83% specificity) in the COPDGene population.

Conclusions: Milder and severe emphysema as assessed by quantitative CT can be accurately estimated by a mathematical model based on the MEFV curve. The model was created uniquely on unstandardized functional data derived from the MEFV curve, avoiding the use of percent-predicted values, anthropometric and ethnicity parameters. These characteristics make this approach convenient for clinical trials as well as for clinical routine.

Chapter 9 - Which criteria to define COPD?

In the previous chapters we have shown that statistical models including either BMI and functional data or parameters of the flow-volume curve can estimate with a considerable accuracy the emphysema extent as assessed on quantitative CT in a population of subjects diagnosed with COPD. However, the criteria to define expiatory airflow obstruction are still matter of international debate (1)(2).

We aimed at investigating the functional and radiological presentation of those subjects defined as COPD by Global Initiative for Chronic Obstructive Lung Disease (GOLD) criterion ($FEV_1/FVC<0.70$) but excluded by European Respiratory Society/American Thoracic Society criterion ($FEV_1/FVC<LLN$).

Unmasking COPD in patients excluded by the lower limit of normality

Mariaelena Occhipinti, M Paoletti, C Nardi, M Palazzi, G Camiciottoli, R inchingolo, S Colagrande, AR Larici, M Pistolesi

(Oral presentation at the ESTI Congress - European Society Thoracic Imaging, Geneva, 24-26/05/2018)

9.1 Background

Airflow limitation has been defined by the GOLD when the post-bronchodilator fixed ratio of FEV_1 to FVC is less than 0.7, regardless of age and sex of the patient (3). Despite of the its simplicity of use in daily clinical practice (4), the fixed ratio does not take into account the normal age-dependent decline in lung function, with a consequent overdiagnosis of chronic obstructive pulmonary disease (COPD) in older people and underdiagnosis in younger people (5, 6). At 80 years of age 20–25% of the reference population would have low values compatible with pathological airflow limitation instead of the expected 5%, with a consequent high rate (75–80%) of false positive results (5).

Due to the general aging of the population, age differences are going to play an important role in the definition of disease in next future. To overcome the issue of overdiagnosis in the elderly, the European Respiratory Society/American Thoracic Society task force recommended to use a criterion based on the lower limit of normal (LLN) values, appropriate for age, sex, and ethnicity of the individual to define obstruction at spirometry (1, 2, 7). Equations to predict the correct reference values for spirometry in each individual were derived from about 80,000 subjects of both sexes and many ethnicities, across all ages (3 to 95 years) (8). According to the LLN criterion, patients diagnosed with COPD by GOLD criteria may be excluded and considered as non-obstructed.

As the population gets older, recognition of the imaging features of “normal” aging is likely to become increasingly important to differentiate from clinically significant disease (9). The lungs age and it has been suggested that COPD is a condition of accelerated lung aging (10). The distinction between normal aging lung

and COPD is a big challenge and of great interest nowadays. Post-processing imaging tools enable the quantification of parenchymal destruction as well as small airway disease. However, qualitative analysis of chest CT images provides invaluable data on the presence not only of COPD signs but also of paraphysiological abnormalities due to aging.

We aimed at investigating the presence of imaging findings indicative for COPD with both quantitative and qualitative analyses of CT scans in those subjects excluded by LLN criteria, a group older than those included by LLN criteria. Furthermore, we used qualitative analysis to define the COPD subtypes in this subset of population and to assess the concordance between readers. Finally, we evaluated the accuracy of our predictive statistical models in estimating the risk of having emphysema at CT in the group of subjects included by GOLD and in those included by ERS criteria.

9.2 Methods

This was a two-center study approved by the institutional Ethics Committees of the University of Florence and the Catholic University of Sacred Heart in Rome. The study was based on a retrospective interpretation of prospectively acquired data. From January 2012 to December 2016, subjects with diagnosis of COPD (FEV1/VC<0.70) (2, 7, 11) were considered for inclusion if they satisfied the following inclusion criteria: age 40-85 years, smoking history >10 pack-years, no COPD exacerbations within one month, no diagnosis of asthma or cardiac disease, and acceptance to participate by written informed consent. Sixteen out of 232 eligible subjects were excluded because of incomplete data. Part of the 216 subjects enrolled participated in previous studies (12-14).

9.2.1 Functional evaluation

Subjects underwent complete pulmonary function tests by using a mass-flow sensor and multigas analyser (V6200 Autobox Body Plethysmograph Sensor Medics, Yorba Linda, USA, or Platinum Elite™ Body Plethysmograph, Medical Graphics Corporation, St. Paul, MN, USA), arterial blood gases by Radiometer ABL90 FLEX or ABL800 FLEX (Brønshøj, Denmark). Pre- and post-bronchodilator spirometry, lung volumes, and single-breath DLco were obtained according to standard ATS/ERS (American Thoracic Society/European Respiratory Society) recommendations (15-17). All subjects had $FEV_1/FVC<0.70$ and 157 also below the lower limit of normality (LLN) criterion, defined as the 5^{th} percentile of the reference population (Table 1) (2, 7, 11). LLN individual values were obtained by using the online calculator (http://gligastransfer.org.au/calcs/spiro.html) by the Global Lung Function Initiative of the ERS. The automated calculator uses prediction equations derived from about 80,000 subjects of both sexes and many ethnicities (8).

9.2.2 CT scanning technique and analysis

In each center volumetric chest CT scans were obtained by the same team and the same CT scanner (SOMATOM Sensation 64, Siemens, Erlangen, Germany, or SOMATOM Definition FLASH 128, Siemens,

Erlangen, Germany) within 48 hours of the functional evaluation. CT scans were acquired at full inspiration and forced end-expiration using the acquisition protocol adopted in the COPDGene Study (18) with the following parameters: 120 kVp, 200 mAs, rotation time 0.5 sec, slice thickness 0.6 mm, pitch 1.1 and reconstructions kernels b31f (smooth) and b70f (sharp). Subjects were instructed on how to perform respiratory maneuvers while lying supine in the CT scanner with arms fully abducted. No contrast medium was injected.

Quantitative analysis was performed on images with reconstruction kernel b31f by using two different software programs (VIDA and Imbio LDA). VIDA software provided relative volumes of lung attenuation areas with values below -950 HU at inspiration ($\%LAA_{-950insp}$) and below -856 HU at expiration ($\%LAA_{-856exp}$) to quantify emphysema and total gas trapping, respectively. Imbio LDA provided relative volumes of functional low density area (%fLDA), persistent low density area (%pLDA), and normal lung (%Normal).

Qualitative analysis was performed according to the Fleischner Statement criteria to define COPD subtypes, including advanced destructive emphysema (ADE), confluent centrilobular emphysema, moderate centrilobular emphysema, mild centrilobular emphysema, trace centrilobular emphysema, panlobular emphysema, mild paraseptal emphysema, substantial paraseptal emphysema, and airway-predominant disease (19). Two radiologists (one dedicated thoracic radiologist and one general radiologist) evaluated all CT scans first separately and then after 4 months in consensus.

9.2.3 Statistical model application

The binary logistic regression models presented in Chapter 3 (BMI, $FEV_1\%$, FEV_1/VC, DLco%) and Chapter 5 (BMI, FEV_1/FVC, slope of the flow-volume curve between 25% and 50% of FVC) were applied to the whole group of subjects ($FEV_1/FVC < 0.7$) as well as in the subgroup with $FEV_1/FVC <$ LLN.

9.2.4 Data analysis and statistics

Welch's *t*-test was used to evaluate differences in functional, anthropometric, and CT metrics data among groups included and excluded by LLN criterion.

Agreement between the two readers was tested by using k-Cohen coefficient.

ROC curve (AUC) analysis was used to calculate the accuracy of the models considering a logistic probability threshold (p_{th}) at value of 0.5.

The software programs included Mathcad (version 2001; Mathsoft), SPSS/PC WIN 11.5.1 (SPSS, Chicago, IL), and C++ programming language. Values of p lower than 0.05 indicated statistical significance. Data are expressed as mean and standard deviation (SD).

9.3 Results

The use of the LLN to our population excluded 46/216 (21.3%) patients. The anthropometric, functional, and imaging characteristics of the group excluded by LLN criteria is detailed in Table 1. Sex, age, BMI, and

smoking history were not statistically different between the group included and the group excluded by LLN criteria. The group excluded by LLN criteria had a significantly higher FEV_1/FVC, FEV_1/VC, DLco% and lower TLC, RV, FRC, RV/TLC. Emphysema and gas trapping were significantly lower in the group excluded by LLN criteria, with average values of normality (19, 20).

Patients complained of cough (28/46, 61%), sputum (18/46, 39%), and wheezing (1/46, 2%), with an average modified Medical Research Council questionnaire of 2. Smoking history was similar to those defined COPD by using the GOLD criteria.

At *quantitative CT* analysis the group excluded by LLN differed significantly from those included as of amount of emphysema ($\%LAA_{-950insp}$ and %pLDA), total gas trapping ($\%LAA_{-856exp}$), and functional gas trapping (%fLDA) (Table 1).

At *qualitative CT* analysis consensus reading identified signs of COPD in all 46 subjects excluded by LLN criteria. In particular, 3 subjects presented with airway disease, 16 with paraseptal emphysema, and 27 with centrilobular emphysema (Table 2). Nineteen out of 46 cases (41%) were moderate-to-severe emphysema subtypes, by grouping those with any kind of moderate-to-severe emphysema (substantial paraseptal emphysema, advanced destructive emphysema, confluent centrilobular emphysema, and moderate centrilobular emphysema). Sixteen out of 46 cases (35%) excluded by LLN criterion had paraseptal emphysema, which is a higher rate than in the general COPD population reported in literature.

Concordance between the readers was good (k= 0.61) (Figure 1). This result suggests that a dedicated training is not mandatory to classify COPD subtypes. The biggest difference was noted between airway disease and mild centrilobular emphysema, as the cases defined as airway disease by the thoracic radiologist were classified as either mild or trace centrilobular emphysema by the general radologist (Figure 2).

The binary logistic regression model including the slope of the flow-volume curve between 25% and 50% of FVC (S_{25-50}), BMI, and FEV_1/FVC predicted the probability of having emphysema with 85% accuracy (87% sensitivity and 81% specificity) in the whole group of subjects (GOLD criterion) and 82% accuracy (82% sensitivity and 83% specificity) in the subgroup with FEV_1/FVC<LLN (ERS/ATS criterion) (Figure 3). The probabilistic model including BMI, FEV1%, FEV1/FVC, and DLco% predicted the probability of having emphysema with 80% accuracy in the whole group of subjects (GOLD criterion) and 77% accuracy in the subgroup with FEV_1/FVC<LLN (ERS/ATS criterion) (Figure 3).

9.4 Tables

Table 1. Anthropometric, pulmonary function, and CT metrics data of: A) GOLD dataset (patients with COPD enrolled according to GOLD criterion of the fixed ratio of FEV_1/FVC <0.70); B) LLN dataset (patients with COPD enrolled according to LLN criterion); C) patients excluded by LLN criterion. Data are reported as mean (SD). Welch's *t* robust test was used to test the hypothesis that the two B-C subgroups had equal means. Smoking history is expressed as pack-years.

	A) GOLD dataset	B) LLN dataset	C) Patients excluded by LLN criteria	Welch's t test (B vs C)
N	216	170	46	
Sex (M:F)	169:47	131:39	39:7	-
Age (years)	70.2 (8.0)	69.9 (8.3)	71.2 (7.2)	ns
BMI (kg/m^2)	26.5 (4.6)	26.3 (4.5)	27.5 (4.84)	ns
Smoking history	51.7 (27.0)	50.8 (23.9)	55.1 (37.3)	ns
FEV_1%	62.6 (25.8)	56.0 (22.6)	90.0 (21.0)	p<.01
FEV_1/VC (%)	47.5 (13.2)	43.9 (11.6)	62.8 (7.2)	p<.01
FEV_1/FVC (%)	52.3 (13.1)	48.6 (11.5)	67.6 (7.1)	p<.01
TLC%	108.2 (16.5)	110.7 (16.6)	97.6 (11.3)	p<.01
DLco%	68.9 (23.5)	64.3 (22.1)	86.6 (22.3)	p<.01
RV%	137.0 (46.7)	146.3 (45.5)	97.7 (26.8)	p<.01
FRC%	129.5 (32.6)	135.7 (32.0)	103.9 (19.6)	p<.01
RV/TLC (%)	49.9 (14.1)	52.6 (13.9)	38.7 (8.2)	p<.01
$\%LAA_{-950insp}$	14.3 (11.7)	16.3 (12.0)	6.1 (5.2)	p<.01
$\%LAA_{-856exp}$	45.2 (20.3)	49.2 (19.0)	28.4 (16.7)	p<.01
%fLDA	36.9 (13.7)	38.8 (12.8)	28.3 (14.5)	p<.01
%pLDA	12 (11.7)	16.3 (12.0)	7.5 (5.2)	p<.01

Legend: BMI = body mass index, DLco% = percentage of predicted diffusing capacity of lung for carbon monoxide, FEV_1% = percentage predicted of forced expiratory volume in 1 second, %fLDA = percentage of functional low density area, FRC% = percentage of predicted functional residual capacity, FVC% = percentage of predicted forced vital capacity, $\%LAA_{-950insp}$ = percentage of lung attenuation area with values below -950 Hounsfield Units at inspiratory CT scan, $\%LAA_{-856exp}$ = percentage of lung attenuation area with values below -856 Hounsfield Units at expiratory CT scan, %pLDA = percentage of persistent low density area, RV% = percentage of predicted residual volume, TLC% = percentage of predicted total lung capacity, VC = vital capacity.

Table 2. Qualitative analysis of chest CT scans. Distribution of COPD subtypes in subjects with FEV_1/FVC >LLN. Data represent case numbers.

Centrilobular emphysema (27)						Paraseptal emphysema (16)		Airway disease
ADE	Confluent	Moderate	Mild	Trace	Panlobular	Substantial	Mild	
2	4	6	6	9	0	7	9	3

9.5 Figures

Figure 1. Distribution of COPD subtypes at qualitative CT analysis performed by a dedicated thoracic radiologist and a general radiologist in 46 subjects excluded by LLN criterion. Differences in classification were greater in airway disease and mild centrilobular emphysema.

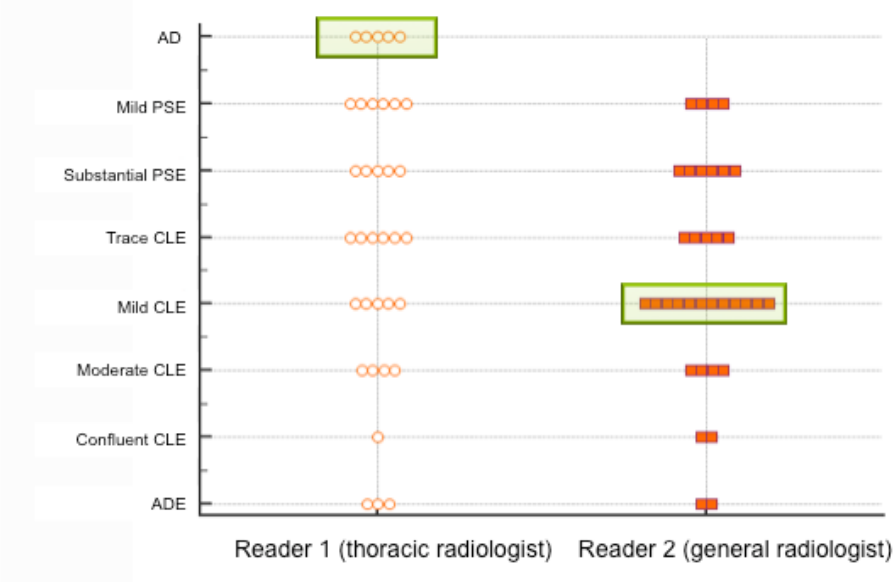

Legend: AD=airway disease, ADE= advanced destructive emphysema, CLE= centrilobular emphysema, PSE= paraseptal emphysema.

Figure 2. Similarities and dissimilarities in classification of COPD subtypes at qualitative CT analysis performed by a dedicated thoracic radiologist and a general radiologist in 46 subjects excluded by LLN criterion.

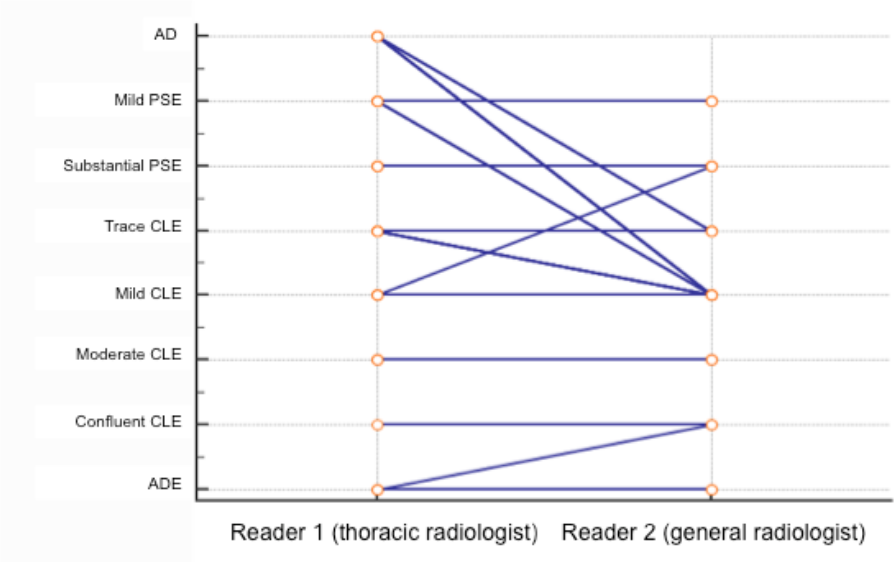

Legend: AD=airway disease, ADE= advanced destructive emphysema, CLE= centrilobular emphysema, PSE= paraseptal emphysema.

Figure 3. ROC curves of the two logistic models. The *black curves* represent the MEFV curve-based model for subjects with $FEV_1/FVC<0.70$ (*left panel*) and for subjects with with $FEV_1/FVC<LLN$ (*right panel*). The *grey curves* represent the DLco-based model for subjects with $FEV_1/FVC<0.70$ (*left panel*) and for subjects with with $FEV_1/FVC<LLN$ (*right panel*). *Grey curves* data are derived from reference (21).

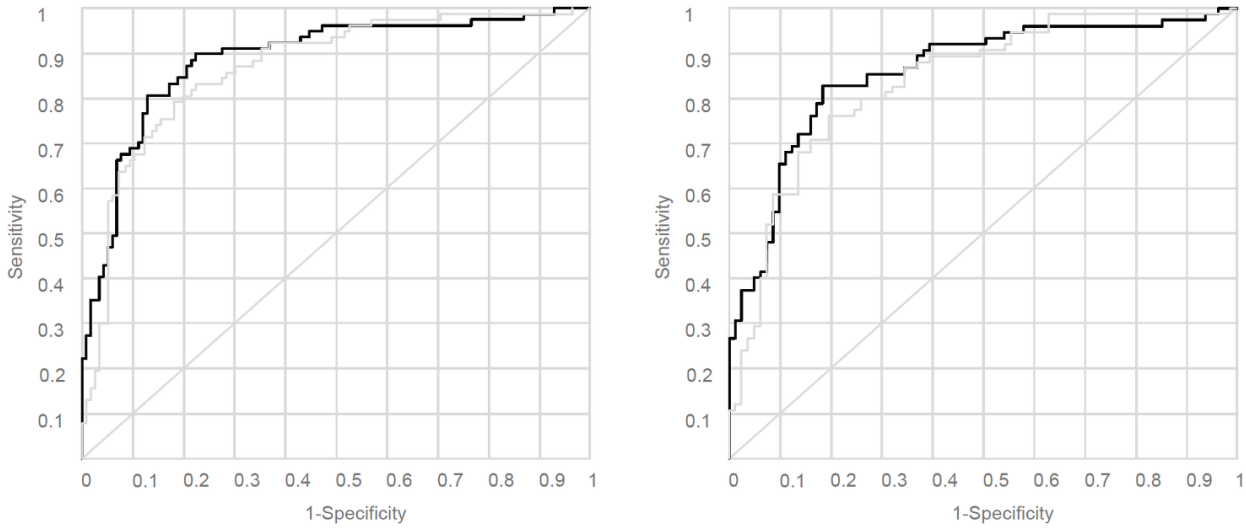

9.6 References

1. Smith LJ. The lower limit of normal versus a fixed ratio to assess airflow limitation: will the debate ever end? Eur Respir J 2018; 51.

2. Brusasco V. Spirometric definition of COPD: exercise in futility or factual debate? Thorax 2012; 67:569-570.

3. (GOLD) GIfCOLD. Global Strategy for the Diagnosis, Management and Prevention of COPD 2017 [Available from: http://goldcopd.org.

4. Vogelmeier CF, Criner GJ, Martinez FJ, Anzueto A, Barnes PJ, Bourbeau J, et al. Global Strategy for the Diagnosis, Management, and Prevention of Chronic Obstructive Lung Disease 2017 Report: GOLD Executive Summary. Eur Respir J 2017; 49.

5. Quanjer PH, Hall GL, Stanojevic S, Cole TJ, Stocks J, Global Lungs I. Age- and height-based prediction bias in spirometry reference equations. Eur Respir J 2012; 40:190-197.

6. Mohamed Hoesein FA, Zanen P, Lammers JW. Lower limit of normal or FEV1/FVC < 0.70 in diagnosing COPD: an evidence-based review. Respir Med 2011; 105:907-915.

7. Pellegrino R, Viegi G, Brusasco V, Crapo RO, Burgos F, Casaburi R, et al. Interpretative strategies for lung function tests. Eur Respir J 2005; 26:948-968.

8. Quanjer PH, Stanojevic S, Cole TJ, Baur X, Hall GL, Culver BH, et al. Multi-ethnic reference values for spirometry for the 3-95-yr age range: the global lung function 2012 equations. Eur Respir J 2012; 40:1324-1343.

9. Copley SJ, Wells AU, Hawtin KE, Gibson DJ, Hodson JM, Jacques AE, et al. Lung morphology in the elderly: comparative CT study of subjects over 75 years old versus those under 55 years old. Radiology 2009; 251:566-573.

10. MacNee W, Rabinovich RA, Choudhury G. Ageing and the border between health and disease. Eur Respir J 2014; 44:1332-1352.

11. Pauwels RA, Buist AS, Calverley PM, Jenkins CR, Hurd SS, Committee GS. Global strategy for the diagnosis, management, and prevention of chronic obstructive pulmonary disease. NHLBI/WHO Global Initiative for Chronic Obstructive Lung Disease (GOLD) Workshop summary. Am J Respir Crit Care Med 2001; 163:1256-1276.

12. Camiciottoli G, Bigazzi F, Paoletti M, Cestelli L, Lavorini F, Pistolesi M. Pulmonary function and sputum characteristics predict computed tomography phenotype and severity of COPD. Eur Respir J 2013; 42:626-635.

13. Paoletti M, Cestelli L, Bigazzi F, Camiciottoli G, Pistolesi M. Chronic Obstructive Pulmonary Disease: Pulmonary Function and CT Lung Attenuation Do Not Show Linear Correlation. Radiology 2015; 276:571-578.

14. Castaldi PJ, Benet M, Petersen H, Rafaels N, Finigan J, Paoletti M, et al. Do COPD subtypes really exist? COPD heterogeneity and clustering in 10 independent cohorts. Thorax 2017; 72:998-1006.

15. Miller MR, Hankinson J, Brusasco V, Burgos F, Casaburi R, Coates A, et al. Standardisation of spirometry. Eur Respir J 2005; 26:319-338.

16. Macintyre N, Crapo RO, Viegi G, Johnson DC, van der Grinten CP, Brusasco V, et al. Standardisation of the single-breath determination of carbon monoxide uptake in the lung. Eur Respir J 2005; 26:720-735.

17. Wanger J, Clausen JL, Coates A, Pedersen OF, Brusasco V, Burgos F, et al. Standardisation of the measurement of lung volumes. Eur Respir J 2005; 26:511-522.

18. Regan EA, Hokanson JE, Murphy JR, Make B, Lynch DA, Beaty TH, et al. Genetic epidemiology of COPD (COPDGene) study design. COPD 2010; 7:32-43.

19. Lynch DA, Austin JH, Hogg JC, Grenier PA, Kauczor HU, Bankier AA, et al. CT-Definable Subtypes of Chronic Obstructive Pulmonary Disease: A Statement of the Fleischner Society. Radiology 2015:141579.

20. Silva M, Nemec SF, Dufresne V, Occhipinti M, Heidinger BH, Chamberlain R, et al. Normal spectrum of pulmonary parametric response map to differentiate lung collapsibility: distribution of densitometric classifications in healthy adult volunteers. Eur Radiol 2016; 26:3063-3070.

21. Occhipinti M, Paoletti M, Bigazzi F, Camiciottoli G, Inchingolo R, Larici AR, et al. Emphysematous and Nonemphysematous Gas Trapping in Chronic Obstructive Pulmonary Disease: Quantitative CT Findings and Pulmonary Function. Radiology 2018; 287:683-692.

Chapter 10 - Future directions

The evolution of knowledge concerning COPD covers 200 years (1). Although recently the interest towards COPD has increased and research in the field is growing fast, there are still many questions to answer.

Our next studies will focus on the *longitudinal evaluation* of patients with COPD in order to investigate the natural history of this disease by using on one hand cutting-edge radiological methodologies and on the other hand a close clinical approach. The collaboration with researchers with great expertise in the field (the COPDGene Study research group) will be the key to answer interesting questions of basic research that may rapidly translate into key points for patient treatment.

A few physicists around the world are developing post-processing imaging techniques to assess *pulmonary vessels* without the need of contrast media injection (2). The application of these tools may contribute to an accurate characterization of the different endotypes. Many years ago post-mortem studies have already shown significant differences in lung vascularization between patients with emphysema and those with small airway disease (3, 4). However, the *in vivo* characterization of lung vessels could help in the management of those patients that are prone to develop pulmonary hypertension.

The use of innovative radiological tools will be combined with an accurate *qualitative assessment* of chest CT scans, according to the Fleishner Society Statement (5). The evaluation will not be limited to the definition of CT-subtypes, but it will take into account associated features of COPD, such as tracheobronchomalacia, bronchiectases, coexistence of interstitial lung disease, pulmonary hypertension, morphology of chest wall and large airways.

Further development of the *online App* based on the ESI model described in Chapter 6 is ongoing to eventually help pulmonologists and primary care physicians in defining COPD endotypes tomorrow and in targeting therapy accordingly.

10.1References

1. Petty TL. The history of COPD. Int J Chron Obstruct Pulmon Dis 2006; 1:3-14.

2. Rudyanto RD, Kerkstra S, van Rikxoort EM, Fetita C, Brillet PY, Lefevre C, et al. Comparing algorithms for automated vessel segmentation in computed tomography scans of the lung: the VESSEL12 study. Med Image Anal 2014; 18:1217-1232.

3. Andoh Y, Shimura S, Aikawa T, Sasaki H, Takishima T. Perivascular fibrosis of muscular pulmonary arteries in chronic obstructive pulmonary disease. Chest 1992; 102:1645-1650.

4. Hale KA, Niewoehner DE, Cosio MG. Morphologic changes in the muscular pulmonary arteries: relationship to cigarette smoking, airway disease, and emphysema. Am Rev Respir Dis 1980; 122:273-278.

5. Lynch DA, Austin JH, Hogg JC, Grenier PA, Kauczor HU, Bankier AA, et al. CT-Definable Subtypes of Chronic Obstructive Pulmonary Disease: A Statement of the Fleischner Society. Radiology 2015:141579.

Chapter 11 - Conclusions

This thesis describes the use and development of innovative tools, both radiological and bioengineering, in supporting clinical diagnosis and phenotypization of chronic obstructive pulmonary disease (COPD). Radiology was coupled with pulmonary function to better understand this complex and heterogeneous disease and to describe its phenotypes and endotypes.

An overview of the clinical complexity and heterogeneity of COPD and the current role of imaging is presented in chapter 1. Chapter 2 explains the current role of qualitative and quantitative imaging, recent advances in post-processing image analysis and imaging tools dedicated to research in this field.

The studies described from chapter 3 to chapter 7 are the core of the thesis, consisting of the models developed from clinical and functional data to evaluate the presence of emphysema in patients with expiratory airflow obstruction. Imaging tools are used to assess CT endotypes and as referring gold standard for the models. In chapter 3 we demonstrated that standard imaging metrics obtained by inspiratory and expiratory CT scans can be used to identify and quantify the relative contribution of emphysematous and non-emphysematous gas trapping, allowing a better definition of COPD patient subtypes. The definition of the prevalent CT subtype (i.e. emphysema versus airway disease) of COPD could potentially be used to target patient therapy to the underlying COPD endotype. Moreover, a logistic model combining BMI, DLco%, FEV_1%, and FEV_1/VC proved to be accurate in predicting CT-based quantification of emphysema grade, which may prove useful when assessing COPD patients who do not undergo chest CT.

In chapter 4 and 5 we further explored the chances to use functional parameters to estimate the presence of emphysema at CT by using statistical models. In chapter 4 we tried to exclude DLco and to use only functional parameters directly derived from the spirometric flow-volume curve without standardization for sex, age, and ethnicity data. In chapter 5 we took into account the shape of the flow-volume curve itself. The level of accuracy of both models was high and suitable for clinical practice as well as for pharmacologic trials.

The deep thoughts on the flow-volume curve inspired us to develop a mathematical model (ESI) entirely based on the curve, as described in chapter 6. This model classifies patients with milder or more severe emphysema, as defined by quantitative CT metrics, without the need of anthropometric or standardized parameters. Moreover, in this chapter lung texture analysis was used to study the presentation of lung patterns in COPD patients. An unsupervised radiomics approach identified three clusters of patients and their presentation at pulmonary function tests was described. The ESI model created from a cohort of Caucasians was then validated in the largest population of COPD patients ever studied (the COPDGene Study) including different ethnicities (chapter 7). The application of the ESI model to such a big and heterogeneous population supported the results obtained in our small cohort. This result put the foundations for using ESI model in randomized controlled trials to test treatment efficacy according to COPD endotypes and not only to the simplistic approach of FEV_1 reduction and exacerbation rate that overlook the physio-pathogenetic mechanisms underlying airflow obstruction.

In chapter 8 and chapter 9 we examined the ongoing questions and future directions of research in the field. In particular, in chapter 7 we wonder about the criteria to define COPD, as the adoption of the LLN criterion excluded subjects with relevant COPD findings at CT scan. Moreover, we explored the concordance between a dedicated thoracic radiologist and a general radiologist to define COPD CT-subtypes. In chapter 8 I discussed the future research directions towards the need for longitudinal studies, assessment of lung vessels, qualitative assessment of COPD subtypes, and development of a handy App for clinicians to define the presence of emphysema without undergoing chest CT scan.

All the work presented is the result of a strict and passionate collaboration of experts in different fields: pulmonologists, radiologists, and bioengineers. This collaboration is challenging, intriguing, stimulating, and fundamental for making advances in research when the topic is as complex and heterogeneous as COPD.

Curriculum Vitae

Mariaelena Occhipinti, M.D.

Ragusa, February 6, 1984
Via Pescara, 18 - Marina di Ragusa (RG), 97010 - Italy • Mobile: (+39) 335-6456321
email: mariaelena.occhipinti@gmail.com / mariaelena.occhipinti@unifi.it

Education

PhD Course on Clinical Sciences (October 2015 to date)
University of Florence – Medical School – "Careggi" Hospital, Florence (IT)
Dept. Clinical and Experimental Medicine, Thoraco-Pulmonary Section
Tutor: Prof. Massimo Pistolesi
Curriculum: Experimental and Clinical Medicine
PhD title: *Phenotyping COPD: clinical-radiological correlation of COPD phenotypes*

Research Fellowship in Thoracic Imaging (June 2018)
Department of Physiology and Biomedical Engineering, Mayo Clinic, Rochester (MN)
Tutor: Prof. Brian J. Bartholmai
Topic: Quantitative CT in COPD patients.

European Diploma in Radiology (October 2015)

Research Fellowship in Thoracic Imaging (January 2014 – December 2014)
Harvard Medical School, Beth Israel Deaconess Medical Center, Boston (MA)
Tutor: Prof. Alexander A. Bankier
Topics: Quantitative CT of the lung in normal subjects; Lung nodules in oncologic patients; Masses of posterior mediastinum.

Residency Program in Radiology (May 2010 – May 2015)
Catholic University of the Sacred Heart - Medical School - Rome (IT)
"A. Gemelli" Hospital, Radiology Dept.
Tutors: Prof. Lorenzo Bonomo, Prof. Anna Rita Larici
Vote: 50/50 *Cum laude*

License to Practice Medicine in Italy (February 2010)
Vote: 270/270

Canada, Montréal – Research Exchange Program (July 2009 - September 2009)
Université du Québec à Montréal, Département de Radiologie/Laboratoire de Biorhéologie et d'Ultrasonographie Médicale, Centre de Recherche.
Topic: Development of an animal model of atherosclerotic plaque.

Medical School, Catholic University of the Sacred Heart - Rome, IT (October 2003 – October 2009)
Medical Doctor, 110/110 *Cum Laude*
Thesis: "Diagnostic PET/CT vs PET/CT alone in staging and re-staging of non small cell lung cancer"
Relators: Prof. Lorenzo Bonomo, Prof. Anna Rita Larici.

University College for Excellence - Rome, IT (October 2003 – October 2009)
Fondazione Comunità "Domenico Tardini", in partnership with the European University College Association.

Scientific High School, Liceo Scientifico Statale "E. Fermi" – Ragusa, IT (September 1998 - July 2003)
Vote: 100/100 *Cum Laude*

International collaborations

Member of ATS/ERS Task-Force for combined pulmonary fibrosis and emphysema (CPFE)

Lung Nodule Evaluation Project

COPDGene Study Investigators

Mayo Clinic (Rochester, MN)

Ludwig Boltzmann Institute Lung Vascular Research, Graz (AT)

University Medical Center Heidelberg (DE)

Research Grants

Research Grant "Fondazione CR Firenze" (July 2018 to date)
Project title: "DECODE: Diagnosi e fEnotipizzazione della bpCo attraverso un approccio integrato di biofOtonica, raDiomica e machinE learning". In collaboration with CNR Institute of Applied Physics "N. Carrara" IFAC.

Research Grant at University of Florence (January 2018 to date)
Dept. Rheumatology
Careggi University Hospital
Topic: In search for the parenchymal and vascular features in SSc-ILD: how to address the challenge of quantitative analysis of CT images and correlation with clinical and instrumental data. Grant of GILS (Gruppo Italiano Lotta Sclerodermia), 1st classified. Grant of FIRA (Fondazione Italiana per la Ricerca sull'Artrite), 1st classified.

Research Grant at University of Florence (January 2016 to date) – "Menarini Foundation"
Dept. Clinical and Experimental Medicine, Thoraco-Pulmonary Section
Careggi University Hospital
Topic: Quantitative CT in COPD patients and functional predictive models.

Research Grant "Fondazione Roma" (June 2017-October 2017)
Dept. Radiological Sciences
Catholic University of the Sacred Heart - Medical School - Rome (IT)
Topic: Personalized pharmacological treatment of chronic obstructive pulmonary disease based on phenotyping.

Research Grant "Istituto Giuseppe Toniolo" (September 2015 - December 2015)
Dept. Radiological Sciences
Catholic University of the Sacred Heart - Medical School - Rome (IT)
Topic: Quantitative CT in patients with Systemic Sclerosis associated with interstitial lung involvement.

List of publications

- **Occhipinti M**, Paoletti M, Bigazzi F, Camiciottoli G, Inchingolo R, Larici AR, Pistolesi M.
"Emphysematous and non-emphysematous gas trapping in COPD: quantitative CT findings and pulmonary function"
Radiology. 2018;287(2):683-692

- Nardi C, Calistri L, Grazzini G, Desideri I, Lorini C, **Occhipinti M**, Mungai F, Colagrande S.
Is Panoramic Radiography an Accurate Imaging Technique for the Detection of Endodontically Treated Asymptomatic Apical Periodontitis?
J Endod. 2018;44(10):1500-1508. doi: 10.1016/j.joen.2018.07.003.

- Nardi C, Salerno S, Molteni R, **Occhipinti M**, Grazzini G, Norberti N, Cordopatri C, Colagrande S.
"Radiation dose in non-dental Cone Beam CT applications: A systematic review"
Radiol Med. 2018 Oct;123(10):765-777. doi: 10.1007/s11547-018-0910-7.

- Sacconi B, Valente G, **Occhipinti M**.
Book chapter: "Mediastinal non-neoplastic conditions"
In: *Diagnostic imaging for thoracic surgery*. Editors: Michele Anzidei, Marco Anile. In press for Springer.

- Torricelli E, **Occhipinti M**, Lavorini F, Cresci C, Arcangeli C, Cavigli E, Bigazzi F, Pistolesi M.
"Pulmonary hypertension nosography: are all patients classifiable?"
Intern Emerg Med 2017. https://doi.org/10.1007/s11739-017-1700-2

- **Occhipinti M**, Larici AR, Bonomo L, Antonelli Incalzi R.
"Aging Airways: between Normal and Disease. A Multidimensional Diagnostic Approach by Combining Clinical, Functional, and Imaging Data"
Aging and Disease 2017; 8 (4): 471-485.

- **Occhipinti M**, Heidinger BH, Pfannenberg C, Munden RF, Eisenberg RL, Bankier AA.
"Managing incidental lung nodules in patients with a history of oncologic disease. A survey of thoracic radiologists"
J Thorac Imaging 2017; 32(2):115-120.

- Pistolesi M, **Occhipinti M**.
Book chapter: "Chest Radiography: pulmonary venous hypertension"
In: *The ESC Textbook of Cardiovascular Medicine*. 3rd edition. In press for Oxford University Press.

- Pistolesi M, Bigazzi F, **Occhipinti M**, Paoletti M, Camiciottoli G.
Book chapter: "COPD: airways and lung parenchyma"
In: La pneumologia interventistica nell'enfisema e nell'asma. In press for Springer.

- Silva M, Nemec S, Dufresne V, **Occhipinti M**, Heidinger B, Charberlain R, Bankier AA.
"Normal spectrum of pulmonary parametric response map: distribution of densitometric classifications in healthy adult volunteers"
Eur Radiol 2016; 26(9):3063-70. doi: 10.1007/s00330-015-4133-1.

- **Occhipinti M**, Heidinger BH, Franquet E, Eisenberg RL, Bankier AA.
"Posterior mediastinum: a multimodality approach"
Diagn Interv Radiol 2015; 21(4):293-306. doi: 10.5152/dir.2014.14467

- Heidinger BH, **Occhipinti M**, Bankier AA, Eisenberg RL.
"Large airways disorders"
AJR Am J Roentgenol 2015; 205(1):41-56. doi: 10.2214/AJR.14.13857

- Franchi P, Larici AR, **Occhipinti M**, Ciliberto M, Staglianò S, Inzani F, del Ciello A, Calandriello L, Bonomo L.
"Pulmonary adenocarcinoma: radiological-pathological correlation with the new multidisciplinary classification and guidelines for subsolid nodules management"
Radiol Med 2015; 2: 67-77.

- Larici AR, Franchi P, **Occhipinti M**, Contegiacomo A, del Ciello A, Calandriello L, Storto ML, Marano R, Bonomo L.
"Diagnosis and management of hemoptysis"
Diagn Interv Radiol 2014; 20(4):299-309. doi: 10.5152/dir.2014.13426.

- Petronelli S, Zurlo MT, Giambersio S, Danieli L, **Occhipinti M.**
"A single-centre experience of 200 consecutive unselected patients in percutaneous EVAR"
Radiol Med 2014; 119(11): 835-41. doi: 10.1007/s11547-014-0399-7.

- Larici AR, Franchi P, **Occhipinti M**, Devicienti E, Mereu M, del Ciello A, Bonomo L.
Book chapter: "Airway disease" In: Geriatric Imaging (2013), Part III, pp: 319-352. Editors: Guglielmi G, Peh WCG, Guermazi A. Springer Berlin Heidelberg. doi: 10.1007/978-3-642-35579-0_14

Invited lectures at conferences

- ECR 2019, Vienna. Lectures:
"Radiologic anatomy: Chest - Mediastinal"
"Fundamentals of chest imaging"
"Back to basics: how to interpret a chest radiograph? Mediastinal syndrome".
- SIICP 2018. Otranto, 12-13 October 2018. Lecture: "Role of imaging in chronic respiratory diseases"
- ESTI/ESCR 2018. Geneva (CH), May 2018. Lecture: "Organising pneumonia" at the joint session ESTI/ESCR on multimodality imaging in cardiopulmonary inflammation.
- ECR 2018, Vienna. Moderator at scientific session: "Quantitative CT: a new diagnostic and functional tool"
- Italian Congress of Thoracic Imaging, Rome. October 2017. Lecture: "Role of CT in diagnosis, quantification, and phenotypization of COPD"
- PneuMed. Genoa, May 2017. Course on "Respiratory physiopathology and functional imaging"
- ECR 2017, Vienna. Lecture: "Still tricky after all these years: the mediastinum". Moderator of Master Class session on the "Airways"
- International Symposium on COPD, Florence. June 2016. Discussant at the session "Imaging of COPD".
- Respiro Stresa. May 2016. Lecture: "COPD: new phenotypes and old genotypes"
- ECR 2016, Vienna. Lecture: "Role of CT in mediastinal masses"
- ESTI 2015, Barcelona. Lecture: "Posterior mediastinum"
- SIRM 2014, Rome. Lecture: "Subsolid lung nodules: diagnosis and management".

Awards in Radiology

- **Trainee Research Prize, RSNA 2016** (Radiologic Society of North America), Chicago. Project title: "Spectrum of Pulmonary Parametric Response Maps in Asthmatic Patients: A Promising Innovative Tool in Defining Asthma Subtypes".

- ESTI Congress 2012, London. Poster presentation: "Reproducibility of semi-automated airway measurements on 64-detector row CT at inspiratory and expiratory scans: impact of two reconstruction algorithms". AR Larici, E Devicienti, M Occhipinti, M Amato, L Calandriello, A del Ciello, L Bonomo.
Awarded with a Certificate of Merit.

- ECR 2012, Vienna. Poster presentation: "Upper airway diseases in the elderly: pictorial review of MDCT findings". M Occhipinti, AR Larici, E Devicienti, P Franchi, A del Ciello, M Mereu, FM Danza, L Bonomo.
Awarded with a Certificate of Merit.

Reviewer for Scientific Journals

- European Radiology (2015-19)

- European Radiology Experimental (2018-19)

- Diagnostic and Interventional Radiology (2017)

- Journal of Anatomy (2016)

- Journal of Thoracic Imaging (2014)

Scientific presentations at Conferences

- SIRM (Italian Society of Radiology) 2018. Genoa (IT). Oral presentation. "Investigando sui criteri diagnostici di BPCO: superiorità dell'esame TC sui criteri funzionali LLN e GOLD".

- ESTI (European Society Thoracic Imaging) 2018, Geneva (CH). Oral presentation. "Unmasking COPD in patients excluded by the lower limit of normality" Occhipinti M, Paoletti M, Nardi C, Palazzi M, Camiciottoli G, Inchingolo R, Colagrande S, Larici AR, Pistolesi M.

- RSNA (Radiological Society North America) 2017, Chicago (IL). Oral presentation. "Evaluating Treatment Response in Patients with Systemic Sclerosis and Diffuse Interstitial Lung Involvement: Quantitative CT as a New Outcome Measure" Occhipinti M, Bosello S, Westmore MS, Cicchetti G, Sisti LG, Larici AR.

- ERS (European Respiratory Society) 2017, Milan. Poster presentation with discussion. "Pulmonary Parametric Response Maps: an innovative tool in defining asthma subtypes" Occhipinti M, Hatt C, Fuso L, Sbarra M, Condoluci C, Macis G.

- ERS 2017, Milan. Poster presentation. "A predictive model for classifying COPD patients according to CT emphysema extent by using functional data and BMI" Occhipinti M, Paoletti M, Bigazzi F, Camiciottoli G, Inchingolo R, Larici AR, Pistolesi M.

- Italian Congress of Thoracic Imaging 2017, Rome. Oral presentation. "Pulmonary parametric response maps in severe asthma" Occhipinti M, Hatt C, Fuso L, Condoluci C, Macis G.

- World Congress of Thoracic Imaging 2017, Boston (MA). Oral presentation. "Assessment of small airway disease contribution to pulmonary dysfunction in COPD" Occhipinti M, Paoletti M, Bigazzi F, Camiciottoli G, Bonti V, Pistolesi M.

- RSNA 2016, Chicago (IL). Oral presentation. "Spectrum of Pulmonary Parametric Response Maps in Asthmatic Patients: A Promising Innovative Tool in Defining Asthma Subtypes" Occhipinti M, Hatt C, Fuso L, Sbarra M, Condoluci C, Bonomo L, Macis G.

- ESTI (European Society Thoracic Imaging) 2016, Krakow. Oral presentation. "Game over for old scoring systems? LTA in interstitial lung involvement of Systemic Sclerosis". Oral presentation. Occhipinti M, Larici AR, Cicchetti G, Bosello S, Rucco M, Bonomo L.

- SIRM 2016, Naples (IT). Oral presentation. "TC quantitativa nell'interessamento interstiziale da sclerosi sistemica: obiettivando i risultati della terapia". Occhipinti M, Larici AR, Bosello S, Cicchetti G, Pirronti T, Bonomo L.

- ECR (European Congress of Radiology) 2016, Vienna. Oral presentation. "Lung cancer screening program in a large Italian cohort: baseline results". Occhipinti M, Franchi P, Cicchetti G, Ciliberto M, Larici AR, Bonomo L.

- STR (Society of Thoracic Radiology) 2015 "Thoracic imaging", Carlsbad (CA). Poster presentation. "Posterior mediastinum: a multimodality approach". Occhipinti M, Heidinger H, Franquet E, Eisenberg RL, Bankier AA.

- STR 2015 "Essentials in lung cancer screening programs", Carlsbad (CA). Oral presentation. "CT Lung Cancer Screening: baseline results from a large Italian screening program compared to the NLST data". Occhipinti M, Franchi P, Tonetti L, Ciliberto M, Bonomo L.

- RSNA 2014, Chicago. Oral presentation. "Lung volume and heterogeneity: CT quantification of lobar contribution". Silva M, Heidinger BH, Occhipinti M, Nemec SF, Molinari F, Dufresne V, Bankier AA.

- RSNA Congress 2013, Chicago (IL). Oral presentation. "Role of MDCT-virtual lobectomy in the prediction of post-operative lung function in patients undergoing surgical lobectomy". M Occhipinti, E Devicienti, AR Larici, R Inchingolo, MR Calvello, L Bonomo.

- ECR 2013, Vienna. Poster presentation. "Pediatric Tuberculosis: pictorial review of CXR and MDCT findings". M Occhipinti, AR Larici, A del Ciello, P Franchi, E Devicienti, L Calandriello, A Contegiacomo, F Maggi, L Bonomo.

- ECR 2013, Vienna. Poster presentation. "Lung Adenocarcinoma: radiological-pathological correlation according to the new multidisciplinary classification". P Franchi, AR Larici, M Occhipinti, A del Ciello, A Contegiacomo, L Calandriello, F Inzani, G Rindi, L Bonomo.

- ESTI Congress 2012, London. Poster presentation. "Airway diseases in the elderly". M Occhipinti, AR Larici, E Devicienti, P Franchi, A del Ciello, M Mereu, L Bonomo.

- RSNA Congress 2012, Chicago (IL). Poster presentation. "Pediatric Tuberculosis: A Pictorial Review". M Occhipinti, AR Larici, A del Ciello, P Franchi, E Devicienti, L Bonomo.

- ECR 2012, Vienna. Poster presentation. Pulmonary lymphatic drainage in non-small cell lung cancer. P Franchi, AR Larici, M Amato, A del Ciello, M Occhipinti, E Devicienti, M Ciresa, A Contegiacomo, L Bonomo

- ESTI Congress 2011, Heidelberg (Germany). Poster presentation. "Incidental asymptomatic pulmonary embolism on MDCT: a prospective study of prevalence in oncology inpatients". A del Ciello, AR Larici, F Maggi, L Calandriello, A Contegiacomo, M Occhipinti, R Silvestri, L Bonomo.

Languages

Italian (native)

English (Advanced: level C1 in CEFR - Common European Framework of Reference for Languages, equivalent to 3/3+ in ILR - Interagency Language Roundtable Scale)

Spanish (Intermediate)

French (Basic)

References

Massimo Pistolesi, MD
Dept. Clinical and Experimental Medicine – "Careggi" Hospital – Largo A. Brambilla, 3, 50134 Florence (IT)
University of Florence
massimo.pistolesi@unifi.it

Lorenzo Bonomo, MD
Dept. of Radiological Sciences – "A. Gemelli" University Hospital – Largo A. Gemelli, 8 - 00168 Rome (IT)
Catholic University of Sacred Heart
lorenzo.bonomo.md@gmail.com

Alexander A. Bankier, MD, PhD
Dept. Radiology, Beth Israel Deaconess Medical Center, 330 Brookline Ave, 02215 Boston (MA)
Harvard Medical School
abankier@bidmc.harvard.edu

Ronald L. Eisenberg, MD
Dept. Radiology, Beth Israel Deaconess Medical Center, 330 Brookline Ave, 02215 Boston (MA)
Harvard Medical School
rleisenb@bidmc.harvard.edu

Brian Bartholmai
Dept. Radiology, Mayo Clinic, 1216 2nd St SW, 55902 Rochester, MN (MN)
bartholmai.brian@mayo.edu